SOME COMPENSATION TECHNIQUES APPLIED TO A LABORATORY POWER SYSTEM

A Thesis

Submitted To The Faculty of Graduate Studies

In Partial Fulfilment Of The Requirements For The Degree

Of Master Of Science

The University of Manitoba

Department of Electrical Engineering

by

E.M. Ryczkowski

Winnipeg, Manitoba

May 1977

"SOME COMPENSATION TECHNIQUES

APPLIED TO A LABORATORY POWER SYSTEM"

by

E.M. Ryczkowski

A dissertation submitted to the Faculty of Graduate Studies of the University of Manitoba in partial fulfillment of the requirements of the degree of

MASTER OF SCIENCE

ACKNOWLEDGEMENT

The author gratefully acknowledges the efforts of Dr. G.W. Swift for his guidance and encouragement in the development of this topic. The cooperation extended by the staff of the Electrical Engineering Department is also appreciated. In addition, the financial support provided by the National Research Council is acknowledged with thanks. Finally, the patience and careful attention of Catharine Souliere in the typing of this thesis is much appreciated.

ABSTRACT

The object of this thesis was to investigate the possibility of using complex pole - zero compensation on a generator infinite bus system employing frequency as the feedback signal. A complex compensator was implemented on a real machine infinite bus model power system and its performance was compared to that of a real root compensator having the form $\frac{Ks}{1 + Ts}$. The results indicate that the complex compensator can produce favorable results for a particular system configuration with a substantial range of operating conditions for that particular configuration. However, it is observed that real root compensation can perform just as favourably as complex root compensation.

TABLE OF CONTENTS

NOMENCLATURE

E_1 - the generated voltage behind the machine transient reactance. (L-L volts)

E_b - the infinite bus voltage (L-L volts)

Xe - the external system reactance between the generator and the infinite bus. (p.u.)

Re - the external system resistance (p.u.)

δ - angle between the quadrature axis and the infinite bus.

ω - frequency or speed (when p.u. values are used either definition applies)

ω_n - undamped natural frequency

ω_d - damped natural frequency

ζ - damping ratio

P_m - mechanical power due to prime mover (p.u.)

P_e - electrical power (p.u.)

T_m - mechanical torque due to prime mover (p.u.)

T_s - synchronizing torque component

T_D - damping torque component

T_{shaft} - torque applied to machine shaft

ν - machine speed (radians/second)

J - moment of inertia of the synchronous machine rotor

e_t - terminal voltage

e_r - reference voltage

E_{fld} - generator field voltage

E'_q - voltage proportional to direct axis flux linkages

D - prime mover damping (p.u.)

M - inertia constant (sec)

ke - exciter gain

k_1-k_6 Heffron - Phillips constants

Te - exciter time constant (sec)

T'_{d0} - open circuit field time constant (sec)

T'_{dz} - effective field time constant under load ($T'_{dz} = k_3 T'_{d0}$ sec.)

T_d' - short circuit field time constant (sec)

X_d - direct-axis synchronous reactance (p.u.)

X_d' - direct-axis transient reactance (p.u.)

X_d'' - direct-axis subtransient reactance (p.u.)

X_q - quadrature-axis synchronous reactance (p. u.)

X_q' - quadrature-axis transient reactance (p.u.)

X_q'' - quadrature-axis subtransient reactance (p.u.)

R_s - stator resistance (p.u.)

X_{ls} - stator leakage reactance (p.u.)

X_{ms} - magnetizing reactance (p.u.)

E_{ms} - voltage accross the magnetizing reactance (air gap voltage)

n' - current reatio between stator current and field current

I_f - field current

I_s - stator current

V_s - stator voltage (during frequency response tests)

$L_{d(j\omega)}$ operational inductance for the direct axis.

L_{du} - unsaturated synchronous inductance

L_m - mutual inductance

L_l - leakage inductance

Z_s - impedance measured at the stator terminals during frequency response tests

Z_{eq} - impedance of the machine equivalent circuit referred to the stator terminals

L_1 - inductane of the first branch of the equivalent circuit

R_1 - resistance of the first branch of the equivalent circuit

L_2 - inductance of the second branch of the equivalent circuit

R_2 - resistance of the second branch of the equivalent circuit

$G(s)$ - uncompensated system transfer function

$G_c(s)$ - compensator transfer function

t_s - 2% settling time (sec)

σ - magnitude of the real part of the dominant root of the system in the s-plane

s - Laplace operator

Δ - used as a prefix to indicate small change

NOTE: All quantities are in per unit on the machine base unless otherwise indicated.

CHAPTER I

INTRODUCTION

Stability of large electric power systems has been subjected to much concern and discussion of late. In recent years there has been a trend to extensive interconnection of power systems so as to increase reliability and to obtain the economic benefits of new blocks of generation. However, these aims can only be realized if the interconnected system remains intact and does not break up and lose synchronism when subjected to disturbances. Because of these developments, the problem of stability has created more concern.

Increasingly large power systems not only contribute to inherent instability but, as a direct consequence of their size, they turn the problem of analysis into an extremely difficult task. A large system can possess a wide range of operating conditions and be subjected to a large variety of disturbances. Also, because of the nonlinear nature of A.C. power transmission, the ability to extrapolate from one operating condition to the next cannot be done with confidence. Bearing this in mind, it can be seen that any particular solution to a stability problem will probably have only a limited range of application unless some means of adapting or updating the solution to changing operating variables is found.

Interconnected system stability is degraded when certain parts of the system exhibit tendencies toward dynamic instability. Small speed variations occur continuously during normal operation with corresponding variations in angle differences and generator loads. The system is dynamically stable if these variations diminish with time. Conversely,

if these variations increase with time dynamic instability will result. Power oscillations may be initiated spontaneously or as a result of a disturbance and if the system is dynamically unstable they will build in magnitude until synchronism is lost. A common factor in such behavior is long transmission lines. As a result of this phenomenon the capacity for stable power flow between machine groups is reduced and low natural oscillation frequencies that are poorly damped occur.

In view of the above discussion, this thesis will endeavor to investigate the performance of a complex compensator when applied to a machine infinite bus system with a long transmission line in the hope of increasing the dynamic stability limit of such a system and, if possible, increase the transient stability limit. The concept of complex compensation is pursued since the roots of the uncompensated system generally occur in complex conjugate pairs. It would then seem logical to expect that a properly selected complex compensator should be able to alter the location of the system eigenvalues for a reasonable range of operating values and thereby result in a more stable system. Because the system eigenvalues occur in complex conjugate pairs this would seem to detract from the effectiveness of a compensator using real poles and zeroes. The following chapters will attempt to determine the effectiveness of a complex compensator as opposed to a real root compensator of the form $\frac{Ks}{1 + Ts}$.

The compensators under consideration shall use frequency as the feedback signal. Frequency has been selected since this is the most widely used feedback signal among most utilities although one could have just as easily selected a feedback signal proportional to power deviation.

In Chapter II the characteristics of a machine-infinite-bus-system

is developed. Since this particular area has had extensive coverage in numerous other publications [1, 2, 3, 4, 5] the development will be brief and will only serve to introduce the most important concepts. The development will then turn to the analytic representation of a machine-infinite-bus-system utilizing the Heffron - Phillips model [1] and from this model the system transfer function will be obtained. Finally, the real-machine-infinite-bus-model-power-system will be described and the individual parameters of the system will be determined. It should be noted that a rather novel approach utilizing frequency response techniques was employed to determine the parameters of the synchronous machine.

In Chapter III the complex compensator design is presented. The design procedure is based on the use of the root locus method and frequency response techniques. Although the system transfer function is fairly involved the root locus plots were easily obtained using a PDP 11/40 digital computer. The above methods are then applied to the real pole-zero compensator for comparison purposes. Analog computer simulations are run to observe time domain performance.

Finally, in Chapter IV the compensators obtained through analytic methods are implemented on a real-model-power-system and oscillographic results are included. In this way the validity of the model used is confirmed and the method of analysis is checked.

It should be noted that in the paragraphs which follow, the terms compensator and stabilizer will be used interchangeably and are to be understood to imply the same thing.

CHAPTER II

System Models

1. Synchronous Machine and Infinite Bus

In most cases one can model a block of generation or a single generator connected to the rest of the network as a single machine connected via an A.C. transmission line to a very large system. The result of such an approximation can usually give the investigator sufficient insight to be able to determine the conditions leading to instability.

With the machine infinite bus representation the electrical power transfer relationships can be studied. The single line diagram is shown in Fig. 2.1 (a) while Fig. 2.1 (b) demonstrates the vector relation present between voltage and current. The nomenclature used is as follows:

X_d' = the generator transient reactance (ohms)

X_e = the external reactance consisting of the transmission line and transformers which connect the generator to the large system (ohms).

E_1 = the generated voltage behind the transient reactance (L-L volts)

E_b = the infinite bus voltage (L-L volts)

δ_{1b} = the angle between the generated voltage and the infinite bus voltage.

From Fig. 2.1(b), neglecting saliency (if $X_d \neq X_q$ an extra term will be added to the power equation) [2];

$$I = \frac{E_1 \angle \delta_{1b} - E_b \angle 0^\circ}{(X_d' + X_e) \angle 90^\circ}$$

$$I = \frac{E_1 \angle \delta_{1b} - 90^\circ}{Xd' + Xe} - \frac{E_b \angle -90^\circ}{Xd' + Xe} \quad \text{- - - - - - - - - - - - (2.1)}$$

Also

$$P = E_b I \cos \phi \quad \text{- (2.2)}$$

but

$$I \cos \phi = \frac{E_1 \cos(\delta_{1b} - 90^\circ)}{Xd' + Xe} - \frac{E_b \cos(-90^\circ)}{Xd' + Xe}$$

$$= \frac{E_1 \sin \delta_{1b}}{Xd' + Xe} \quad \text{- - - - - - - - - - - - - - - - (2.3)}$$

Therefore

$$P = \frac{E_b E_1 \sin \delta_{1b}}{Xd' + Xe} \quad \text{- - - - - - - - - - - - - - - - - - (2.4)}$$

where P is the power transferred in watts (the above equation neglects resistance which would modify the above relation in that the maximum power transferred would be reduced). Eq'n. (2.4) is shown graphically in Fig. 2.2 and is commonly termed as the power angle diagram. From the equation the maximum theoretical power that can be transferred is

$$P_{max} = \frac{E_b E_1}{Xd' + Xe} \quad \text{- - - - - - - - - - - - - - - - - - - (2.5)}$$

Having shown the relationship between power and angle it is now possible to relate this to the concept of stability. Stability, according to the American Standards Association, is that attribute of the power system which enables it to develop restoring forces between the elements thereof equal to or greater than the disturbing forces. Concurrently,

the stability limit is the maximum power flow possible through some point in the system when the entire system or that part of the system to which the stability limit refers is operating with stability. To inter-

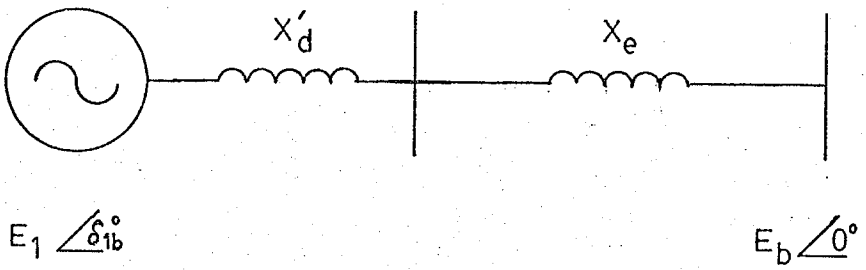

Fig. 2.1(a) Machine infinite bus single line diagram

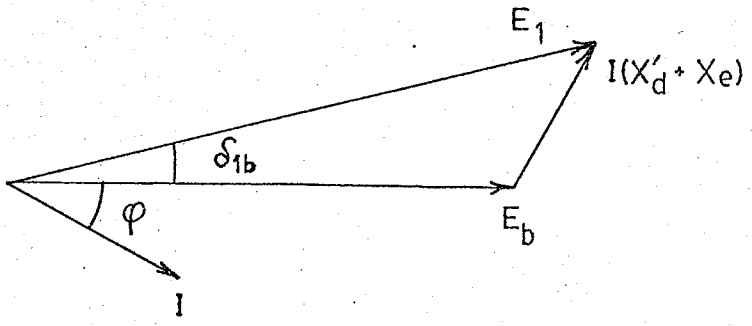

Fig. 2.1(b) Machine infinite bus vector diagram

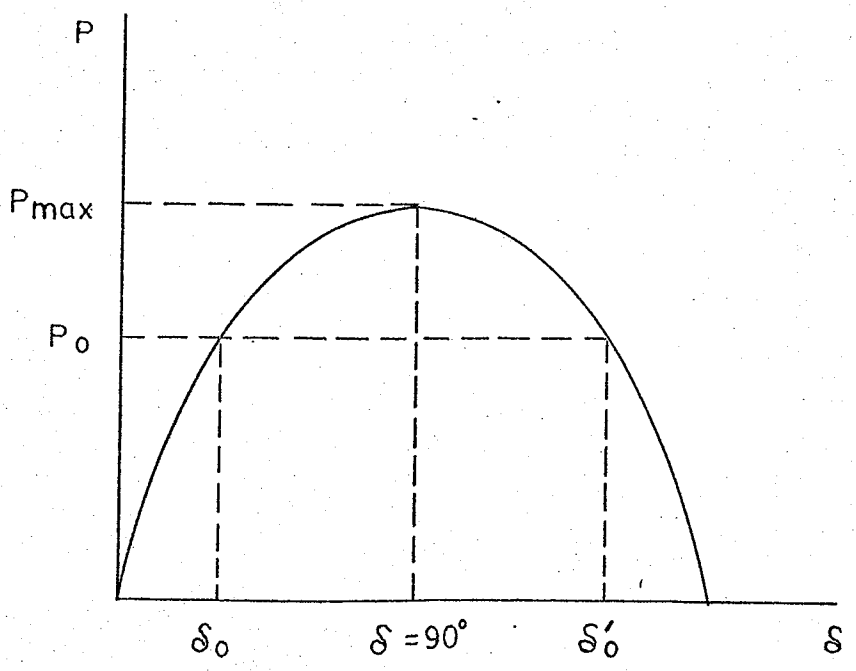

Fig. 2.2 Power-Angle diagram

pret the above in terms of the power angle diagram we can select an operating point P_0 on the curve corresponding to an angle δ_0. If we assume that the input torque is constant then a small disturbance causing a slight reduction in δ will also mean that the power transmitted is reduced. Assuming no losses, it can be seen that the input power exceeds the power transmitted thus causing the generator rotor to accelerate which tends to increase the angle δ. This causes the generator output to shift back towards P_0 and ultimately to a new point above P_0 as determined by system damping. At this point the input power is now less than the power transmitted and thus the generator rotor will decelerate causing δ to decrease. The system therefore moves back towards the original operating point at P_0. When system damping is not negligible the oscillations will eventually die out (the settling time is dependent on the amount of damping the system exhibits) and stability will be maintained. For any operating point corresponding to $\delta \geq 90^{\circ}$ it can easily be seen that the forces present will tend to move the system away from these points resulting in instability.

The above discussion can be used to determine the critical point in system oscillations. If we recall Fig. 2.2, it can be seen that the critical point corresponds to the angle δ_0' for a given internal voltage, reactance and power flow condition. For a system operating with stability at δ_0 it can theoretically stand disturbances which cause the angle to swing about δ_0 and up to δ_0' without losing synchronism. If the angle swings beyond δ_0' the previous discussion has shown the forces within the system will cause the angle to increase even further resulting in instability.

Having gained some insight into the mechanism associated with stability we can now discuss some of the terms frequently used. The steady-state stability limit for the system under consideration can be theoretically expressed by eq'n (2.5). This gives the maximum power which can be transmitted with stability and corresponds to an angle δ of 90^{o}.

Dynamic stability relates to the conditions associated with the system for a particular operating point when forces are set up to return the system to the original operating condition in the face of small disturbances such as speed deviations during normal operation. A system is dynamically unstable if these disturbances increase in magnitude with time.

Transient stability refers to the system's ability to maintain synchronism when subjected to major disturbances such as load increases, switching operations and faults with subsequent circuit isolations. These disturbances alter the system configuration and thus it is required that the new system be stable at its new operating point when subjected to these transient disturbances. Usually a system will lose synchronism after a disturbance because of the relatively large speed deviations, rotor angle differences and power shifts which are initiated. Analysis of the effects resulting from transient disturbances can be determined using the power-angle diagram [2].

2. The Heffron - Phillips Model

a) Description and Analysis

Using the single machine infinite bus situation a great deal of

work has been done on the stability of synchronous machines subjected to small perturbations. To facilitate these studies a linearized small perturbation model was developed by Heffron and Phillips [1]. The block diagram of the model is shown in Fig. 2.3. In total, one can observe the presence of six constants (k_1-k_6) which are usually referred to as the Heffron - Phillips constants. Each of these constants is dependent to a greater or lesser extent on the operating conditions. Calculation of these constants is involved but is required in order that the model represent the specific operating condition under consideration. For a detailed description of the equations refer to Appendix A. Once the model parameters have been determined one can study the effect that small distrubances can have on any of the pertinent operating variables within the system. These studies are usually carried out with the aid of an analog computer. It is to be noted that this model includes the weak interaction present between the real power and angle loop and that of the reactive power and voltage loop through the interacting coefficients k_2, k_4 and k_5.

Through the analysis of the model one can identify the parameters which affect the different aspects of the system's performance. Because this model is based on small perturbations of the operating variables one can set any variable to zero if it is assumed to be constant. In this way certain sections of the model can be isolated.

Examining the performance of the system, assuming constant d-axis flux linkages, leads one to the reduced block diagram of Fig. 2.4. It can be seen that this diagram forms a torque - speed - angle loop. Resolving this system into its characteristic equation will indicate that

the response is that of a damped oscillation with a frequency of $\omega_n \sqrt{1 - \zeta^2}$ and a damping ratio ζ where

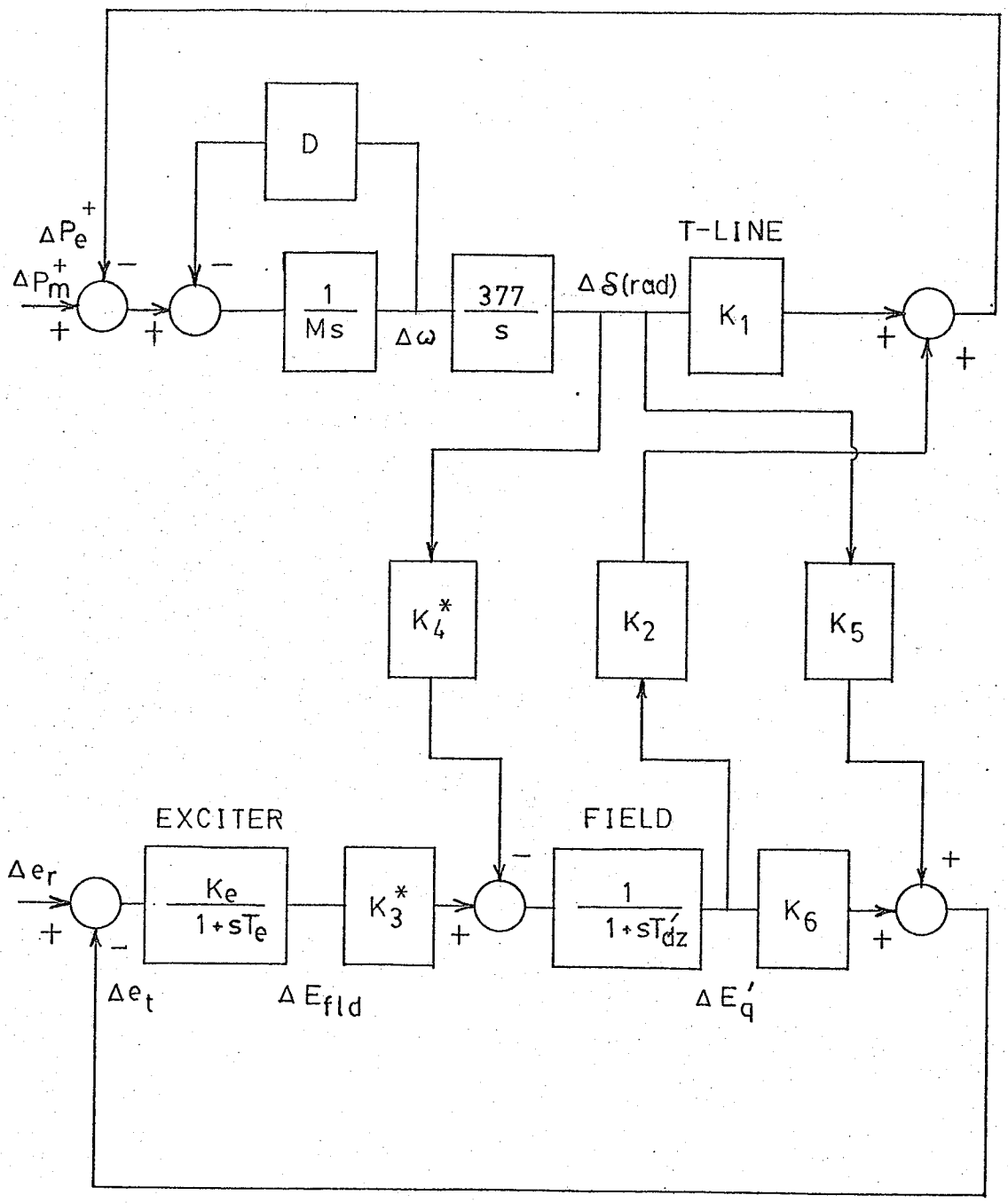

Fig. 2.3 Heffron - Phillips model of a synchronous machine infinite bus system.

* See Appendix A for alternative definition of k_3 and k_4.

+ $\Delta P = \Delta T$ since per unit values are being used.

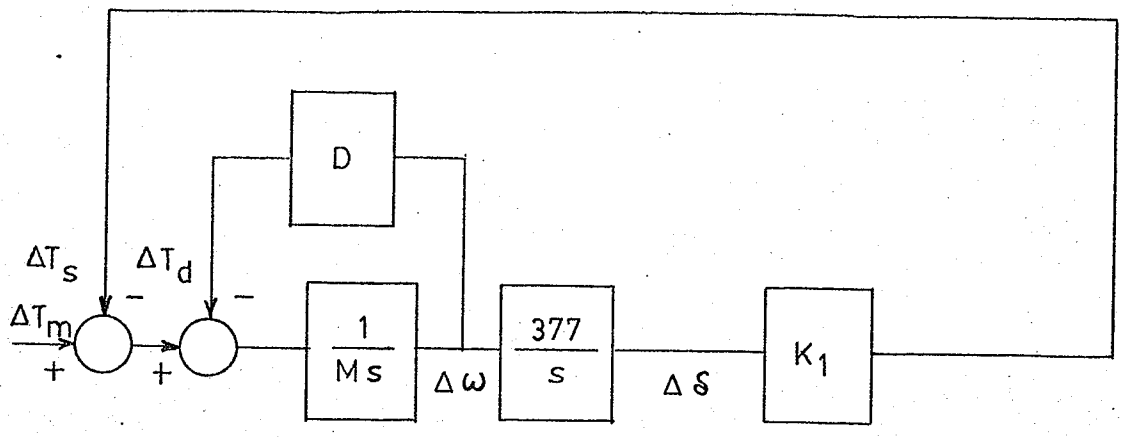

Fig. 2.4 Torque - speed - angle loop

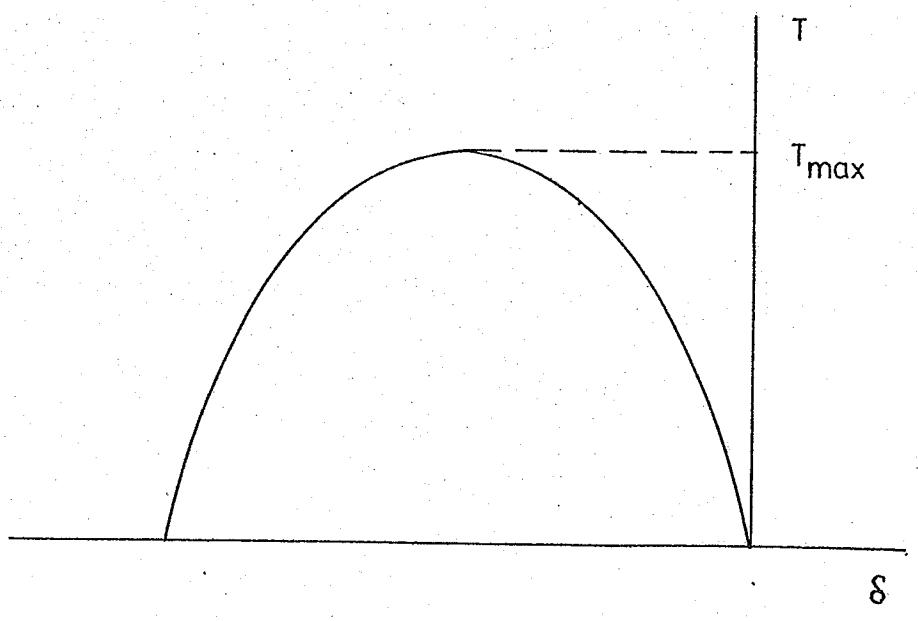

Fig. 2.5 Torque - angle diagram

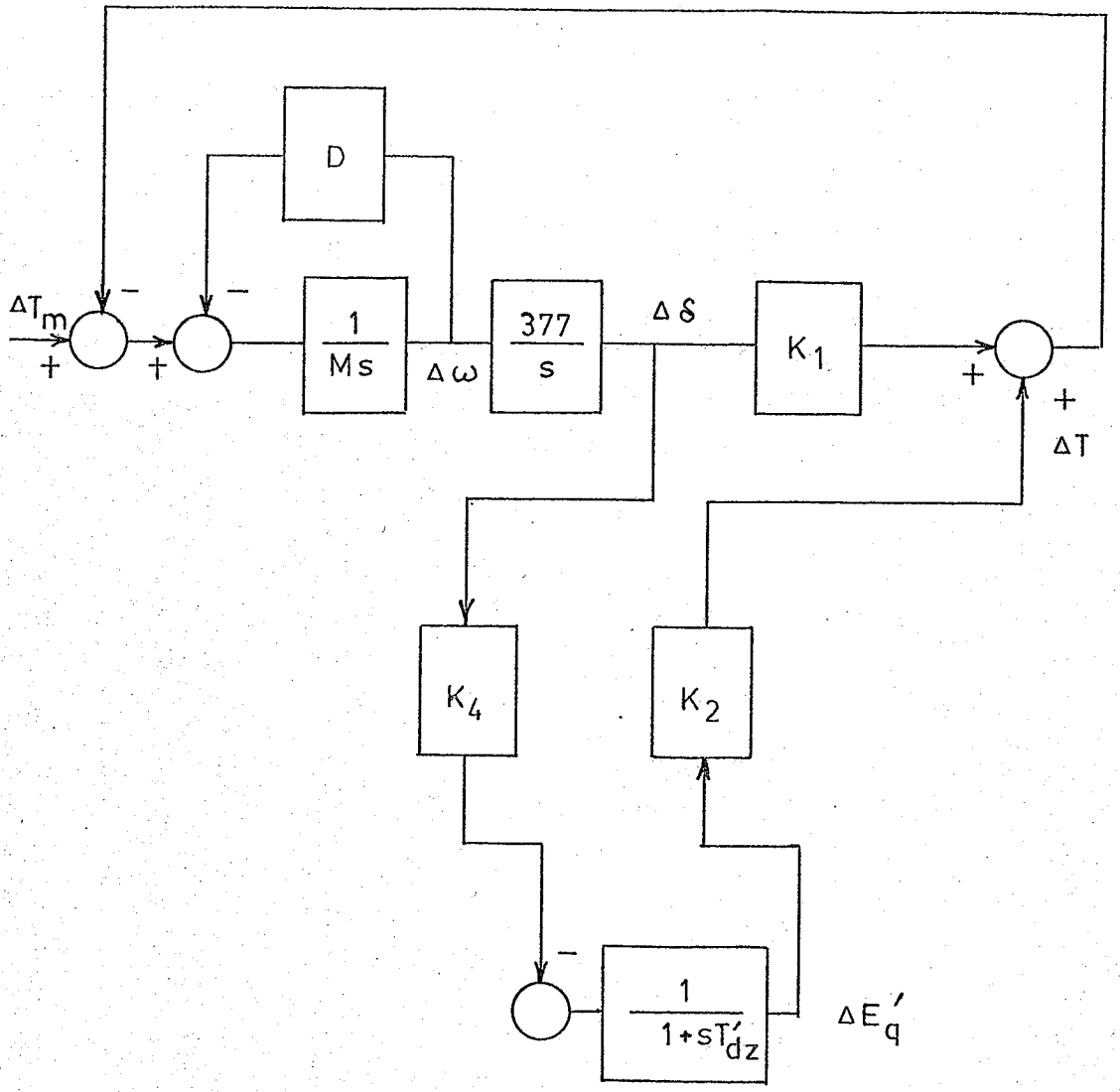

Fig. 2.6 Torque - speed - angle loop including effect of field losses.

$$\omega_n = \sqrt{\frac{K_1 377}{M}} \qquad \text{- (2.6)}$$

and

$$\zeta = \tfrac{1}{2}D/\sqrt{K_1 377M} \qquad \text{- (2.7)}$$

Damping is provided by a component of torque which is proportional to speed. As damping goes to zero the frequency of oscillation approaches ω_n. Observing that ω_n is proportional to K_1 and inversely proportional to M, it can be seen that light inertia systems (small M) and high transient power coefficients K_1, will produce high oscillation frequencies. Looking at the equation for K_1 (Appendix A) it is easy to observe that systems with high machine and external impedances cause K_1 to take on lower values. This corresponds to the observed phenomena that systems with long transmission lines are prone to low oscillation frequencies. In most situations of practical interest K_1 is positive. Using the normal range of values for damping, inertia and loading, the oscillation frequencies observed will take on values from about .5Hz to 2Hz.

Synchronous machine theory will indicate that there are two components of torque created by the machine windings. For any frequency of oscillation braking torques are developed which are either in phase with rotor speed or rotor angle. That component of torque which is in phase with rotor speed is termed as damping torque. Negative damping torques will lead to situations of instability. That component of torque which is in phase with rotor angle is termed as synchronizing torque. Positive synchronizing torques are required for the desired restoring forces to be set sup. Further insight into the torques arising from the

operation of synchronous machines can be obtained by examining the differential equation describing its dynamic behavior [6]. The equation is as follows:

$$J \frac{d\nu}{dt} = T_{shaft} + T \quad \text{- - - - - - - - - - - - - - - - - (2.8)}$$

where J is the moment of inertia, T_{shaft} is the torque applied to the rotor shaft and T is the torque produced by the machine windings. Both torques are measured in the direction of positive speed ν.

To maintain synchronism the above equation indicates that the instantaneous speed of the rotor cannot vary appreciably. Since speed is proportional to the derivative of rotor angle δ we can write

$$K \frac{d^2\delta}{dt^2} = T_{shaft} + T \quad \text{- - - - - - - - - - - - - - - - - (2.9)}$$

where K is a proportionality constant. Now, the accelerating torque corresponding to a disturbance on the system is expressed as $T_{shaft} + T$, where T is either negative or zero. It is intuitively obvious that T must be negative since the accelerating torque cannot be greater than T_{shaft}. From analysis [6] it has been shown that the machine torque is related to the rotor angle δ in the same way that electrical power is related to rotor angle (Fig. 2.2) except for the sign change. The diagram showing the torque angle relation is found in Fig. 2.5 and the associated equation is

$$T = -T_s \sin \delta \quad \text{- (2.10)}$$

Substituing this into eq'n 2.9 produces:

$$k \frac{d^2\delta}{dt^2} = T_{shaft} - T_s \sin \delta \quad \text{- - - - - - - - - - - - - (2.11)}$$

The solution to this equation for δ in response to a small change in shaft torque will result in a response possessing an undamped oscillation. In real situations the oscillation eventually dies away due to a damping action arising from mechanical losses and from a speed dependent torque in the load. In addition a damping action is created as a result of currents that are induced in the short circuited rotor damper windings when speed varies from its synchronous value. This component can be expressed as

$$T = -T_D' \nu = -T_D \frac{d\delta}{dt} \quad \text{- - - - - - - - - - - - - - - - (2.12)}$$

where the proportionality constants between ν and δ have been incorperated in T_D. If this is added to eq'n (2.11) we have:

$$k \frac{d^2\delta}{dt^2} + T_D \frac{d\delta}{dt} = T_{shaft} - T_s \sin \delta \quad \text{- - - - - - - (2.13)}$$

In conclusion, it is evident that the torques created by the machine windings are composed of a component in phase with rotor angle (synchronizing torque) and a component in phase with rotor speed (damping torque).

To further examine the Heffron-Phillips model we look at the performance of the system when field voltage is assumed to be constant. The reduced block diagram for this case is shown in Fig. 2.6. The relationship, between the component of torque and angle is given by

$$\frac{\Delta T}{\Delta \delta} = \frac{-k_2 k_4}{1+ST'_{dz}} \qquad \text{- (2.14)}$$

The component of torque is proportional to angle in the steady state and is equal to $-k_2 k_4 \Delta\delta$. This becomes part of the synchronizing torque with the overall steady state value being equal to $k_1 - k_2 k_4$. Therefore, stability can only be maintained as long as the term $k_1 - k_2 k_4$ is greater than zero. When the oscillation frequency gets large ($\omega >> \frac{1}{T'_{dz}}$) the phase angle of this relation becomes almost equal to positive 90^o which puts the component of torque in phase with machine rotor speed. The torque is therefore almost entirely a damping torque. However, because of the large frequencies involved, the magnitude of this torque component becomes small and thus the field contribution to damping is only minor.

Finally to complete this discussion, one must examine the effects on stability resulting from the voltage regulator loop. The pertinent section of the model is shown in Fig. 2.7. The voltage regulator excitation system has the standard form typical of thyristor type exciters. The form as indicated in the diagram is:

$$\frac{\Delta E_{fld}}{\Delta e_t} = -\frac{k_e}{1+ST_e} \qquad \text{- (2.15)}$$

where k_e is the exciter gain and T_e is its time constant which for this class of excitation system is quite small.

Dealing first with the component of torque produced by the k_4 branch we see that the regulator loop will modify the expression relating

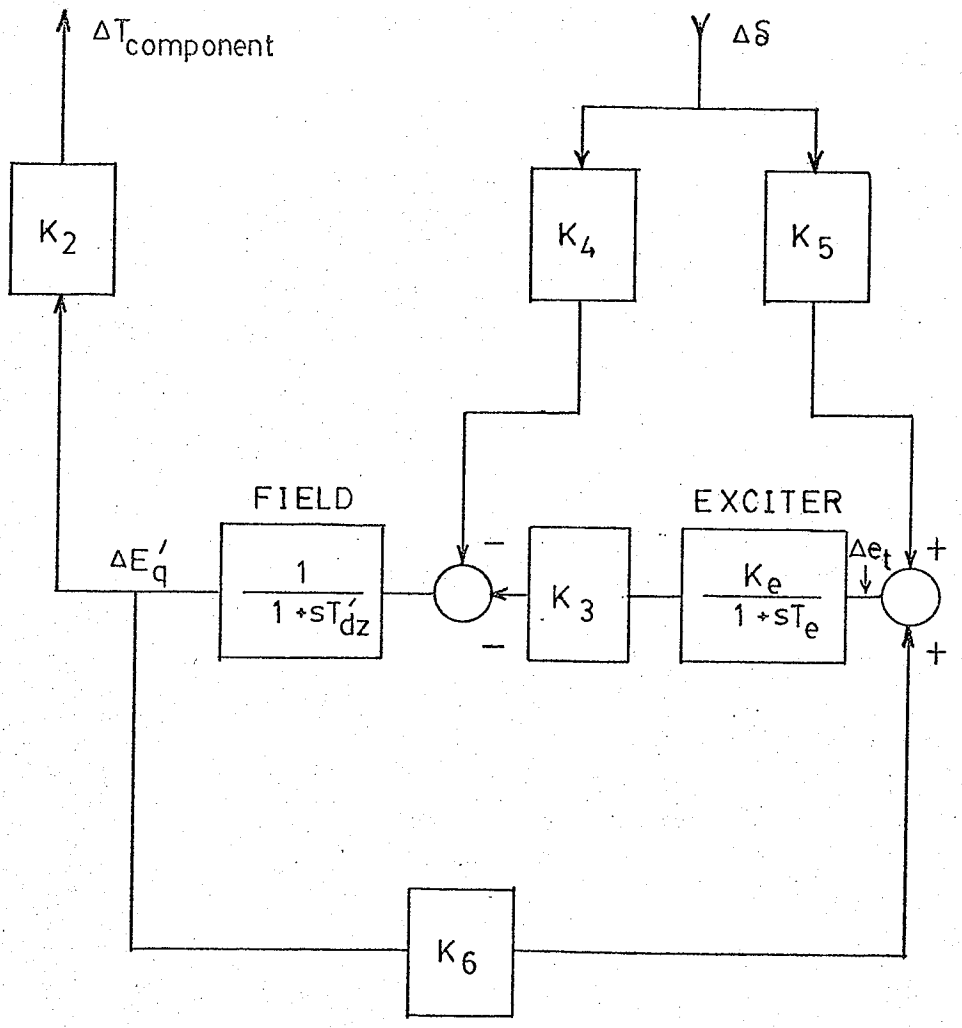

Fig. 2.7 Torque component as a direct result of angle deviations acting on the voltage regulator loop.

torque to angle into the following form.

$$\frac{\Delta T}{\Delta \delta} = \frac{-k_2 k_4 (1+ST_e)}{(1+ST_e)(1+ST'_{dz}) + K_e k_3 k_6} \qquad \text{- - - - - - - - - - (2.16)}$$

Assuming that $1+ST_e$ is approximately equal to one (T_e is normally very small) and that k_e is large, we can approximate eq'n (2.16) with:

$$\frac{\Delta T}{\Delta \delta} \simeq \frac{-k_2 k_4}{k_e k_3 k_6 [1+S\ T'_{do}/k_e k_6]} \qquad \text{- - - - - - - - - - - - - - (2.17)}$$

At low frequencies the magnitude of eq'n (2.17) is much smaller than that of eq'n (2.14) and at high frequencies they approach each other. As a result the net synchronizing component of torque now becomes $k_1 - \frac{k_2 k_4}{k_e k_3 k_6}$ in the steady state and it can be realized that for fairly high exciter gains the negative component is negligible with the obvious implication of improved stability. At the same time the field time constant has been reduced from T'_{dz} to $T'_{do}/k_e k_6$. This creates the effect of a reduced damping component of torque since the phase angle of eq'n (2.17) will approach 90^o at much higher oscillation frequencies. The net effect on both synchronizing and damping torques as a result of the voltage regulator loop through branch k_4 can therefore be assumed to be negligible.

Turning our attention to the k_5 branch leads to the following expression.

$$\frac{\Delta T}{\Delta \delta} = \frac{-k_2 k_5 k_e}{1/k_3 + k_6 k_e + S(\frac{Te}{k_3} + T'_{do}) + S^2 T_e T'_{do}} \qquad \text{- - - - - - - (2.18)}$$

Assuming k_3 to be approximately equal to 1 gives

$$\frac{\Delta T}{\Delta \delta} \simeq \frac{-k_2 k_5}{\frac{T'_{do}}{k_6(1+S\frac{T'_{do}}{k_6 k_e})(1+ST_e)}} \qquad \text{- - - - - - - - - - - - - - (2.19)}$$

If we set $s = j\omega$ the above expression will have the form

$$\frac{\Delta T}{\Delta \delta} = a + jb \qquad \text{- (2.20)}$$

where the real part will correspond to the synchronizing component of torque and the imaginary part to the damping component. The synchronizing component is therefore:

$$\Delta T_s = \frac{-k_e k_2 k_5 (k_e k_6 - \omega^2 T_e T'_{do})}{(k_e k_6 - \omega^2 T_e T'_{do})^2 + \omega^2 (T_e k_e k_6 + T'_{do})^2} \Delta\delta \qquad \text{- - - - (2.21)}$$

If we narrow our concern to frequencies at around 1 Hz and assuming the normal range of parameter values the above can be approximated as:

$$\Delta T_s \simeq \frac{-k_e k_2 k_5}{k_e k_6 - \omega^2 T_e T'_{do}} \Delta\delta \qquad \text{- - - - - - - - - - - - - (2.22)}$$

For low frequencies one can further simplify to obtain

$$\Delta T_s \simeq -\frac{k_2 k_5}{k_6} \Delta\delta \qquad \text{- - - - - - - - - - - - - - - - - (2.23)}$$

and thus the net synchronizing component becomes

$$\Delta T_s = (k_1 - \frac{k_2 k_5}{k_6}) \Delta\delta \qquad \text{- - - - - - - - - - - - - - - - - (2.24)}$$

When k_5 is positive (low to medium external impedance and loading) k_1 is usually quite high so that the net synchronizing component is positive and stability is maintained. When k_5 is negative (moderate to high external impedance and heavy loading) k_1 will usually assume a lower value. The net synchronizing component remains positive.

As the frequency increases the torque component of eq'n (2.22) would get extremely large but, before this effect can make a major contribution to system performance, instability will have developed due to negative damping.

Returning to eq'n (2.19), the damping torque component becomes

$$\Delta T_D = \frac{k_e k_2 k_5 (T_e k_e k_6 + T'_{do})\,\omega}{(k_e k_6 - \omega^2 T_e T'_{do})^2 + \omega^2 (T_e k_e k_6 + T'_{do})}\,\Delta\delta \quad - - - \quad (2.25)$$

The term k_5 will determine whether the above contributes positive damping or negative damping. Most stability problems arise when k_5 is negative. In addition, with k_5 negative, a large value for k_e will enhance negative damping. Conversely if k_e is zero, which correponds to the case where $\Delta Efld$ was assumed to be zero, only a small amount of field damping will be present.

As a result of this development it can be seen that, when k_5 is negative, a voltage regulator will enhance a machine's ability to provide synchronizing torque but, at the same time, it will destroy the natural damping of the machine. It is thus common to observe the case where the addition of a voltage regulator has provided stability to a machine but, that its operation has become extremely oscillatory. For the situation where a long transmission line is present a high regulator gain is most

desirable. Therefore, one way of solving the damping problem has involved the use of an auxilliary stabilizing signal derived from machine speed, frequency or power.

b) System Transfer Function

For the purposes of this investigation the Heffron-Phillips model will be used to analyze the behaviour of the model power system to be described in a subsequent section. As mentioned earlier the feedback signal to be used in this work is terminal frequency. To study the effects of using a signal other than the above would require the appropriate modification of the transfer function.

To begin, the input and output variables of the system without compensation must be established. Referring to Fig. 2.8(a), we define the transfer function as

$$\frac{\Delta\omega}{\Delta e_r} = G(s) \qquad \text{- (2.26)}$$

where the output variable is frequency variation and the input variable corresponds to the change in reference voltage caused by the stabilizer feedback signal. The standard method of determining G(s) when the system being considered is of a complicated nature, consists of Mason's Loop Rule [7]. The formula used is as follows:

$$G(s) = \frac{\Sigma_k P_k \Delta_k}{\Delta} \qquad \text{- (2.27)}$$

where:

P_k = the k_{th} path from the input variable to the output variable

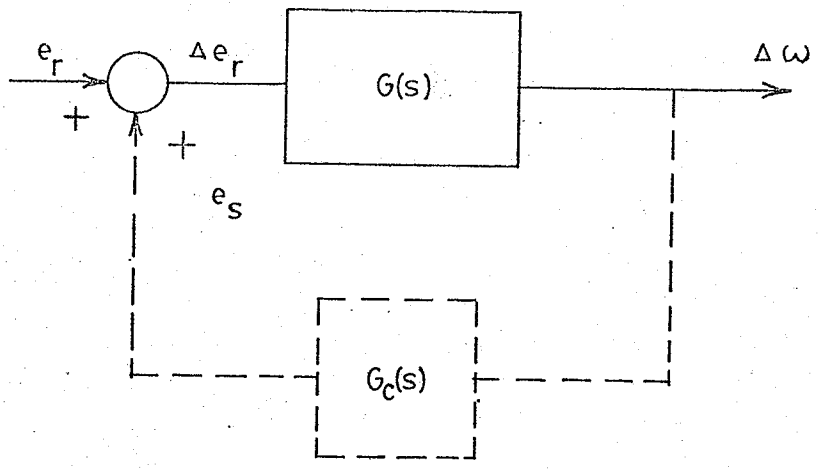

Fig. 2.8(a) Block diagram of system defining the input and output variables and the feedback loop.

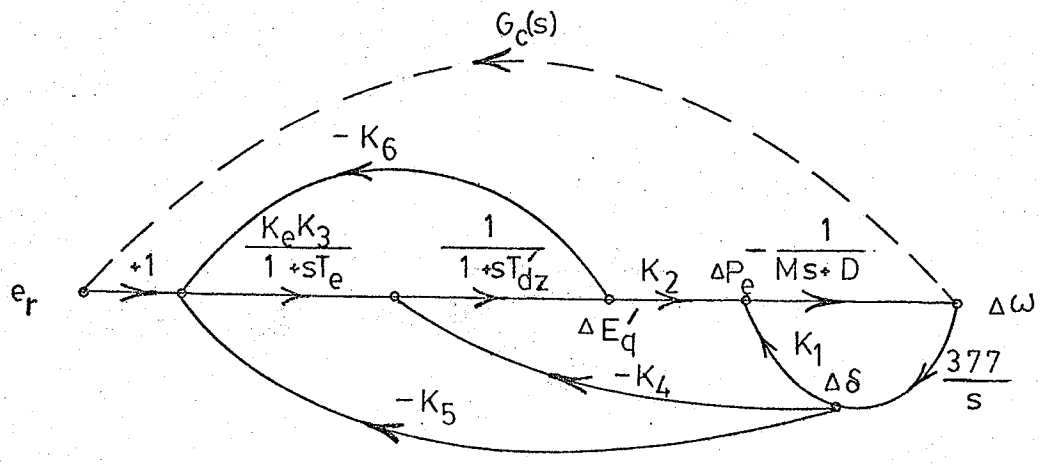

Fig. 2.8(b) Signal flow graph of Heffron Phillips model

Δ = the determinant of the graph

Δ_k = the cofactor for the path P_k

The summation is taken over all possible forward paths from the input to the output. The signal flow graph for the system is found in Fig. 2.8(b)

There is only one feedforward path as is described by:

$$P_1 = \frac{-k_e k_2 k_3}{(Ms+D)(1+sT_e)(1+sT'_{dz})} \qquad \text{- - - - - - - - - - - - (2.28)}$$

Evaluating the determinant of the graph leads to:

$$\Delta = 1 + \frac{377k_1}{S(Ms+D)} - \frac{377\ k_2k_4}{S(Ms+D)(1+ST'_{dz})} - \frac{377k_ek_2k_3k_5}{S(Ms+D)(1+ST_e)(1+ST'_{dz})}$$

$$+ \frac{k_ek_3k_6}{(1+sT_e)(1+sT'_{dz})} + \frac{377\ k_1k_ek_3k_6}{S(Ms+D)(1+sT_e)(1+sT'_{dz})} \qquad (2.29)$$

The cofactor for the forward path is:

$$\Delta_1 = 1 \qquad \text{- (2.30)}$$

Collecting eq'n (2.28), (2.29) and (2.30) and utilizing eq'n (2.27) gives the following result after appropriate manipulation.

$$\frac{\Delta\omega}{\Delta e_r} = \frac{-k_ek_2k_3\ S}{\{[MT_eT'_{dz}]S^4 + [M(T_e+T'_{dz})+DT_eT'_{dz}]S^3 + [M(1+k_ek_3k_6)+D(T_e+T'_{dz})+}$$

$$377k_1T_eT'_{dz}]S^2 + [D(1+k_ek_3k_6)+377\{k_1(T_e+T'_{dz})-k_2k_4T_e\}]S +$$

$$[337\ \{k_1(1+k_ek_3k_6)-k_ek_2k_3k_5-k_2k_4\}]\ \} \qquad (2.31)$$

Eq'n (2.31) is the transfer function of the uncompensated system. The characteristic equation from above corresponds to a fourth order polynomial. Using this polynomial the eigenvalues of the system can be determined for a particular operating condition and the performance can be evaluated using S-plane techniques.

3. Real Synchronous Machine Infinite Bus Model Power System

To better observe the effect on performance that a stabilizing signal might have, the compensator designed by analytic means was implemented on a physical model power system. However, before proceeding to this step it was required to identify the system by determining the pertinent parameters and also to ensure that the behaviour of the physical model was suitably close to that of an actual remote generator.

a) Description

The physical model power system is shown, as it appears in the laboratory in the photograph of Fig. 2.9. A pictorial block diagram of the model appears in Fig. 2.10.

The prime mover for the generator is simulated with a $\frac{1}{4}$ HP,1800 RPM, 120 V, 2.8A direct current machine. A large flywheel has been fixed to its shaft to impart an inertia to the model which is comparable to that of a real system. Torque transfer is accomplished with a toothed belt and pulleys so as to avoid slippage. The generator is represented by a 120 VA, 1800 RPM, 208 V,.33A, 60 Hz, 3ϕ synchronous machine. The terminals of the synchronous machine are connected to a 3ϕ transmission line simulator. This consists of a 3ϕ set of series inductors. Taps on the coils allow the variation of the equivalent transmission line

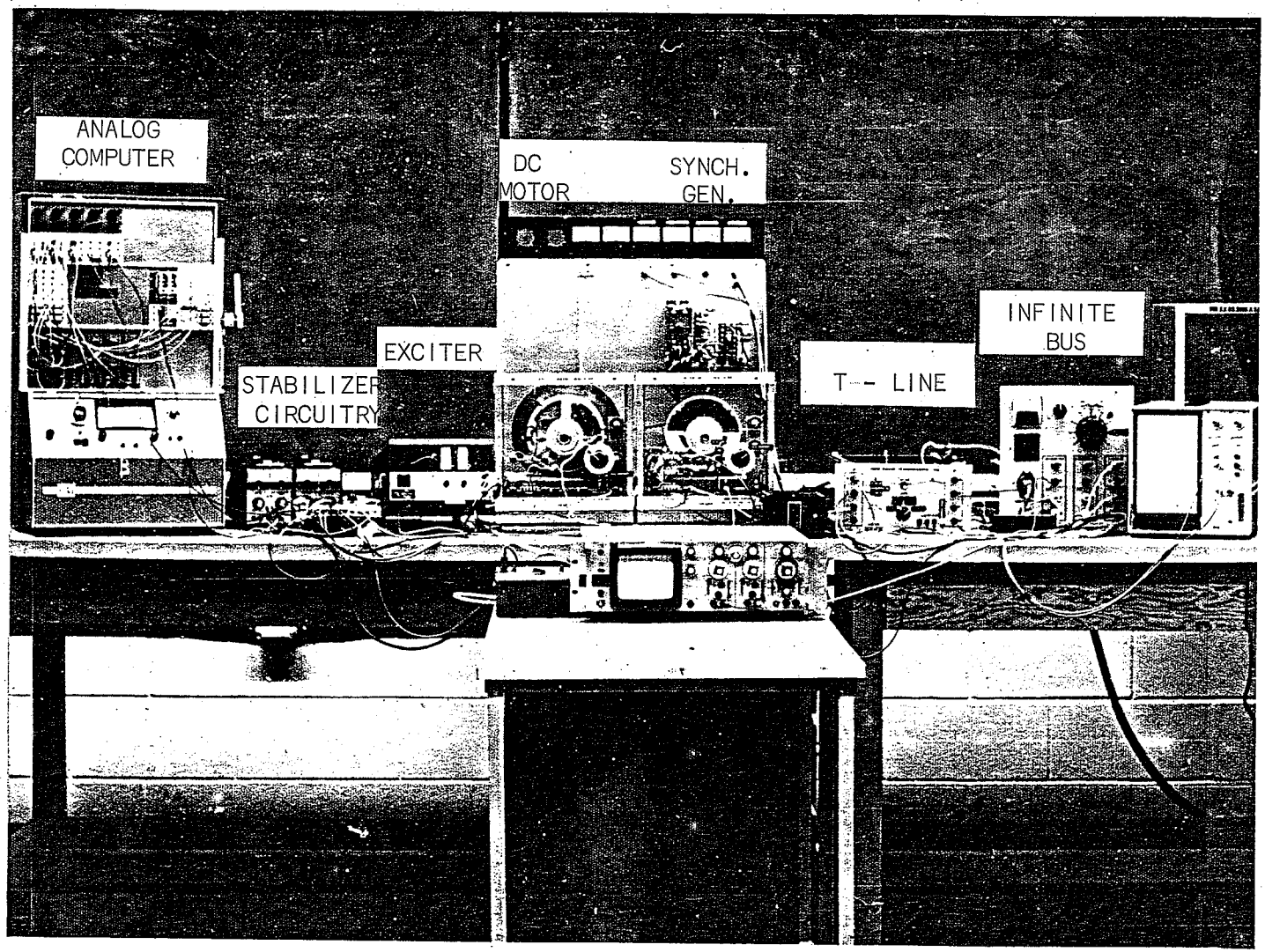

Fig. 2.9 Basic Instrumented Controllable Electric Power System - "BICEPS"

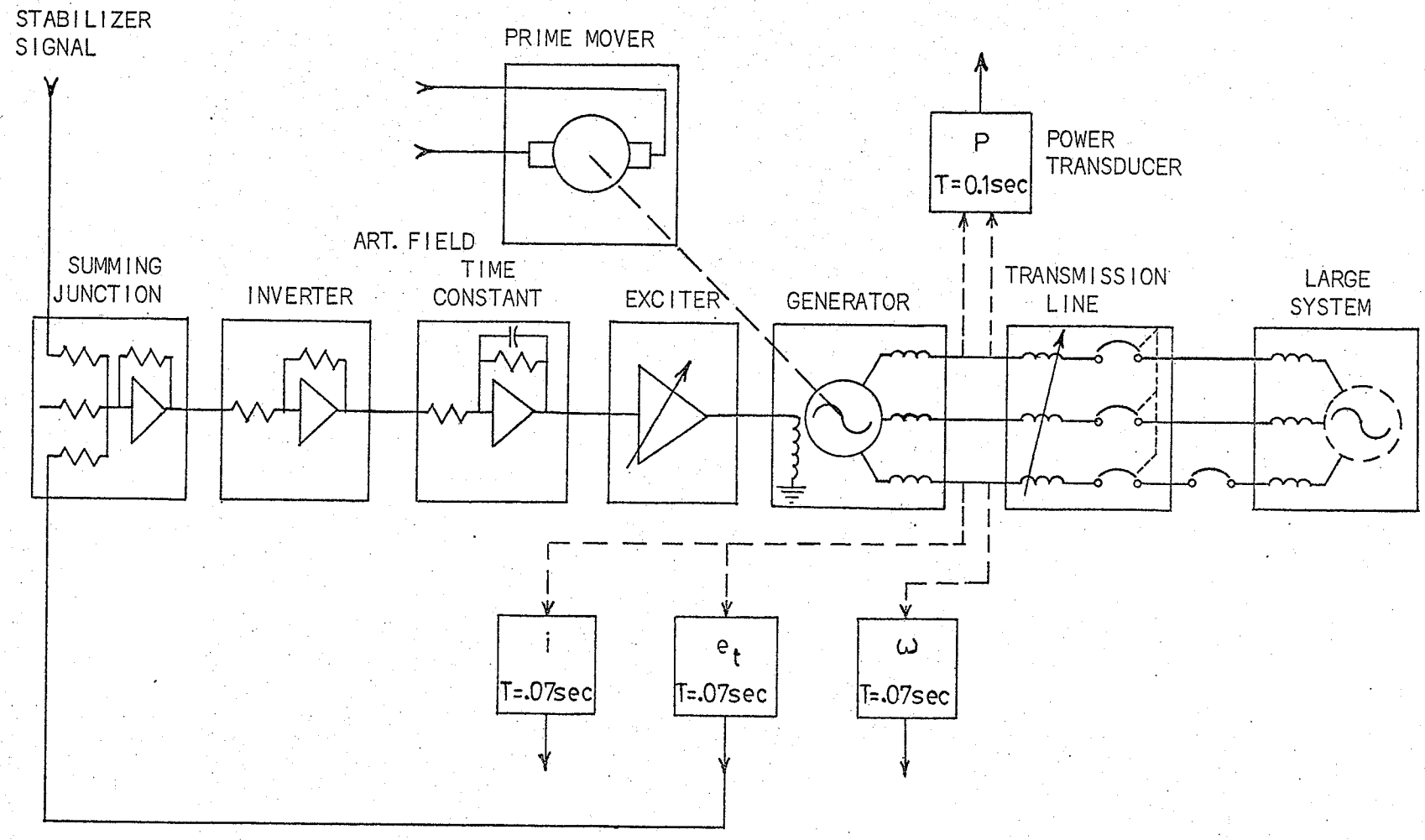

Fig. 2.10 Model power system pictorial block diagram

impedance via a front mounted rotary switch. A front mounted 3ϕ switch serves as a circuit breaker to separate the generator and transmission line from the infinite bus. In addition, a single phase switch is provided to simulate single pole switching. Finally, the generator and transmission line is terminated in a 3ϕ, 4 wire supply (laboratory a.c. power supply) which represents the infinite bus.

The system is equiped with a power transducer (Watts), a voltage and current transducer and a frequency transducer. The outputs from these transducers are permanently connected to panel mounted meters that indicate the magnitude of each variable continuously.

The power transducer is a Hall - effect power computing device designed to provide an isolated low ripple d.c. output current that is accurately proportional to a.c. input power. The time constant of the transducer is about 0.1 seconds.

The voltage and current transducers are average responding rectifying devices. They utilize full wave rectification to provide an isolated low ripple d.c. output that is proportional to voltage and current. Both of these units possess a time constant of approximately 0.07 seconds.

The frequency transducer is a suppressed zero type utilizing a monostable multivibrator to convert the frequency deviation of an input signal into a proportional d.c. output. An input signal of 60 H_z produces zero output while signals above or below that frequency produce a proportional positive or negative d.c. output. Its time constant is approximately equal to 0.07 seconds.

The excitation loop as shown in Fig. 2.10 takes a current signal proportional to the terminal voltage and converts it to a proportional d.c. voltage using a resistance network. This voltage is then applied to an operational amplifier adder circuit where it is subtracted from the reference voltage. The resulting signal is the applied to a low pass filter which is referred to as the artificial field time constant. Its purpose is to modify the time constant of the machine response so that it more closely represents that of the real system. Because the synchronous machine used is very small, its actual field time constant is quite short. To increase this time constant the accepted procedure has been to connect a negative resistance to cancel part of the field resistance and thus alter the generator's field time constant to a more desirable value. The implementation of a negative resistance is a very difficult task and therefore, to avoid this complication and yet obtain reasonable results, it was decided to alter the time constant of the exciter. The exciter in this case is a power operational amplifier whose time constant is approximately 0.001 seconds. Since this is extremely fast, the addition of a time constant with a value greater than 1 second will make the previous time constant insignificant. What is now required is the appropriate analysis of the system to allow the selection of the correct value for this time constant. This topic will be discussed in detail in a later section.

The exciter gain can be set by a variable resistance potentiometer which serves as the feedback resistor on the power operational amplifier.

Synchronization is accomplished with a resistance divider network connected to each end of the transmission line and an oscilloscope. A

lissajous figure is displayed on the oscilloscope and when the pattern forms a straight line with a positive 45^{o} slope the transmission line breaker is closed.

Machine loading is accomplished by increasing the variable dc supply voltage to the dc motor which, in turn, causes the synchronous machine angle to lead that of the infinite bus resulting in the transmission of power down the transmission line. The power factor angle can be altered through the adjustment of terminal voltage.

b) Parameter Determination

i) Machine Parameters

In order that the steady state performance of the synchronous machine may be analyzed it is necessary to obtain the parameters of the machine. The parameters of interest include the stator resistance R_s, stator leakage reactance $X_{\ell s}$, d-axis synchronous reactance X_d, d-axis transient reactance X_d', d-axis subtransient reactance X_d'', the q-axis synchronous reactance X_q, q-axis transient reactance X_q', q-axis subtransient reactance X_q'', and the open circuit field time constant T'_{do}. To obtain these parameters a series of tests were performed which included a direct current resistance measurement made at operating temperature, an open circuit test, a short circuit test, a zero power factor test and a 3ϕ short circuit test with the machine unloaded [6,8]. Because of the difficulty of interpretation of the results from the last test mentioned an additional test utilizing frequency response techniques was performed.

The open circuit test is accomplished by running the machine at

synchronous speed with the stator terminals open circuit. The stator terminal voltage is then plotted as a function of field current. The characteristic for the machine under consideration is shown in Fig. 2.11. For a particular value of air gap voltage E_{ms}, the appropriate value of magnetizing reactance is:

$$X_{ms} = \frac{E_{ms}}{n'I_f} \qquad (2.32)$$

where n' is the current ratio between the magnetizing current and the field current.

For the short circuit test the machine was run at synchronous speed and the field current was measured as a function of stator current. The characteristic for this machine is shown in Fig. 2.12. The relation describing this curve is:

$$|I_s| = \frac{X_{ms}}{[R_s^2 + (X_{\ell s}+X_{ms})^2]^{\frac{1}{2}}} \; n'I_f \qquad (2.33)$$

where X_{ms} for this expression corresponds to the unsaturated value of magnitizing reactance (E_{ms} will be quite small for this test). If the effect of R_s is ignored the expression becomes

$$|I_s| = \frac{X_{ms}}{X_{\ell s} + X_{ms}} \; n'I_f \qquad (2.34)$$

Taking the ratio of $|I_s|$ to I_f will give the slope of the curve.

The zero power factor test was performed as follows. A 3ϕ variable inductor (resistance in assumed to negligible) was connected to the stator terminals and its value is varied to keep stator current constant at a preassigned level while the machine is run at synchronous

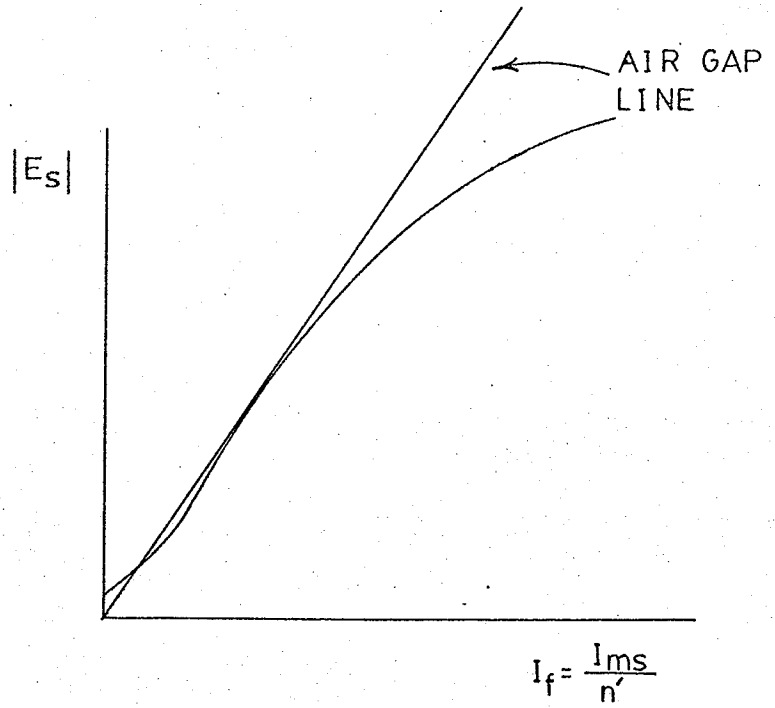

Fig. 2.11 Open circuit magnetization curve for the synchronous generator model.

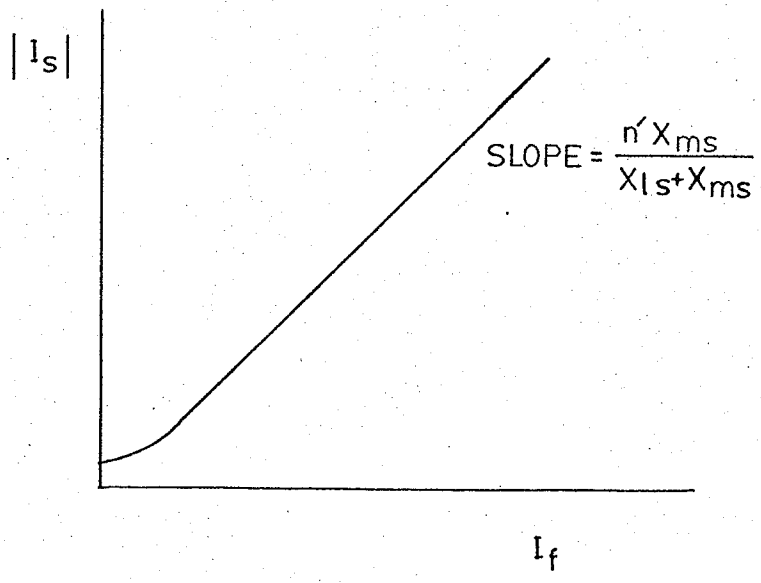

FIG. 2.12 Short circuit curve for synchronous generator model.

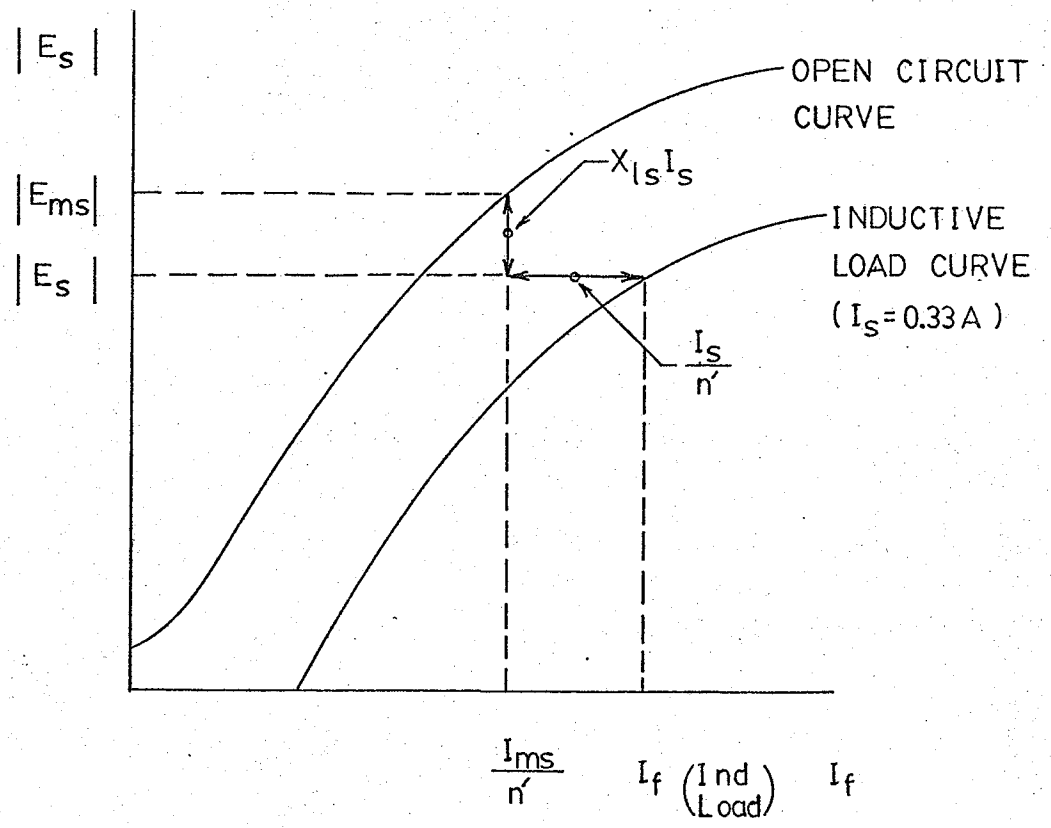

FIG. 2.13 Zero power factor test on synchronous generator model.

speed and the terminal voltage is increased from zero. Terminal voltage as a function of field current was recorded and the resulting characteristic is shown in Fig. 2.13. Analyzing the results leads one to conclude that for a purely inductive load (assume R_s negligible)

$$|E_s|_{\text{(zero P.F. load)}} = |E_{ms}| - |X_{\ell s} I_s| \quad \text{- - - - - - - - -} \quad (2.35)$$

and

$$I_{f\,\text{(zero P.F. load)}} = I_{f\,\text{(open circuit)}} + \left|\frac{I_s}{n'}\right| \quad \text{- - - - -} \quad (2.36)$$

It is thus apparent that one can determine the values for $X_{\ell s}$ and n' by comparing the zero power factor curve with the open circuit curve as shown in Fig. 2.13.

From the above series of tests the following parameter values were determined:

R_s = 11.9 ohms per phase

n' = 2.7

$X_{\ell s}$ = 20 ohms per phase (at 60 H_z)

X_{ms} = 84 ohms per phase (at 60 H_z)

As an additional result from the above measurements one can obtain a value for X_d if the following relation is used:

$$X_d = \frac{I_f \text{ for rated current on short circuit test}}{I_f \text{ for rated voltage on air gap line}} \quad \text{- - -} \quad (2.37)$$

The measured value is approximately 104 ohms per phase which by examination is the same as $X_{\ell s} + X_{ms}$. Converting the above results to per unit on the machine base gives:

$$R_s = 0.03 \text{ pu}$$

$$X_{\ell s} = 0.05 \text{ pu}$$

$$X_{ms} = 0.23 \text{ pu}$$

$$X_d = 0.29 \text{ pu}$$

$$n' = 2.7$$

To obtain values for the remaining reactances and the field time constant it would seem reasonable to attempt a 3ϕ short circuit test. This would involve running the machine at synchronous speed and open circuit with rated terminal volts and suddenly apply a 3ϕ short. The resulting current oscillogram can easily be recorded and the information contained therein should allow the determination of the above parameters after application of established analysis techniques [9]. Although this method is satisfactory in most cases it can prove to be an undesirable approach in instances where the machine is quite large or quite small. Where large machines are concerned the magnitude of the resulting short circuit current as well as the mechanical stresses occurring during such a test could quite probably cause damage to the machine. On the other hand very small machines characteristically have very small time constants and, as a direct consequence of this fact, the short circuit transient will occupy only a very small time interval on the oscillograph. It is therefore easy to realize that meaningful parameter measurements

in this case would be very difficult and the results obtained would be quite subjective. For this particular investigation the latter situation presented itself. Observing the oscillogram obtained from the generator model shown in Fig. 2.14 will confirm the above comments. The only piece of information that could be obtained with certainty from this record is the value for the d - axis synchronous reactance. Measurement showed this value to be 0.29 pu.

Because of this difficulty another technique which could adequately pinpoint the parameter values was required. To fill this need, a method employing frequency response techniques to obtain synchronous machine operational impedances from low voltage measurements at the stator terminals at standstill was attempted [10]. The principle used in this test is the same as that used for the measurement of subtransient reactance by applying a voltage at 60 Hz to the stator terminals. For measurement of the complete characteristic a wider frequency range was used. (0.066 Hz to 100 Hz for this test).

Measurements at the stator terminals will define the following quantity for the d - axis:

$$\frac{V_s}{I_s} = R_s + j\omega L_d(j\omega) \qquad \text{- - - - - - - - - - - - - - - - - -} \quad (2.38)$$

where R_s is the stator resistance and $L_d(j\omega)$ is defined as the operational inductance for the d - axis. $L_d(j\omega)$ may be expressed in henries or in per unit of the inductance corresponding to the impedance base at rated frequency. At low frequencies $L_d(j\omega)$ approaches L_{du} the unsaturated synchronous inductance of the machine.

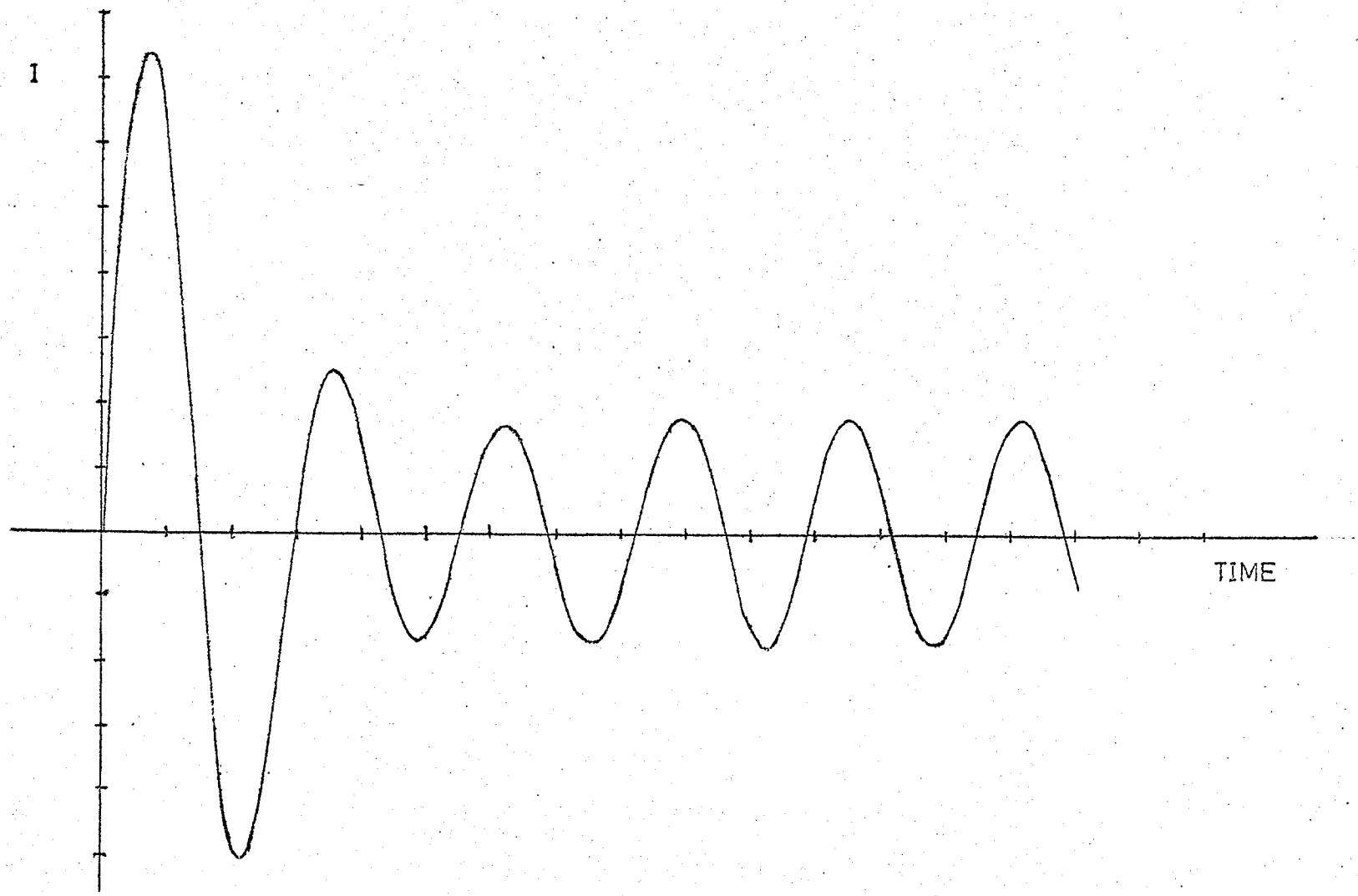

FIG. 2.14 Short circuit current oscillogram

The test arrangement as implemented for d - axis measurements on the synchronous machine is shown in Fig. 2.15. A variable frequency oscillator was connected to the machine terminals via an operational amplifier power supply which served the dual purpose of providing sufficient excitation to the windings in accordance with the oscillator signal and also to isolate the load from the oscillator. The power supply was capable of supplying a 40 volt peak signal. The current level was kept within machine ratings through the use of a noninductive series resistance R_L. The field circuit was left either open circuit or short circuit depending on the test being performed. For the case of a short circuit field a small value resistor was placed across the field terminals in order that the magnitude of the field current could be monitored and thus ensure that it remained within the manufacturers ratings. The voltage across the machine terminals was measured with a differential amplifier equipped oscilloscope while circuit current was obtained by measuring the voltage V_c with an oscilloscope. Because of the fact that the frequency of the voltages varied, the oscilloscope was the only device available that could adequately measure these voltages. Frequency measurement and phase shift was accomplished using an electronic counter Measurement of the time interval between zero crossings of a signal would allow the determination of the frequency of that signal while the phase shift occurring between two different signals could be obtained by measuring the time interval between zero crossings for one signal with respect to the other. To obtain a differential voltage for the electronic counter a differential operational amplifier was constructed. The

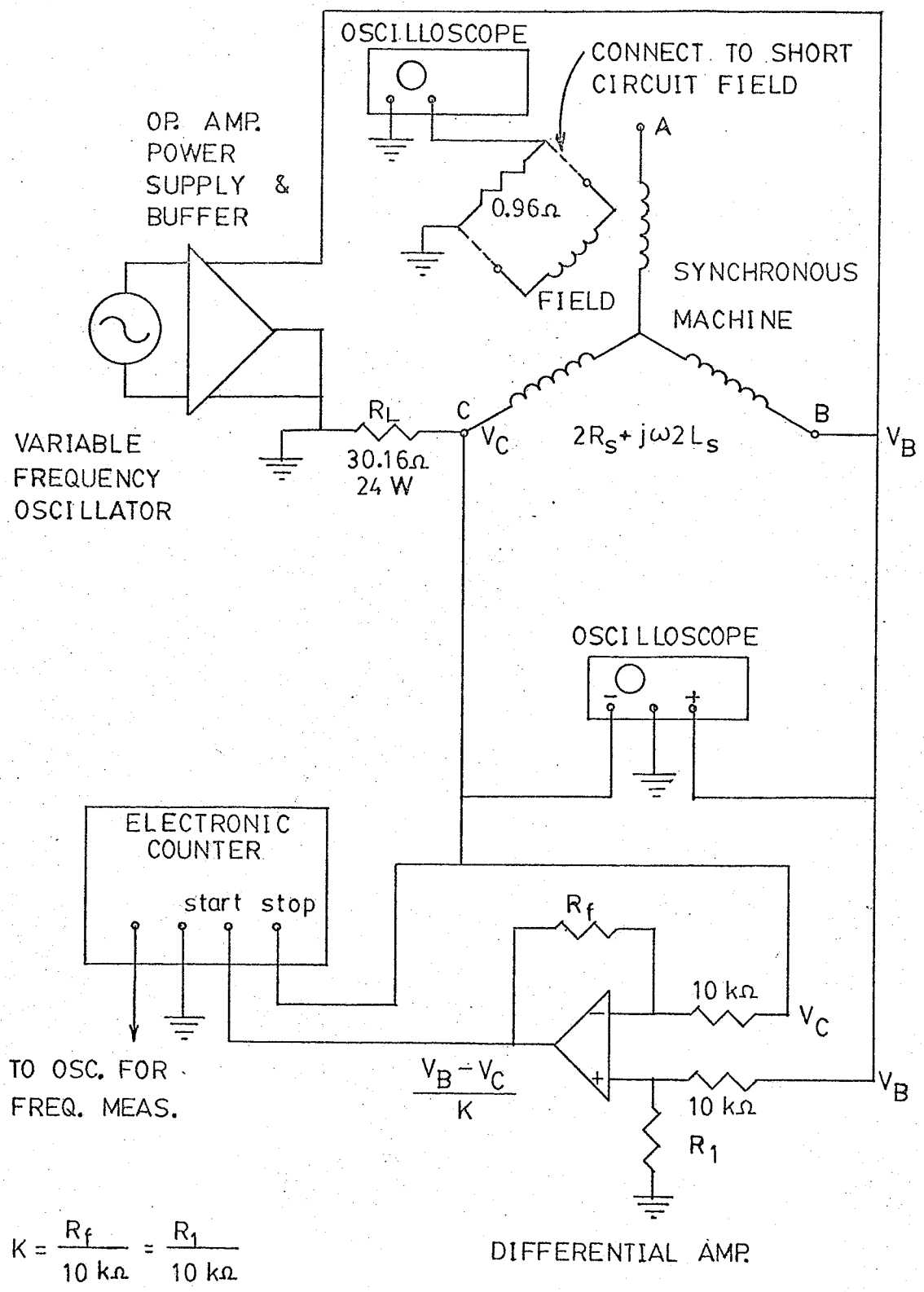

FIG. 2.15 Frequency response test - d-axis measurement circuit.

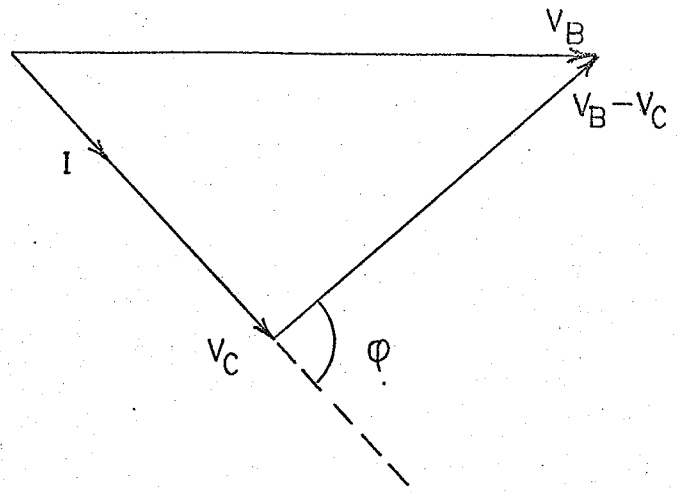

Fig. 2.16 Vector diagram for the frequency response test.

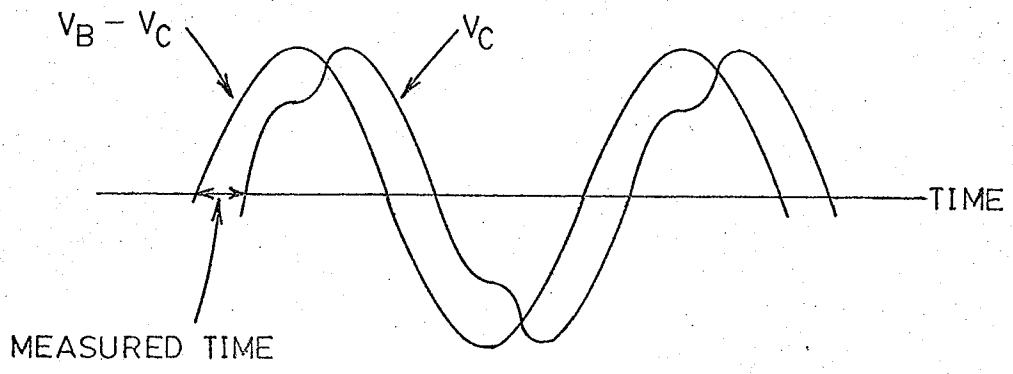

FIG. 2.17 Time interval measurement required to determine phase.

amplifier gain was selected to provide as much voltage as possible to the input of the counter without saturating the amplifier. The operational amplifier circuit was checked to ensure that it did not contribute any phase shift to the input signal and also that the output did not possess any dc offset thus minimizing measurement errors.

A total of four sets of test results were obtained consisting of d - axis impedance measurements with field open circuit and subsequently terminated through a short circuit and also q-axis impedance measure - ments with the two field configurations mentioned above. D - axis measurements with field open circuit will provide a set of measured impedances and time constants. From these measurements only the values for X_d and T_{do}' would be used. On the other hand, the parameters X_d' and X_d'' would be obtained from the test conducted with the field terminated in a short circuit. Since the field circuit effects the short circuit performance of a machine during the subtransient and transient time intervals of the short circuit current, it can be seen that, in order for the results to include this effect, the field circuit should be energized for these measurements. Conversely, the q - axis results for either field termination should be approximately identical since the q - axis of the machine is in phase quadrature with the field winding resulting in no mutual coupling.

To facilitate testing the q - axis of the machine was positioned along A phase of the stator winding by applying a voltage between A phase and neutral and rotating the rotor until zero volts was observed at the field terminals. The rotor was left in this position for each of the four tests mentioned. D - axis measurements were made between term-

inals B and C. Q - axis measurements were made between A phase and B and C phases connected together. When calculating impedances, d-axis measurements were divided by a factor of 2 while q - axis measurements were divided by a factor of 1.5 to obtain per phase quantities.

The vector diagram showing the relation between the voltages in the circuit can be found in Fig. 2.16.

The calculation for the impedance magnitude is as follows:

$$|I| = \frac{V_C}{R_L} = \frac{|V_C|}{30.16} \quad \text{- - - - - - - - - - - - - - - (2.39)}$$

and

$$|Z_s| = \frac{V_B - V_C}{k|I|} \quad \text{- (2.40)}$$

where k is the dividing factor for either the d or q - axis as indicated above.

The calculation of the phase angle is accomplished using the following:

$$\phi = \left[360^{\circ} \times \text{Freq. (Hz)} \times \frac{\text{Meas. Time (ms)}}{1000}\right] \quad \text{- - - - - (2.41)}$$

The measured time is that measurement which is recorded from the electronic counter and its relation to the actual waveforms is shown in Fig. 2.17.

The data for each test is plotted in Fig. 2.18, 2.19, 2.20 and 2.21. The magnitude plots are normalized with respect to the dc measurement of R_s. The curves in each of the above situations must be fitted to the transfer function,

$$\frac{V_s}{kR_sI_s} = \frac{(1+sT_1)(1+sT_2)(1+sT_3)}{(1+sT_4)(1+sT_5)} \quad \text{- - - - - (2.42)}$$

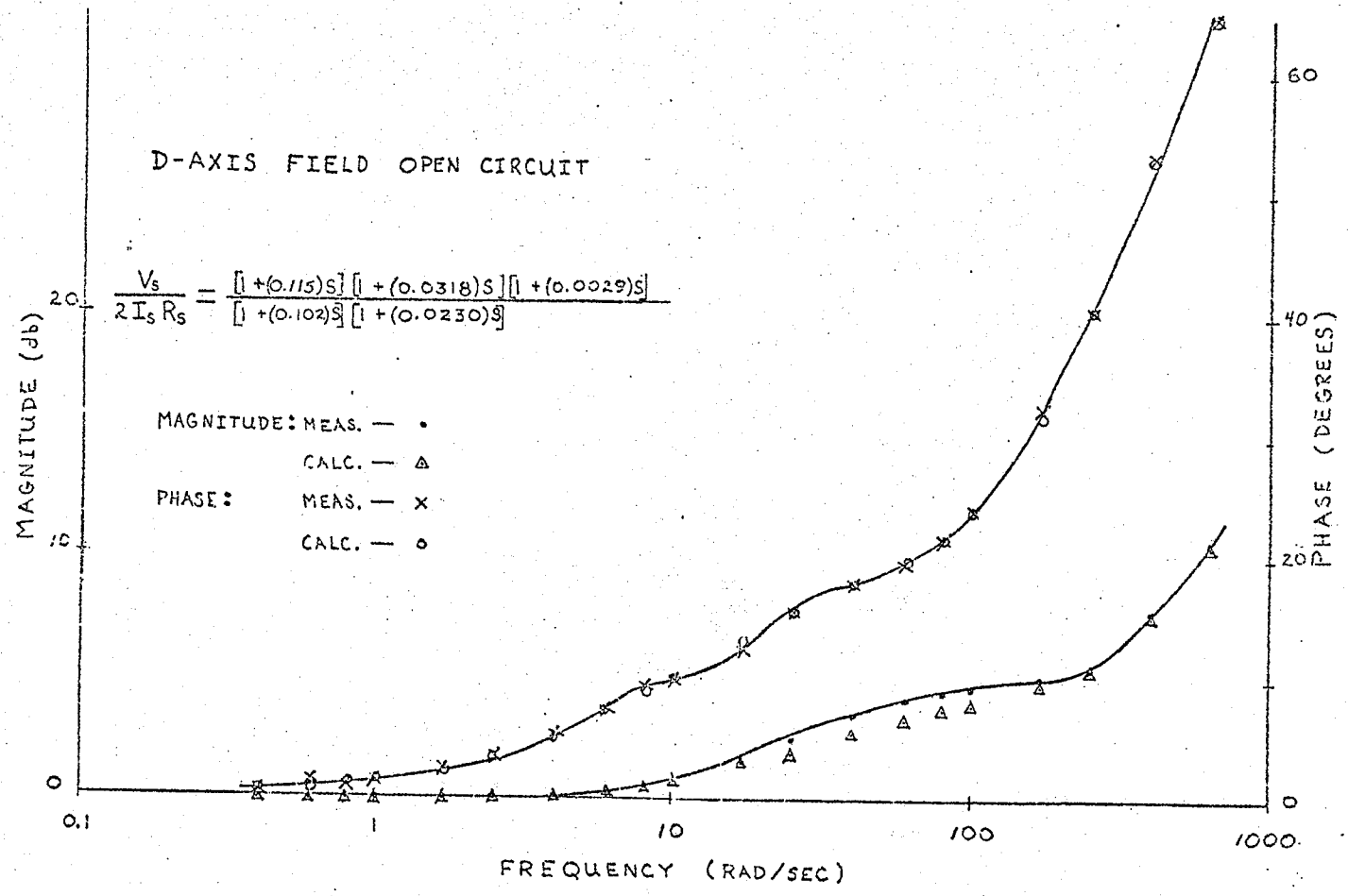
D-AXIS FIELD OPEN CIRCUIT
$\frac{V_s}{2 I_s R_s} = \frac{[1+(0.115)s][1+(0.0318)s][1+(0.0029)s]}{[1+(0.102)s][1+(0.0230)s]}$
MAGNITUDE: MEAS. — •
CALC. — △
PHASE: MEAS. — ×
CALC. — o
MAGNITUDE (db)
PHASE (DEGREES)
FREQUENCY (RAD/SEC)
0
10
20
0
20
40
60
0.1
1
10
100
1000

FIG. 2.18

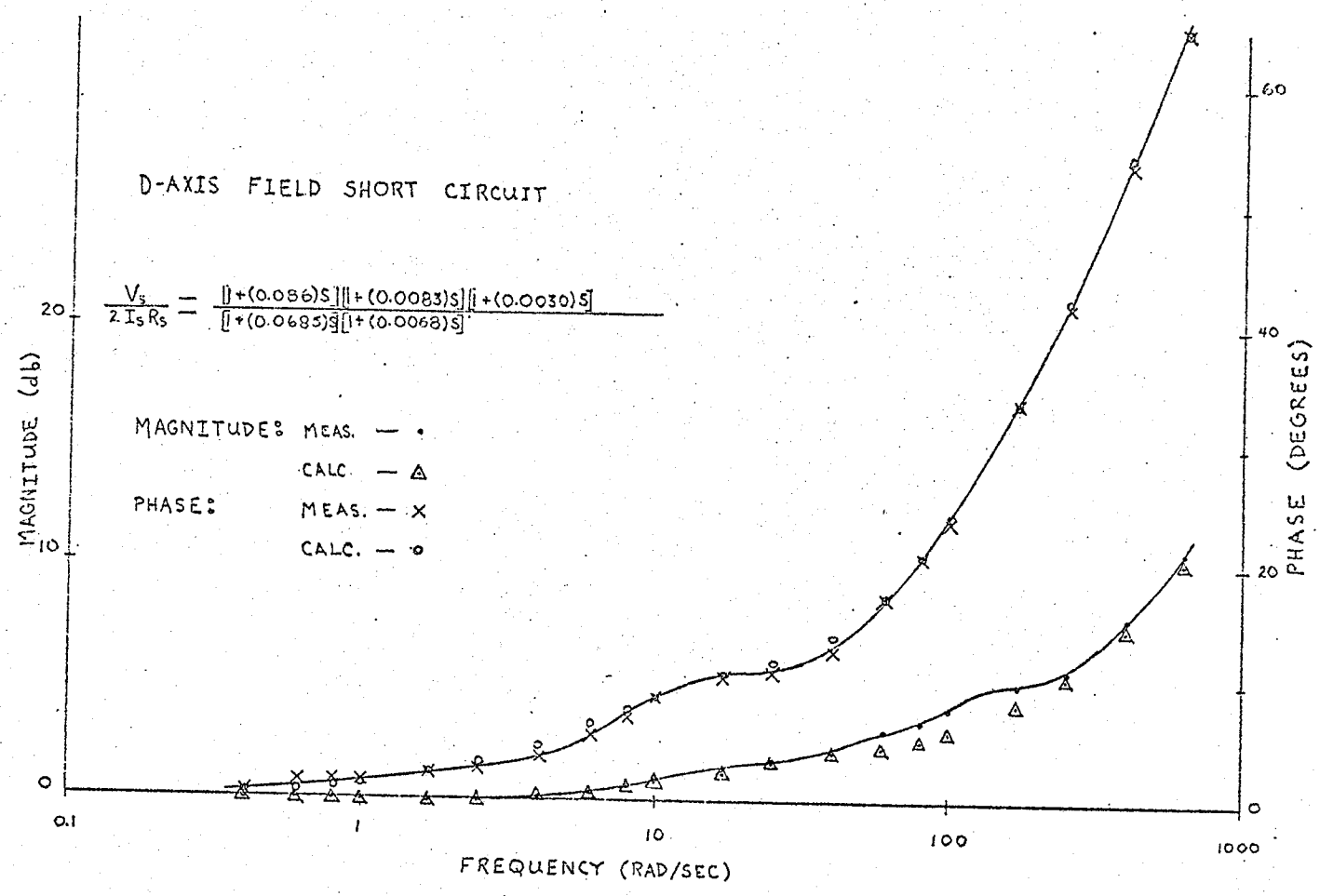
D-AXIS FIELD SHORT CIRCUIT
$\frac{V_s}{2 I_s R_s} = \frac{[1+(0.086)S][1+(0.0083)S][1+(0.0030)S]}{[1+(0.0685)S][1+(0.0068)S]}$
MAGNITUDE: MEAS. — •
CALC. — △
PHASE: MEAS. — ×
CALC. — ○
MAGNITUDE (db)
PHASE (DEGREES)
FREQUENCY (RAD/SEC)
0
10
20
0
20
40
60
0.1
1
10
100
1000

FIG. 2.19

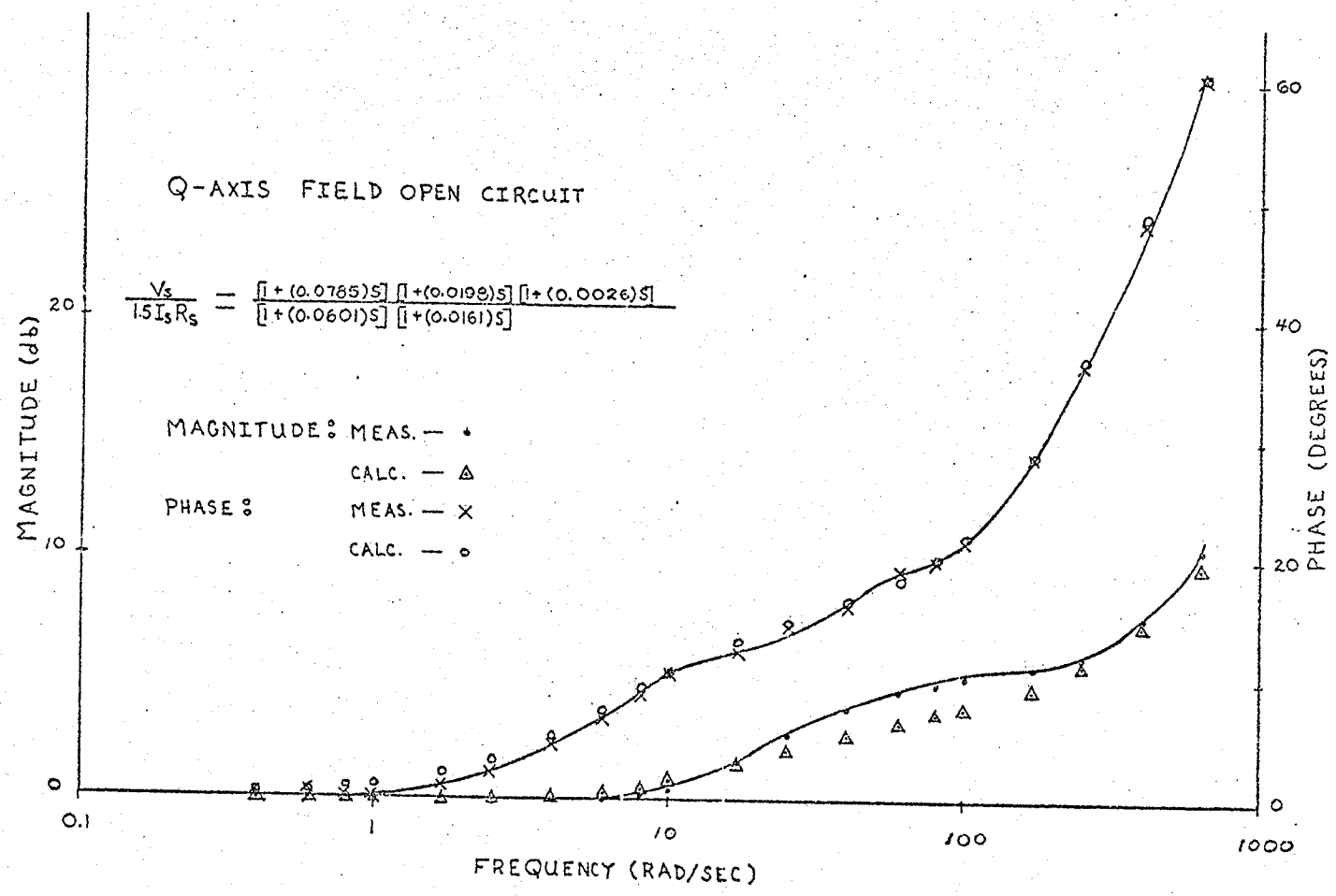
Q-AXIS FIELD OPEN CIRCUIT
$\frac{V_s}{1.5 I_s R_s} = \frac{[1+(0.0785)S][1+(0.0108)S][1+(0.0026)S]}{[1+(0.0601)S][1+(0.0161)S]}$
MAGNITUDE: MEAS. — •
CALC. — △
PHASE: MEAS. — ×
CALC. — o
MAGNITUDE (db)
PHASE (DEGREES)
FREQUENCY (RAD/SEC)
0.1
1
10
100
1000
0
10
20
0
20
40
60

FIG. 2.20

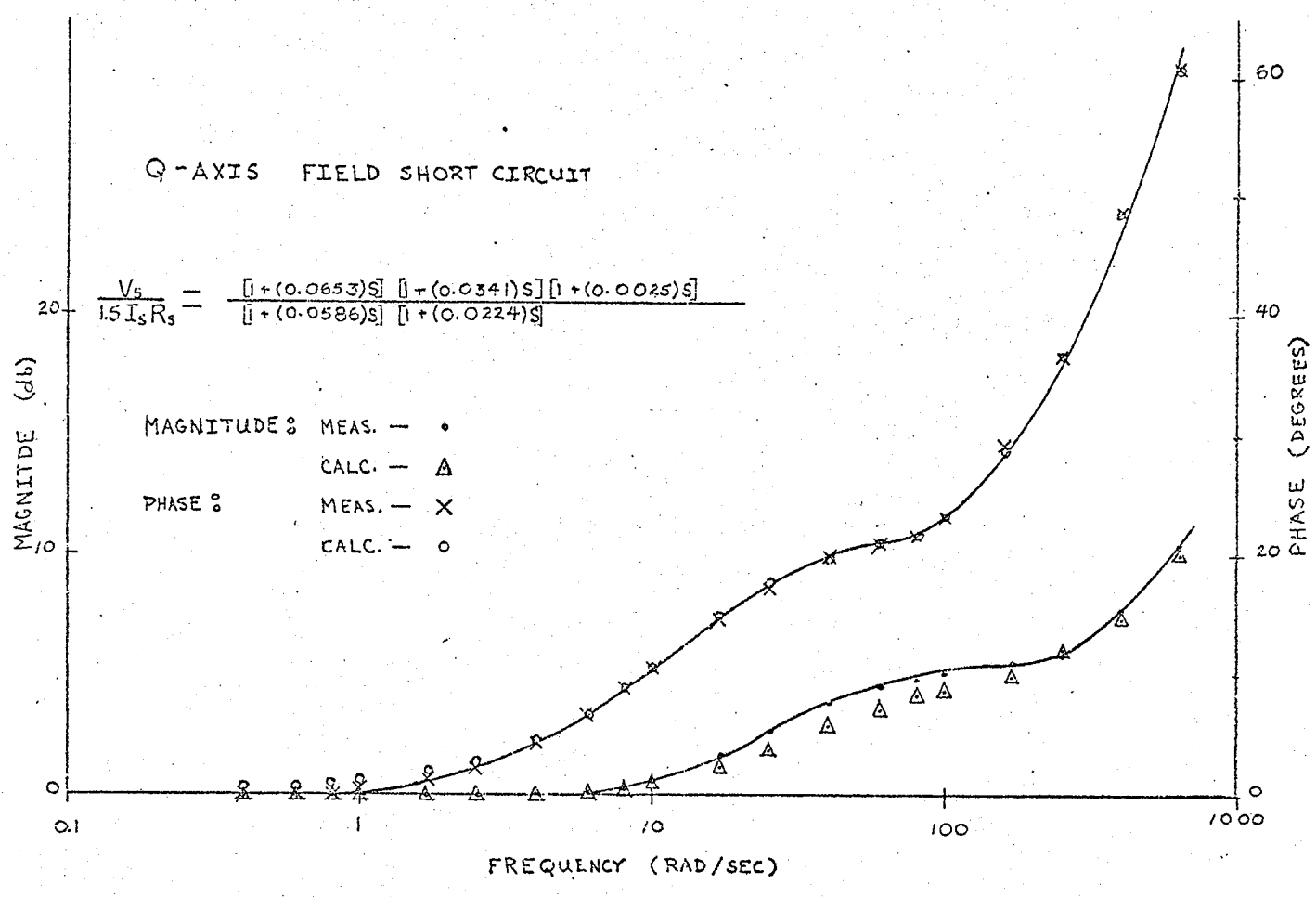
Q-AXIS FIELD SHORT CIRCUIT
$\frac{V_s}{1.5 I_s R_s} = \frac{[1+(0.0653)S]\,[1+(0.0341)S]\,[1+(0.0025)S]}{[1+(0.0586)S]\,[1+(0.0224)S]}$
MAGNITUDE : MEAS. — •
CALC. — Δ
PHASE : MEAS. — X
CALC. — o
MAGNITUDE (db)
PHASE (DEGREES)
FREQUENCY (RAD/SEC)
20
10
0
60
40
20
0
0.1
1
10
100
1000

FIG. 2.21

where the time constants T_1 to T_5, correspond to the break frequencies obtained from the plots. To fit the experimental data to the analytic expression above, a computer optimization routine utilizing the method of least squares was used. Consequently, each of the data plots include points calculated from eq'n (2.42) when the best fit was obtained. The complete expression for each test is shown on each plot.

Having obtained the overall transfer function for the machine impedance, it is then required to derive the transfer function for the operational inductance for each of the four cases above. Using each expression in turn, the impedance for the appropriate equivalent circuit representing the synchronous machine is derived and each of the individual components in the circuit is assigned a value. At this point it is possible to calculate all the reactances and time constants mentioned earlier. Appendix B contains the complete analytic description of the method along with a sample calculation using the results obtained for the d-axis with field open circuit.

The parameter values for the four test cases are summarized in Table 2.1. Mindful of the previous comments, the following list specifies the parameter values to be used for the investigation which follow.

$X_d = 0.29$ pu

$X_d' = 0.14$ pu

$X_d'' = 0.06$ pu

$T_{do}' = 0.10$ sec.

$X_q = 0.29$ pu

$X_q' = 0.23$ pu

PARAM-ETER (pu)	D-AXIS		Q-AXIS		PARAM-ETER (pu)
	O.C. FIELD	S.C. FIELD	O.C. FIELD	S.C. FIELD	
X_d	0.30	0.27	0.31	0.26	X_q
X_d'	0.22	0.14	0.22	0.24	X_q'
X_d''	0.06	0.06	0.05	0.05	X_q''
T_{do}'(sec)	0.10	0.07	0.06	0.06	T_{qo}'(sec)
T_d'(sec)	0.06	0.02	0.03	0.05	T_q'(sec)

Table 2.1 Frequency response measurement results

$X_q'' = 0.05$ pu

$T_{qo}' = 0.06$ sec

It should be noted that the quantity X_d was set at the above value in view of previous measurements which favor the lower value. The q-axis parameters are derived by averaging the results of the two tests (the spread in values could be attributed to inaccuracies in experimental measurements and analytic approximations).

ii) Transmission Line Impedances

As mentioned before the transmission line model consists of a set of series inductors equipped with taps which are selected by means of a front mounted rotary switch. The impedance for each tap setting was measured using a 120 volt supply and the results shown below are expressed in per unit on the machine base.

Low Impedance Setting: $R_e + jX_e = 0.03 + j0.16$ pu

Medium Impedance Setting: $R_e + jX_e = 0.08 + j0.50$ pu

High Impedance Setting: $R_e + jX_e = 0.12 + j0.94$ pu

iii) System Inertia and Damping

Returning to Fig. 2.6 for a moment it can be shown that the transfer function from ΔT_m to $\Delta\omega$ is:

$$\frac{\Delta\omega}{\Delta T_m} = \frac{\frac{1}{M} S\left(S+\frac{1}{T_{dz}'}\right)}{S^3+\left(\frac{M+DT_{dz}'}{MT_{dz}'}\right)S^2+\left(\frac{D+377k_1T_{dz}'}{MT_{dz}'}\right)S+\frac{377(k_1-k_2k_4)}{MT_{dz}'}} \qquad (2.43)$$

This expression has the following standard form [11] when excited with a step input:

$$\Delta\omega(s) = \frac{k(s+Z)}{(s+p)(s^2+2\zeta\omega_n s+\omega_n{}^2)} \qquad (2.44)$$

Using partial fraction expansion:

$$\Delta\omega(s) = \frac{R}{M}\left[\frac{A}{s+p} + \frac{Bs + C}{s^2+2\zeta\omega_n s+\omega_n{}^2}\right] \qquad (2.45)$$

or in the time domain:

$$\Delta\omega_{(t)} = \frac{R}{M}[A\{e^{-pt} - e^{-\zeta\omega_n t}\cos(\omega_n\sqrt{1-\zeta^2}t)\} +$$

$$C^1 e^{-\zeta\omega_n t}\sin(\omega_n\sqrt{1-\zeta^2}t)] \qquad (2.46)$$

where A, B and C are the residues for each of the poles in eq'n. (2.43) and R is the magnitude of the step input. The constant C^1 results from the conversion to the time domain and is equal to $\frac{C+A\zeta\omega_n}{\omega_n\sqrt{1-\zeta^2}}$. From eq'n (2.46) the frequency of the response is:

$$\omega_d = \omega_n\sqrt{1-\zeta^2} \qquad (2.47)$$

For small values of ζ, ω_d will be approximately equal to ω_n. With sufficient experimental data and utilization of the appropriate approximations, it will be possible to determine the values for M and D.

To simulate the above experimentally the model power system must be operated with the regulator loop open (the field voltage is therefore constant). If the synchronous machine is run so as to maintain a constant power output (mechanical torque is constant and thus ΔT_m is zero) and the transmission line impedance is then switched from

one value to another, a step change in electrical power transmitted will occur. By examining the block diagram of Fig. 2.6 one can deduce that this will be equivalent to a step change in ΔT_m. Initiation of this switching operation causes the system to respond with an exponentially decaying oscillation. By recording the terminal voltage, current and power factor prior to the distrubance along with an oscillogram of the oscillation, the constants k_1, k_2, k_4 and T_{dz}' can be calculated and values for M and D can be obtained. When calculating the above constants the transmission line impedance in the circuit during the oscillation should be used.

From measurements:

$$e_t = 0.85 \text{ pu} \qquad I = 1.0 \text{ pu} \qquad \text{power factor} = 1.0$$

$$R_e + jX_e = 0.08 + j\ 0.50 \text{ pu} \quad \text{(final position)}$$

Using the eg'n of Appendix A:

$$k_1 = 0.89 \qquad k_2 = 1.37$$

$$k_3 = 0.81 \qquad k_4 = 0.15$$

$$T_{dz}' = k_3 T_{do}' = 0.08 \text{ sec.} \qquad (T_{do}' = 0.10 \text{ sec})$$

From the system response the following measurements were taken.

$$\text{Frequency} = \frac{2\pi}{\omega_d} = 0.90 \text{ sec.}$$

Time constant of Response, $T = 1.63$ sec.

Prior to using the above measurements, reexamination of eq'n (2.46) indicates that, in addition to the exponentially decaying sine term, there also exists the following:

$$A(e^{-pt} - e^{-\zeta\omega_n t} \cos \omega_n\sqrt{1-\zeta^2}t)$$

If this term is significant it would modify the response in such a manner as to cause the overall waveform to appear nonsinusoidal. The actual experimental result indicated that this was not the case, leading one to believe that A must be very small. In addition, if the denominator of eq'n (2.44) is expanded and equated to the denominator of eq'n (2.43) we have:

$$s^3 + (2\zeta\omega_n + p)s^2 + (2\zeta\omega_n p + \omega_n^2)s + \omega_n^2 p =$$

$$s^3 + \left(\frac{M+DT_{dz}'}{MT_{dz}'}\right)s^2 + \left(\frac{D+377k_1T_{dz}'}{MT_{dz}'}\right)s + \frac{377(k_1-k_2k_4)}{MT_{dz}'} \qquad (2.48)$$

Equating the constant coefficient of each polynomial and using the constants previously calculated leads to:

$$\omega_n^2 p = \frac{3225.7}{M} \qquad (2.49)$$

Assuming ω_n is approximately equal to the measured value of ω_d above (small ζ) will change eq'n (2.49) to :

$$p \simeq \frac{66.2}{M} \qquad (2.50)$$

On a real system M usually ranges between values of 5 and 10. Using eq'n (2.50) the corresponding p values range from 13 to 6.6. Since ζ has been assumed to be small, the real part of the complex conjugate roots will be much smaller than p. The root p can therefore be assumed to be nondominant.

Returning to the measurements obtained from the system it can now be

said with confidence that :

$$\zeta\omega_n = \frac{1}{T} = 0.61 \quad \text{sec}^{-1}$$

and that

$$\omega_d = \omega_n \sqrt{1-\zeta^2} = 6.98 \quad \text{rad./sec.}$$

Manipulation produces $\omega_n = 7.01$ rad/sec and $\zeta = 0.09$. These numerical values confirm earlier assumptions. Also, the residue A can be analytically determined to be:

$$A = \frac{(\frac{1}{T_{dz}'} - p)}{p^2 - 2\zeta\omega_n p + \omega_n^2} \qquad \text{- - - - - - - - - - - - - - - - - - - (2.51)}$$

For $M = 5$ and $p = 13$ the corresponding value for A is -2.5×10^{-3} For $M = 10$ and $p = 6.6$ A becomes 7.0×10^{-2}. In both instances the residue is insignificant as assumed earlier.

To determine numerical values for M and D the following set of equations obtained from eq'n (2.48) must be solved.

$$p = \frac{65.6}{M} \qquad \text{- (2.52)}$$

$$2\zeta\omega_n + p = \frac{M + DT_{dz}'}{MT_{dz}'} \qquad \text{- - - - - - - - - - - - - - - - - - (2.53)}$$

$$2\zeta\omega_n p + \omega_n^2 = \frac{D + 377\, k_1 T_{dz}'}{MT_{dz}'} \qquad \text{- - - - - - - - - - - (2.54)}$$

The values obtained are:

$$M = 5.7 \text{ sec.}$$

$D = 1.8$ per unit

iv) Excitation Loop Parameters

The excitation loop according to the Heffron - Phillips model is defined by the block diagram of Fig. 2.22. The actual circuit existing in the laboratory is shown in Fig. 2.23. The parameter of interest is the exciter gain k_e. To obtain this value the dc gain of the circuit must be determined. To accomplish this the steady state transfer function of each section of the circuit of Fig. 2.23 must be obtained and the results must then be taken together to establish the overall circuit gain. Since the exciter gain is a function of the feedback resistor setting the final result for k_e will be in terms of R_f.

The individual circuit gains are listed below

Voltage Transducer:

$$\text{Gain} = \frac{10^{-3}}{120} \quad \text{AMPS/VOLT}$$

Voltage Divider:

$$\text{Gain} = \frac{5000}{5510} \times 510 \quad \text{VOLTS/AMP}$$

Op. Amp. Adder:

$$\text{Gain} = \frac{R_f}{R_i} = \frac{1 \times 10^6}{5.1 \times 10^2} \quad \text{VOLTS/VOLT}$$

Op. Amp. Inverter:

$$\text{Gain} = \frac{100 \times 10^3}{100 \times 10^3} \quad \text{VOLTS/VOLT}$$

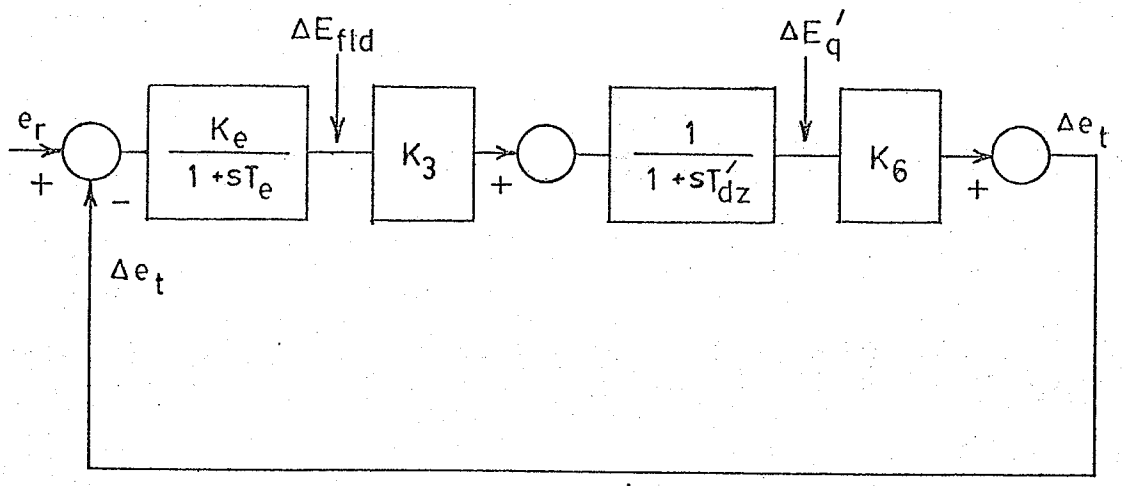

Fig. 2.22 Excitation loop block diagram

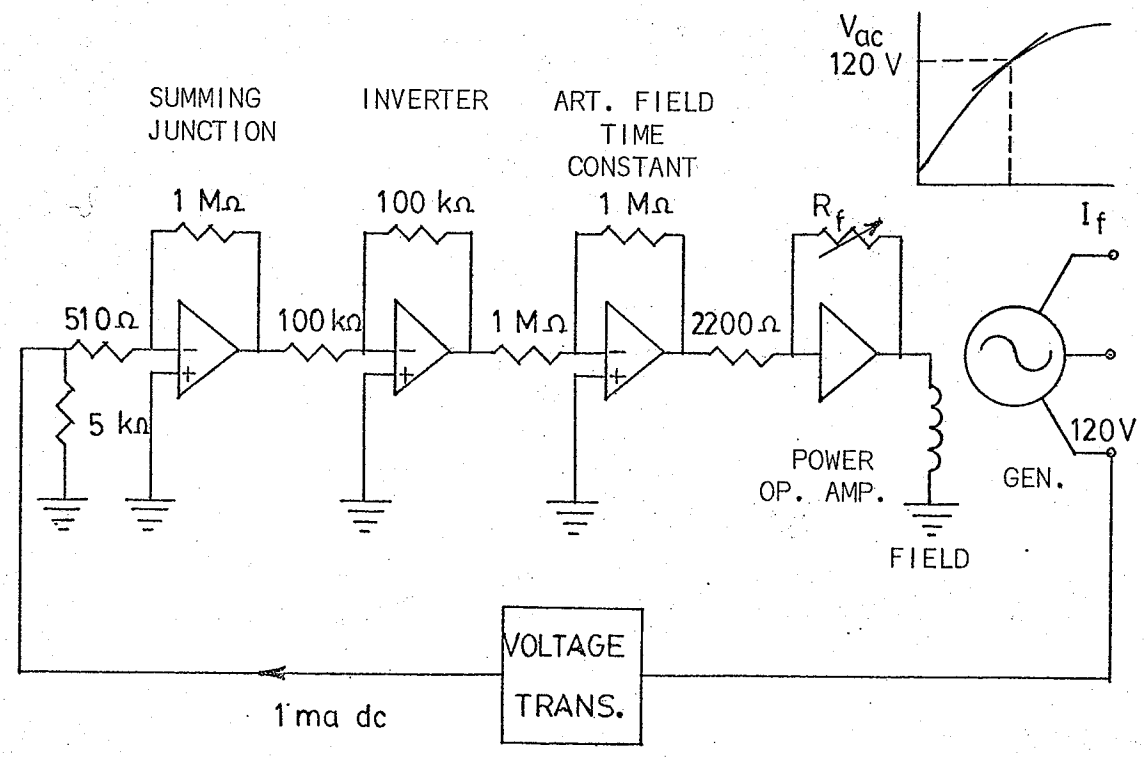

NOTE: Capacitors are not included since steady state is being considered.

FIG. 2.23 Excitation loop circuit.

Artifical Time Constant:

$$\text{Gain} = \frac{1 \times 10^6}{1 \times 10^6} \quad \text{VOLTS/VOLT}$$

Power Op. Amp:

$$\text{Gain} = \frac{R_f}{2200} \quad \text{VOLTS/VOLT}$$

Generator Field:

The dc field resistance measured at operating temperature is 158 ohms. Therefore the gain is 1/158 AMPS/VOLT

Field Circuit to Generator Terminal Voltage:

Using the open circuit characteristic of Fig. 2.11 the slope measured at rated terminal voltage yields a transfer gain of approximately 99 VOLTS (ac)/Amp (dc).

Taking the product of the results above sets the exciter loop gain at $0.0022 \times R_f$. Referring to Fig. 2.22 the exciter loop gain is equivalent to $k_e k_3 k_6$. From Appendix A it is noted that the relation describing k_3 is strictly dependent on the machine and external impedances. Since all the studies to be done in this investigation will only be concerned with the case corresponding to a long transmission line ($X_e = 0.94$ pu), the value assigned to k_3 will be constant at 0.88.

The assignment of k_6, at first glance, looks a little more complex since it is dependent on voltages as well as impedances. However, if the external resistance is assumed negligible the simplified expression of Appendix A may be used. The expression for k_6, upon substitution, becomes:

$$k_6 = 0.87 \frac{e_{q_0}}{e_{t_0}} \qquad (2.55)$$

The expression for the voltage ratio is shown to be:

$$\frac{e_{q_0}}{e_{t_0}} = \frac{e_{t_0} + I_{q_0} X_q}{E_{q_0}} \qquad (2.56)$$

Also

$$E_{q_0} = \sqrt{(e_{t_0} + I_{q_0} X_q)^2 + (I_{p_0} X_q)^2} \qquad (2.57)$$

For the generator considered the value of X_q is 0.29 pu. Therefore, the second term would normally assume a value no greater than $(0.29)^2$ or 0.08. As a result we can say that

$$E_{q_0} \simeq e_{t_0} + I_{q_0} X_q \qquad (2.58)$$

for this particular machine. The value for k_6 can thus be assumed to remain at about 0.87 for normal operating conditions (its actual value would only be slightly lower).

Using these values for k_3 and k_6, an expression for exciter gain as a function of the feedback resistor R_f becomes

$$k_e \simeq (2.8 \times 10^{-3}) \; R_f \qquad (2.59)$$

To achieve exciter gains of 75, 100 and 140 the corresponding resistor settings become 26.8 kΩ, 35.7 kΩ and 50 kΩ respectively.

v) Parameter Determination For An Unstable Operating Condition

To facilitate analysis of the system and consequently allow the design of a suitable type of compensator, it was deemed appropriate to select an unstable operating condition on the model power system and calculate the corresponding Heffron - Phillips constants. By so doing, this operating condition would serve as a basis for determining a particular compensator's effect on system performance. With the Heffron - Phillips constants and the machine parameters determined earlier the characteristic equation of eq'n (2.31) can be identified and its eigenvalues calculated. Through the use of S - plane techniques, the designer can select some sort of compensation to improve the system's performance.

The following measurements were taken with the machine running just beyond its stability limit (X_e = 0.94 pu, artificial time constant = 5 sec).

e_t = 0.85 pu I = 0.64 pu

Power Factor = 1.0 $k_e \simeq 75$

Using the equations of Appendix A where R_e is assumed to be zero, the following values for k_1 -k_6 are calculated:

k_1 = 0.57

k_2 = 0.71

k_3 = 0.88

k_4 = 0.09

k_5 = -0.06

k_6 = 0.85

vi) Artificial Field Time Constant

As mentioned earlier the open circuit field time constant T_{do}' of the generator model is extremely short. Using the model as is would mean that its performance would not be representative of a real system. In addition it was indicated earlier that a negative field resistance was the normal means of correcting this situation. Because this type of approach could easily turn into a rather involved investigation just by itself, the easier approach of adjusting T_e was taken. The value of T_e was adjusted and the resulting roots of the characteristic equation were compared to those occurring for the desired values of T_e and T_{dz}'.

For a steam turbine unit with a solid state exciter the typical values for T_e and T_{dz}' are:

$$T_e = 0.05 \text{ sec.}$$

$$T_{dz}' = 5.0 \text{ sec.}$$

If the constants corresponding to the operating condition observed in the previous section are applied to the characteristic equation along with the above time constant the system eigenvalues are:

$$s_1 = -0.02 + j\,6.35 \qquad s_2 = -0.02 - j\,6.35$$

$$s_3 = -10.23 + j\,11.26 \qquad s_4 = -10.23 - j\,11.26$$

After the trial of several values of T_e, a reasonable result was obtained using the following time constants.

$$T_e = 2.0 \text{ sec}$$

$$T_{dz}' = 0.09 \text{ sec}$$

The resulting eigenvalues became:

$$s_1 = 0.008 + j\,6.38 \qquad s_2 = 0.008 - j\,6.38$$

$$s_3 = -5.96 + j\,16.81 \qquad s_4 = -5.96 - j\,16.81$$

It will be noticed that the third and forth complex conjugate root pair are not comparable to those obtained earlier. Because this root pair is quite removed from the $j\omega$ axis compared to s_1 and s_2 their effect on the system should be negligible. Based on this analysis, the value for T_e obtained above was judged to be adequate. As an aside, it was observed from the $\hat{S}$-plane that the stability of the system was increased if T_e was made smaller. This is consistent with observations made on actual systems.

To confirm the validity of the above approximation, the phase angle of the machine regulator transfer function is calculated for the two sets of time constants indicated above. The expression for the variation in torque due to a variation in reference voltage can be obtained from the Heffron - Phillips model with reference to Fig. 2.7. The equation has the following form.

$$\frac{\Delta T}{\Delta e_t}_{ref} = \frac{-k_2 k_e}{1/k_3 + k_e k_6 + s\left(\frac{T_e}{k_3} + T_{do}'\right) + s^2 T_e T_{do}'} \qquad \text{- - - - - - - (2.60)}$$

Calculation of the phase angle of eq'n (2.60) over the applicable range of frequencies (0 - 2 Hz) shows that the above approximation produces

only a half of the phase lag occurring when $T_e = 0.05$ sec. and $T_{dz}' = 5.0$ sec. This discrepancy arises from the fact that the third and fourth roots of the approximation don't correspond to the desired case. To rectify this situation it was required to increase T_e to 3.3 seconds so that the resulting phase angle of eq'n (2.60) would be comparable. Increasing T_e caused the first two roots to move a little further into the right hand s - phase but, their location is still relatively close to the desired case. The calculated eigenvalues became:

$$s_1 = 0.09 + j\,6.34 \qquad s_2 = 0.09 - j\,6.34$$

$$s_3 = -5.95 + j\,12.65 \qquad s_4 = -5.95 - j\,12.65$$

It should be noted that the usability of the above approximation on this model is possible since the constant k_4 is very small. This situation may not always be the case in practice.

CHAPTER III

COMPENSATOR DESIGN

1. System Transfer Function With Frequency Feedback

The transfer function of the uncompensated system was developed in Chapter II. If a feedback circuit is now added through $G_c(s)$ eq'n (2.29) becomes

$$\Delta = 1 + \frac{377k_1}{s(Ms+D)} - \frac{377\,k_2k_4}{s(Ms+D)(1+sT_{dz}')} -$$

$$\frac{377\,k_ek_2k_3k_5}{s(Ms+D)(1+sT_e)(1+sT_{dz}')} + \frac{k_ek_3k_6}{(1+sT_e)(1+sT_{dz}')} +$$

$$\frac{377k_1k_ek_3k_6}{s(Ms+D)(1+sT_e)(1+sT_{dz}')} + \frac{G_c(s)\,k_ek_2k_3}{(Ms+D)(1+sT_e)(1+sT_{dz}')} \qquad (3.1)$$

Eq'n (2.28) and (2.30) remain unchanged and thus the complete transfer function becomes:

(3.2)

$$\frac{\Delta\omega}{\Delta e_r} = \frac{-k_ek_2k_3\,s}{\{[MT_eT_{dz}']s^4 + [M(T_e+T_{dz}')+DT_eT_{dz}']s^3[M(1+k_ek_3k_6)+D(T_e+T_{dz}')}$$

$$+ 377\,k_1T_eT_{dz}']s^2 + [D(1+k_ek_3k_6) + 377\{k_1(T_e+T_{dz}')-k_2k_4T_e\}]s$$

$$+ 377[k_1(1+k_ek_3k_6) - k_ek_2k_3k_5 - k_2k_4] + k_ek_2k_3G_c(s)S\}$$

The characteristic equation of the compensated system is the denominator of eq'n (3.2). Written in standard form [7], it becomes:

$$1 + \frac{k_e k_2 k_3 G_c(s)\, S}{\{[MT_e T_{dz}']s^4 + [M(T_e+T_{dz}') + DT_e T_{dz}']s^3 + [M(1+k_e k_3 k_6)} = 0 \quad (3.3)$$

$$+ D(T_e+T_{dz}') + 377k_1 T_e T_{dz}']s^2 + [D(1+k_e k_3 k_6) + 377\{k_1(T_e+T_{dz}')$$

$$- k_2 k_4 T_e\}]s + 377[k_1(1+k_e k_3 k_6) - k_e k_2 k_3 k_5 - k_2 k_4]\}$$

Eq'n 3.3 is now amenable to root locus analysis.

2. Investigation of Complex Compensation

a) Complex Compensation Description

The concept of complex compensation was applied to the model - power - system utilizing a feedback signal derived from one of the operating variables in order that the system's performance might be improved. It has been suggested by others [5] that compensation utilizing supplementary signals in conjunction with a real root stabilizer could provide comparable results. To establish whether these comments were justified, it was decided to compare the performance of a complex compensator as opposed to a real root compensator in a feedback path from one of the operating variables. The analytic form of the complex compensator is as shown below.

$$\frac{E_0}{E_i} = \frac{k[s^2+2\zeta_1\omega_1 s+ \omega_1^2]}{s^2+2\zeta_2\omega_2 s+ \omega_2^2} \qquad (3.4)$$

The roots of both the numerator and denominator quadratic are complex.

Two methods of analysis will be employed. The problem will first be investigated using the root locus technique and design in the S-phase. To compare results, the analysis will then be attempted using frequency response methods. The phase angle of the machine function with compensation will form the basis of the analysis. An attempt will then be made to correlate the two results to produce the best design for the model power system.

b) Root Locus Approach

The pole-zero locations for the unstable operating condition calculated in Chapter II are plotted in Fig. 3.1. Examination of this figure indicates that the system has a pair of complex conjugate roots in the right hand S-plane which correspond to an unstable situation. Because of this situation, pole-zero cancellation cannot be used here since cancellation is never exact. If pole zero cancellation were attempted, partial fraction expansion would show that, even though the residues of the unstable characteristic equation roots are very small (a zero has been placed very close to this pole), instability would always occur since an exponential term with a positive real exponent would be present.

To decide on a suitable type of compensation for this system, an examination of what the final S-plane root configuration of the system should look like for good results would be in order. Ideally the domin-

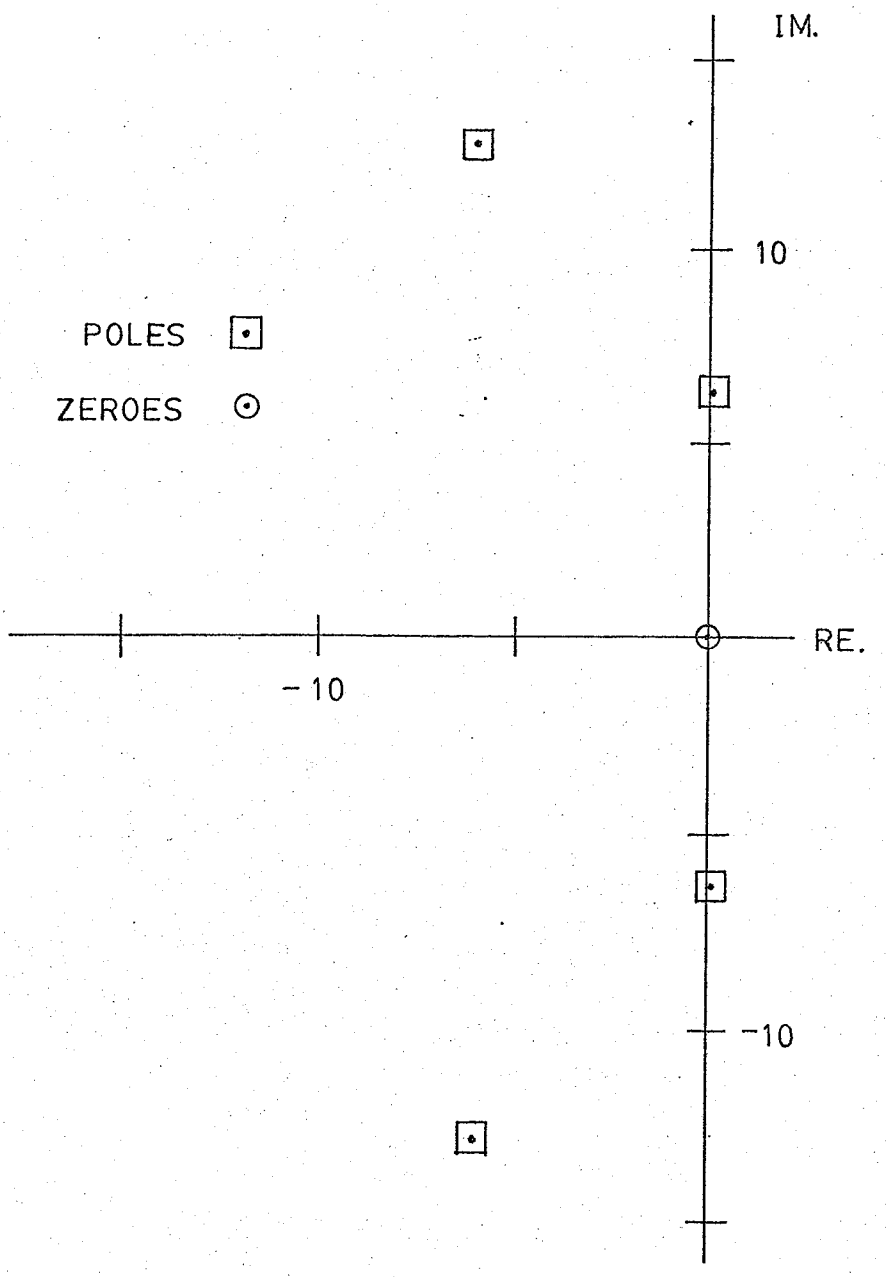

FIG. 3.1 Uncompensated sytem - pole-zero locations

ant unstable poles should be drawn into the left hand S-plane so that the real part of the root is relatively large to ensure good damping. In addition, the imaginary part of the root should not be too large so that the system does not possess a high frequency of oscillation and yet not too small so that the response is sufficiently fast. The required time response of the system should therefore possess a frequency of oscillation of around 1 Hz and an acceptable amount of damping. In addition, the remaining system roots must be nondominant. This can be accomplished by causing the remaining poles to move further to the left in the S - plane or by causing the residues associated with these poles to be very small or a combination of the two. Failing to accomplish these aims could mean that the response would contain a high frequency component. This could lead to undesirable torsional vibrations of the machine rotor shaft and possibly unacceptable mechanical stresses. Finally, the design must ideally maintain the above results in the face of parameter variations and, as a direct consequence of this, exhibit an applicability to a general range of operating conditions.

In terms of some particular design specification one can arbitrarily require that the 2% settling time of the response should be less than 1.5 seconds and that the maximum over shoot be less than 25%. These requirements can be translated to the S-plane using the following well known approximation [11]:

$$t_s \simeq \frac{4}{\sigma} \qquad (3.5)$$

t_s is the settling time and σ is the magnitude of the real part of the dominant root in the S-plane. As a result we can say that $|\sigma| \geq 2.7$. In addition,

graphs are available [11] which relate the damping ratio ζ to the maximum overshoot. For this specification ζ must be greater than 0.4. Now

$$\zeta = \cos\theta \qquad \text{-------------------------} \qquad (3.6)$$

where θ is the angle measured from the negative real axis to a line connecting the pole with the origin. Calculation indicates that θ must be less than 66°. With the above information the dominant root location is established at

$$S \simeq 2.7 \pm j\,6.2$$

A number of complex compensator functionswere tried with the aid of a DECLAB PDP11/40 digital computer. The points on each individual root locus were obtained using the digital computer. These points were then fed into an IBM 370/158 computer to produce the plots shown in Fig. 3.2, 3.3, 3.4 and 3.5. In view of the above requirements the compensation described by Fig. 3.4 seems to produce the most favourable results with the appropriate compensator gain setting. It should be noted that the operating point established in Chapter II was used as the basis for the above plots. Also, the exciter gain was altered and the resulting system roots recalculated to observe the effect of parameter variation on the plot of Fig. 3.4(b).

As can be seen the process of obtaining $G_c(s)$ by the above method is one of trial and error. It is therefore necessary to remember that the compensation described in Fig. 3.4 is not necessarily the optimum case but only the best result obtained from several trials. To

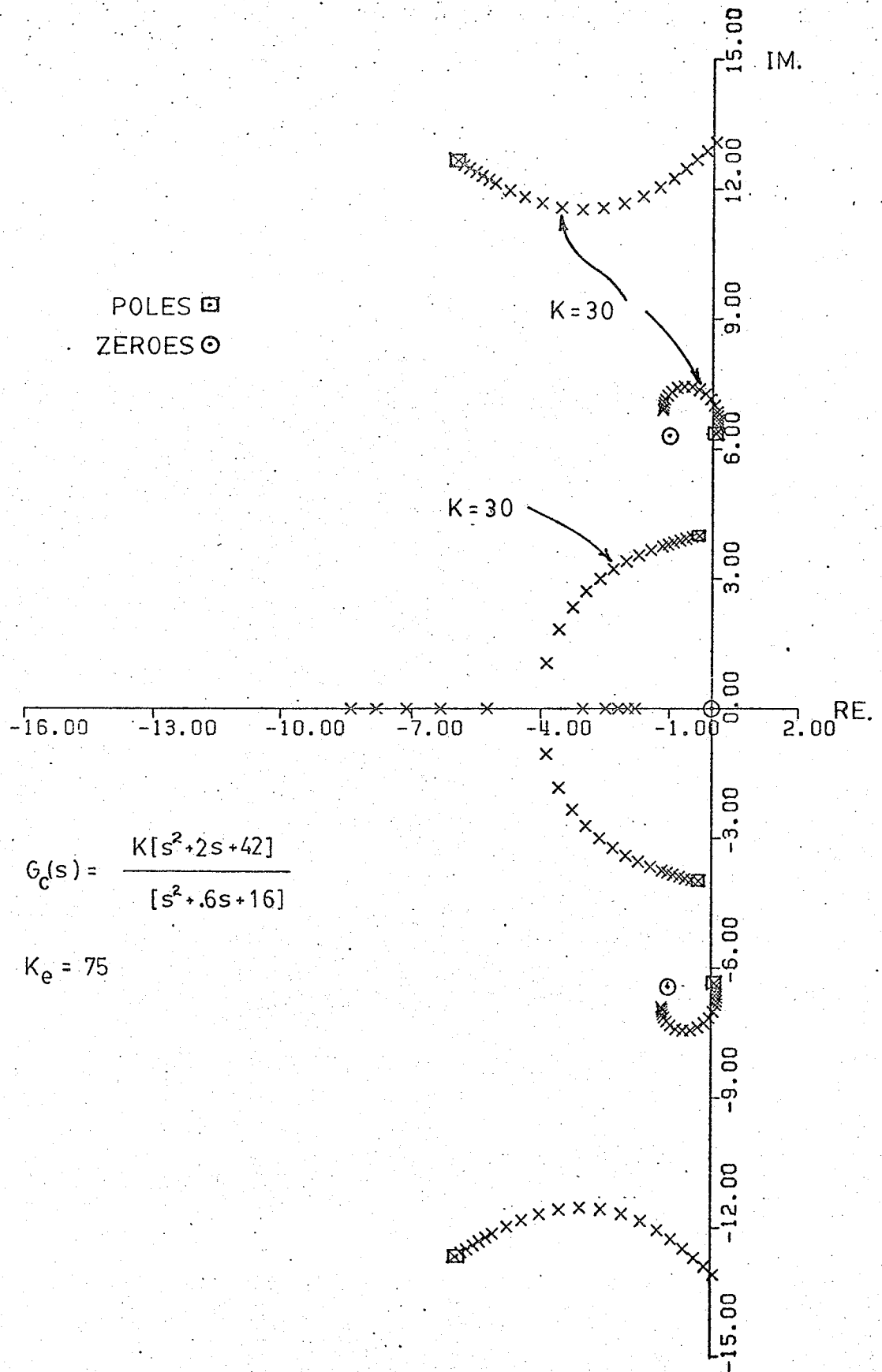

$$G_c(s) = \frac{K[s^2+2s+42]}{[s^2+.6s+16]}$$

$K_e = 75$

FIG. 3.2

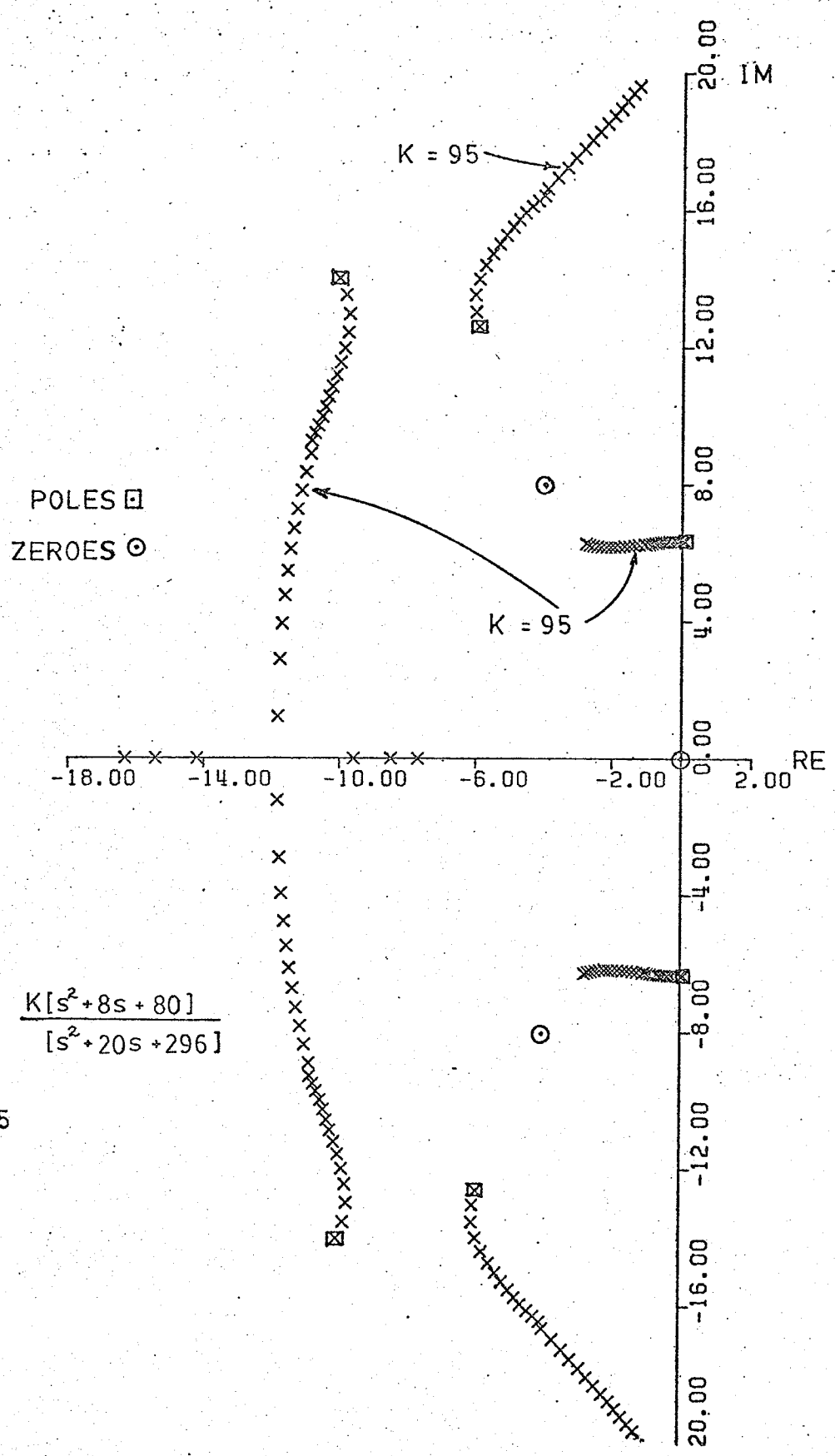

$$G_c(s) = \frac{K[s^2+8s+80]}{[s^2+20s+296]}$$

$K_e = 75$

FIG. 3.13

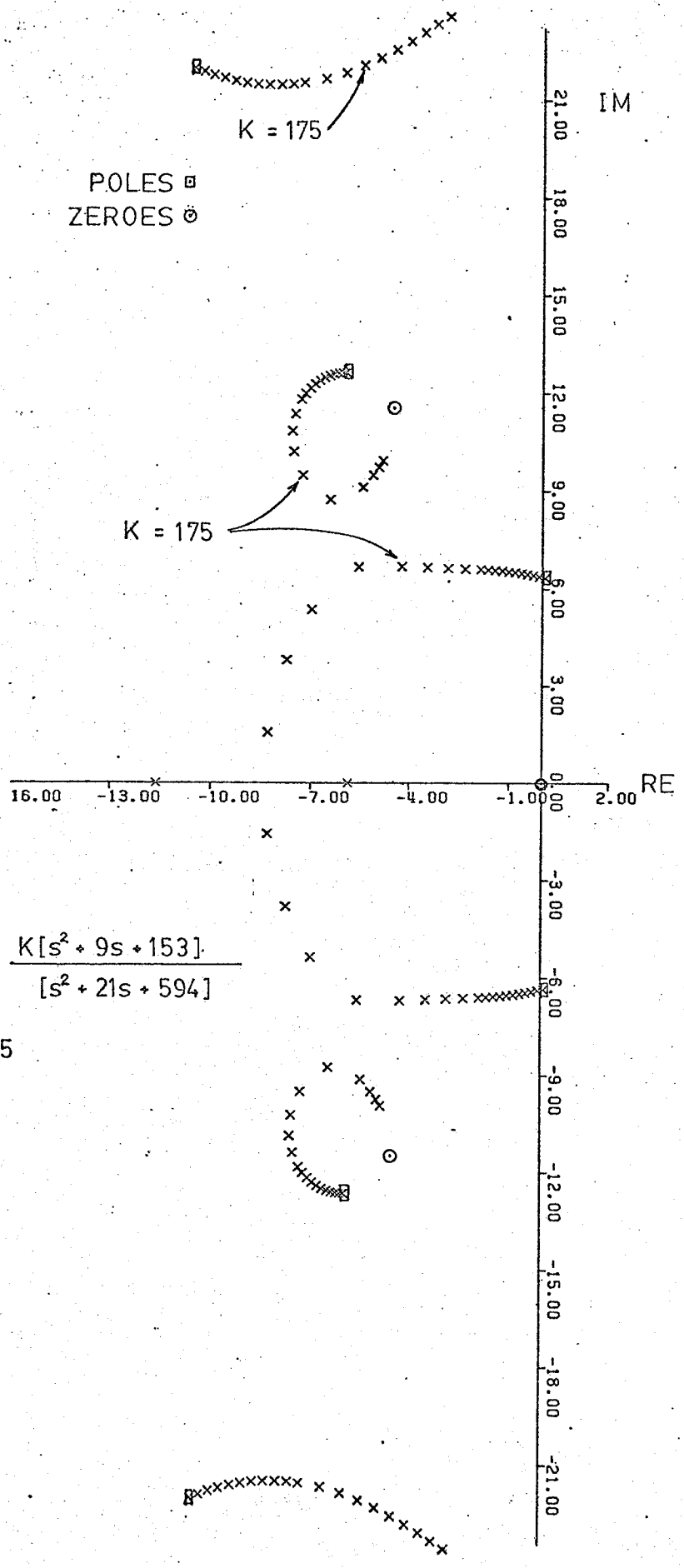

$$G_c(s) = \frac{K[s^2 + 9s + 153]}{[s^2 + 21s + 594]}$$

$K_e = 75$

FIG. 3.4 (a)

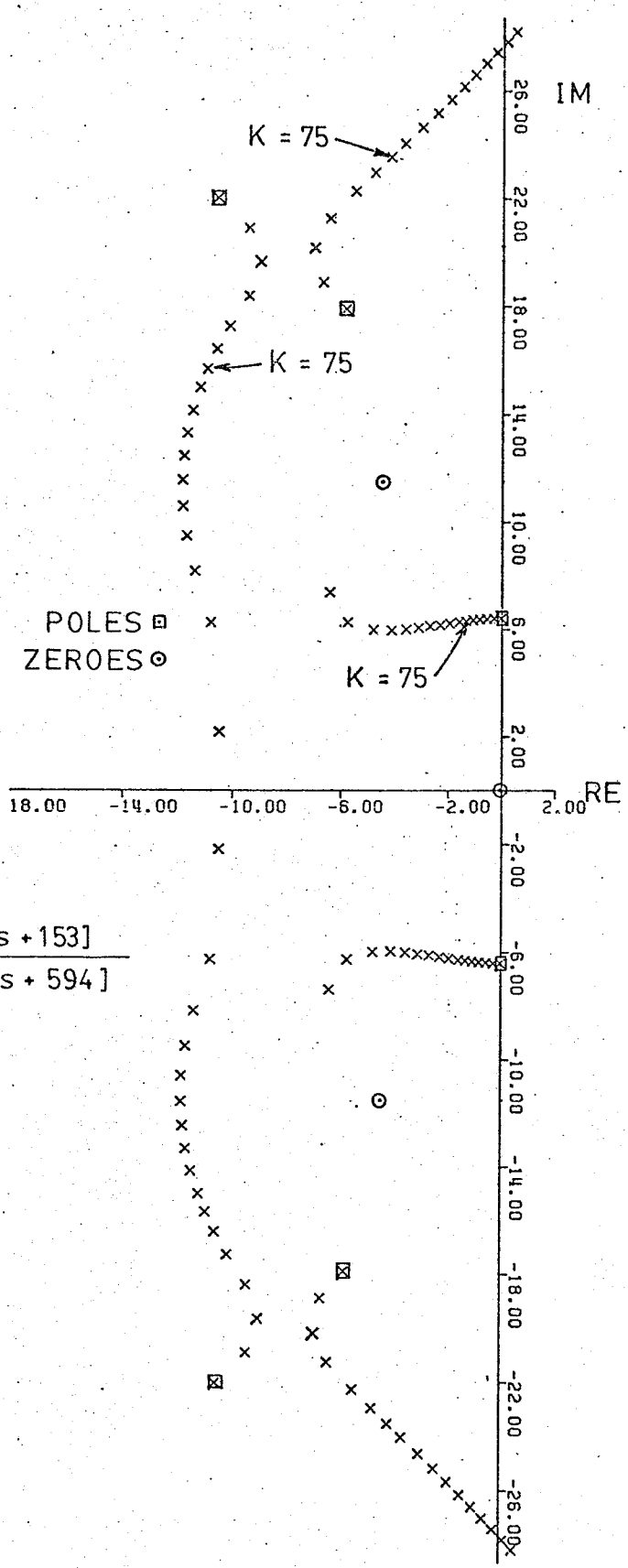

$$G_c(s) = \frac{K[s^2 + 9s + 153]}{[s^2 + 21s + 594]}$$

$K_e = 140$

FIG. 3.4 (b)

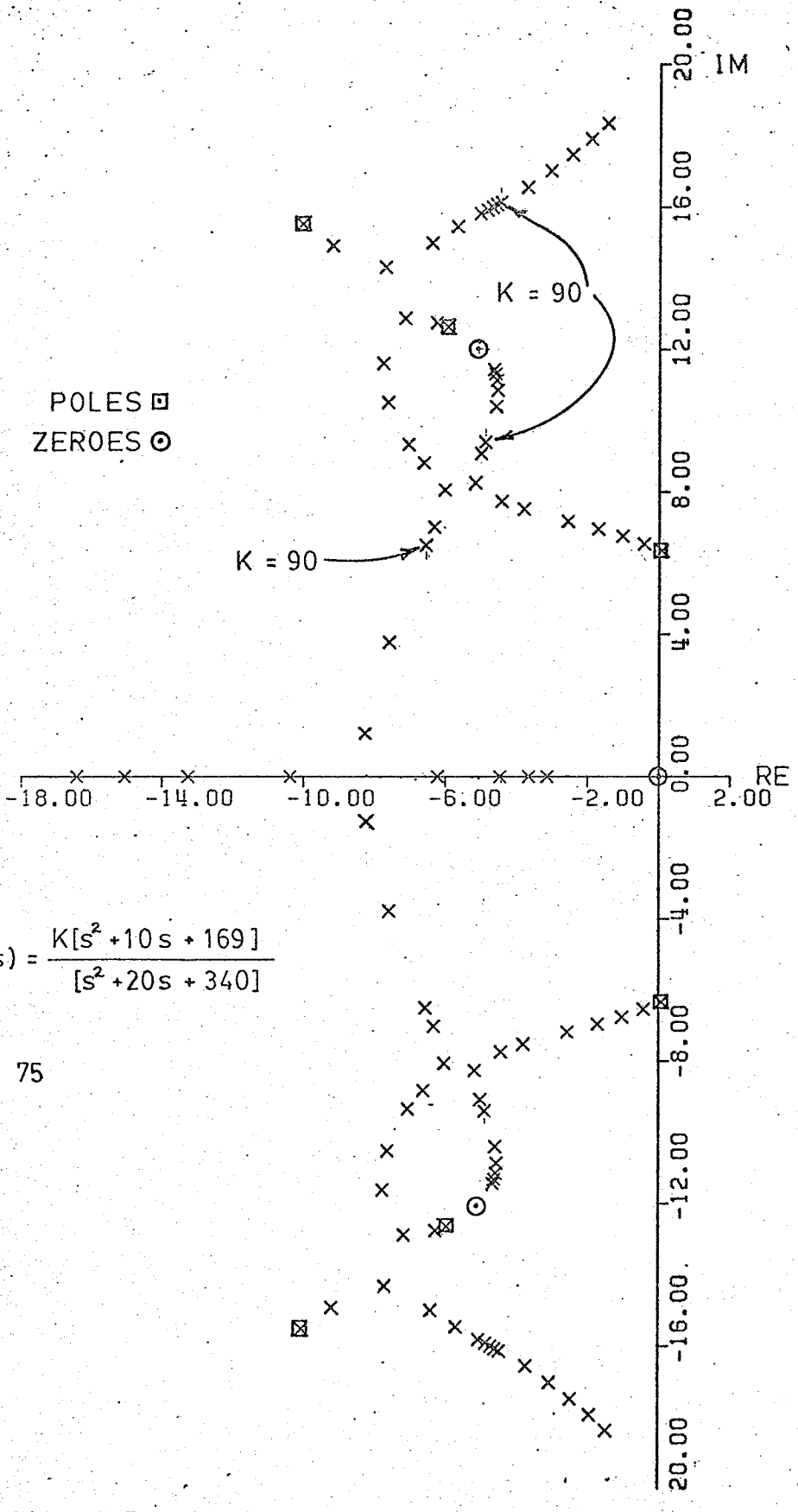

$$G_c(s) = \frac{K[s^2 + 10s + 169]}{[s^2 + 20s + 340]}$$

$K_e = 75$

FIG. 3.5

obtain the optimum case one would have to resort to some sort of computer optimizing routine. Although this approach would probably improve the results it is questionable whether the additional effort and cost associated with such a course of action would allow one to arrive at a dramatically better solution. At any rate, a suitable computer routine is not immediately obvious and, it is thus felt that the method employed is adequate, especially in light of the fact that an entirely different form of analysis will be applied in the following section.

In examining the results for the compensator selected it can be seen that the dominant roots are in the desired location specified earlier. The root locations are rather insensitive to the gain setting on the compensator since a relatively large change in gain is required to produce a marked change in the root locations. The appropriate gain setting seems to be somewhere slightly above 100. Further examination shows that the original high frequency roots of the sytem have been forced to go further into the left hand S-plane. Also, since the compensator zeroes are located in close proximity to the original machine roots, the residues associated with these roots should be small and they should therefore not appreciably contribute to the time response of the system. It should be noted that an excessive compensator gain will cause the system to take on a high frequency type of response due to the dominance of the compensator poles. With the exciter gain set to 140, the plot still proves to be acceptable and thus the compensator should be applicable for a reasonable range of parameter values. Analog computer studies of the above cases confirm these observations and will be discussed further in a subsequent section.

c) Phase Angle Criteria

The phase and magnitude relations for the machine infinite bus system can be determined by referring back to the Heffron - Phillips model. Through careful examination the stabilizer requirements can be derived on the basis of this analysis.

To examine the effect of $G_c(s)$ a block diagram showing the component of torque which it produces from a frequency derived signal is given in Fig. 3.6. The transfer function becomes:

$$\frac{\Delta T}{\Delta \omega} = \frac{G_c(s) k_e k_2 k_3}{1+k_e k_3 k_6+(T_e+T_{dz}')s+T_e T_{dz}' s^2} \quad \text{- - - - - - - -} \quad (3.7)$$

From previous discussions the above component of torque will contribute to damping for low phase angles, while at increasing phase angles the damping component will become less dominant and the synchronizing component will take on prominence. A positive synchronizing component corresponds to lagging phase angles in eq'n (3.7) while negative synchronizing torque corresponds to a leading phase angle.

In view of these observations the following criteria for the synthesis of $G_c(s)$ have been developed [5]. At low frequencies the machine function has small lagging phase angles and thus a small synchronizing component. The function $G_c(s)$ should therefore provide only small leading phase angles which are smaller in magnitude than the lagging angles of the machine function by itself. This will allow the presence of a small positive synchronizing component of torque in eq'n (3.7) which will add to the synchronizing component created through the

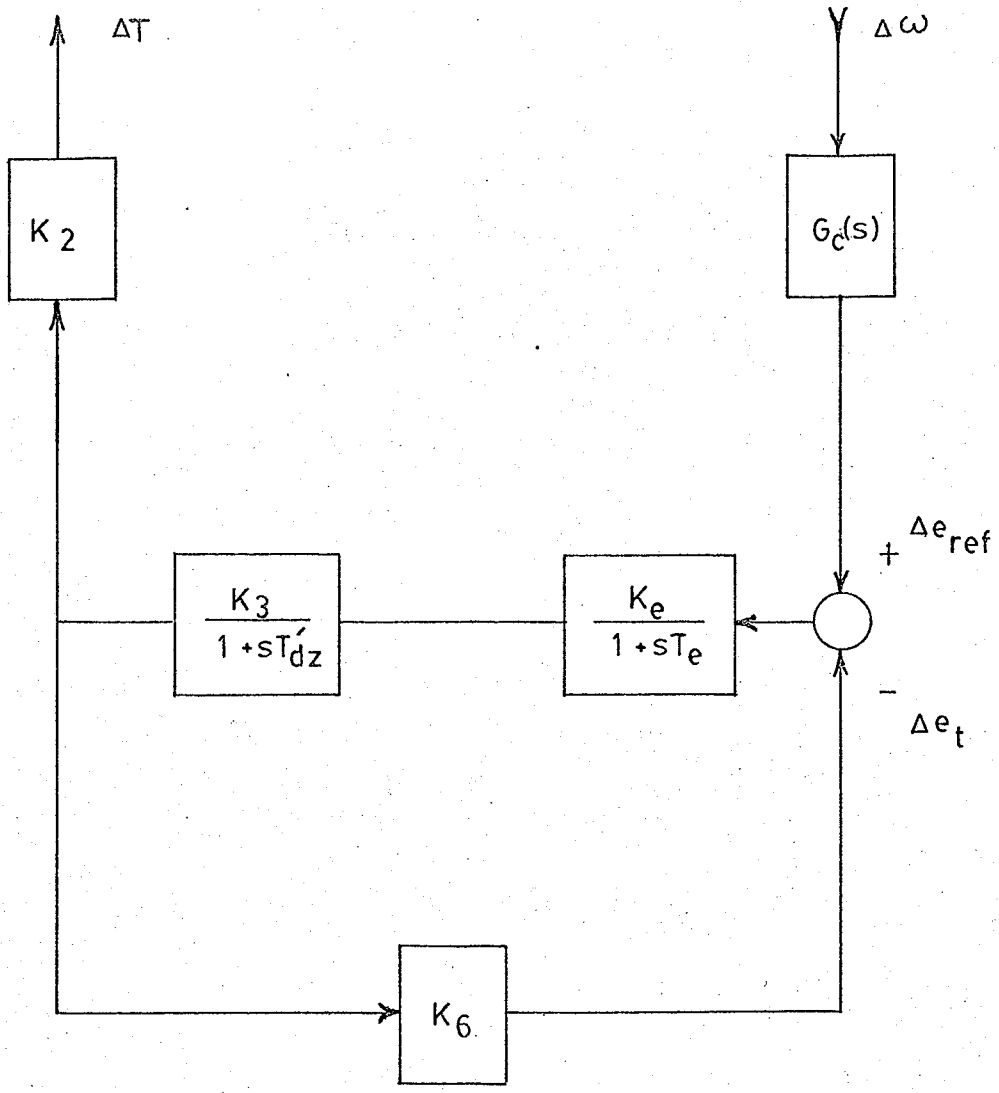

FIG. 3.6 Component of torque produced by voltage regulator action in response frequency derived signal.

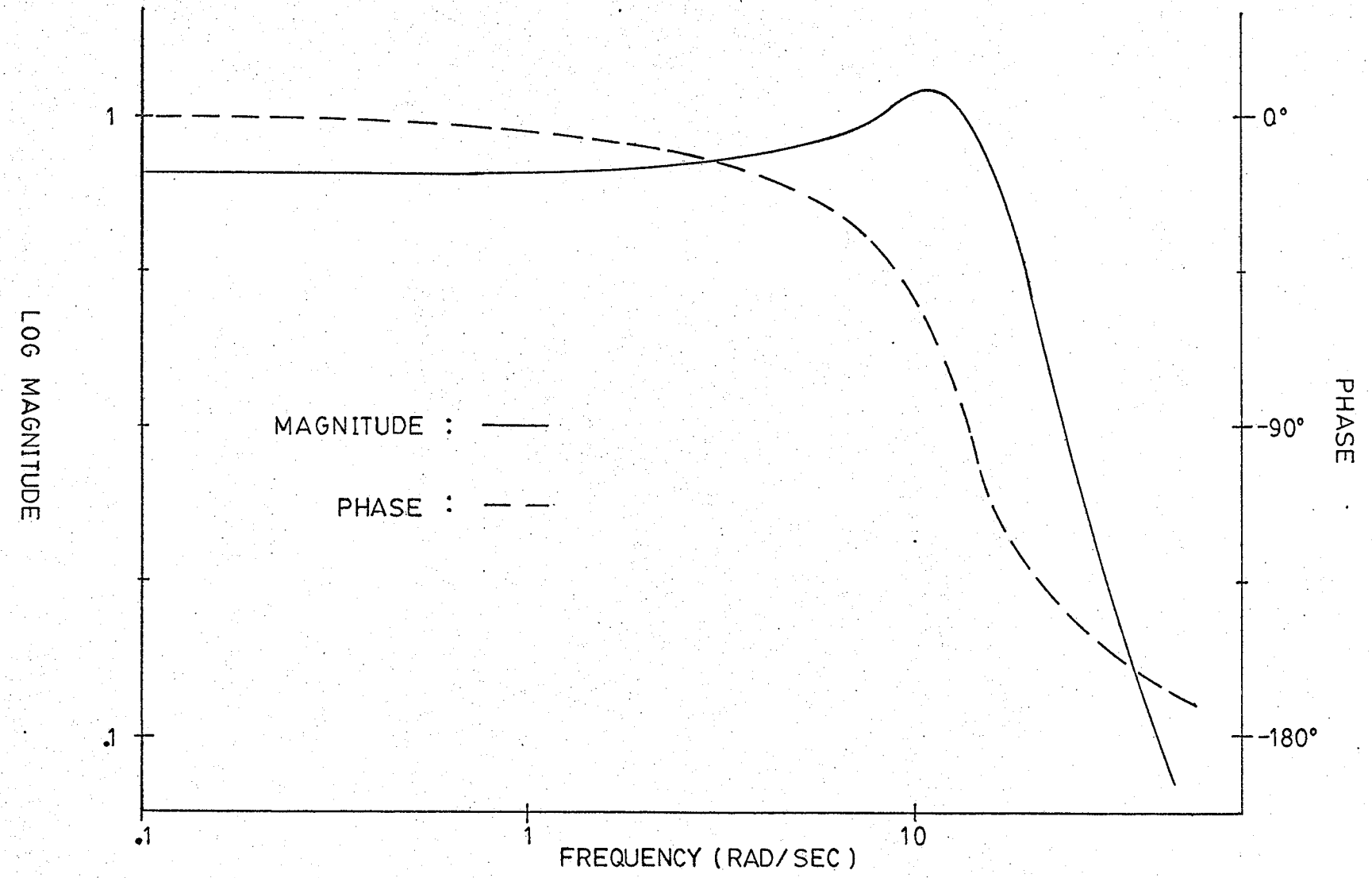

FIG. 3.7 Bode Plot of Mach. Function (k_e = 75)

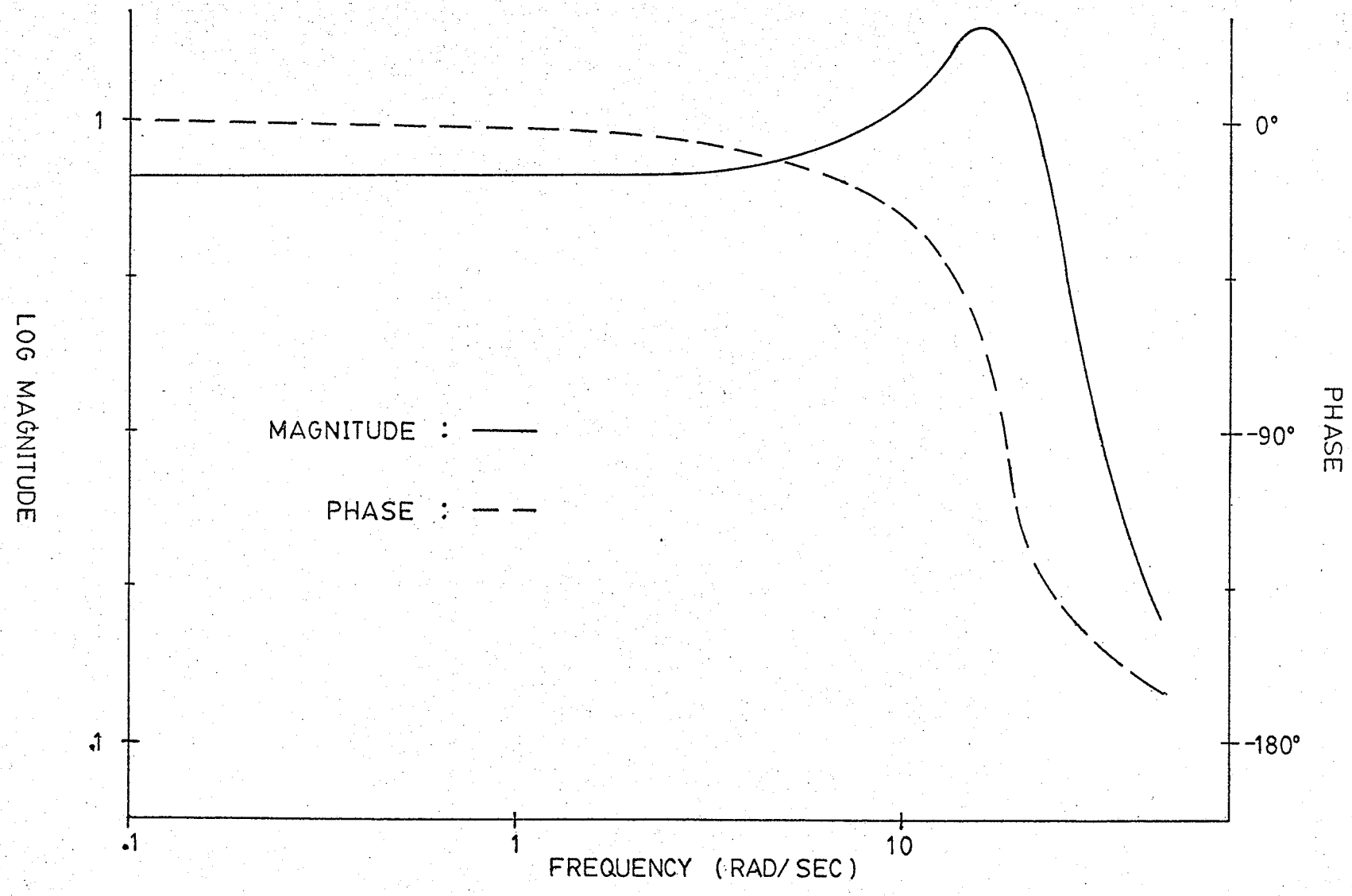

FIG. 3.8 Bode Plot of Mach. Function (k_e = 140)

k_5 loop (using a medium - high regulator gain). Damping will thus be provided without degrading the synchronizing torques.

For higher frequencies, the lag for the transfer function between ΔT and Δe_{ref} will always be greater than the lead which can be provided through $G_c(s)$ due to physical limitations. Therefore, positive synchronizing torques will always be present. However, up to the frequency range of interest, it would be desirable to prevent the overall phase angle from getting too large. Large phase angles would create excessive synchronizing torques which would result in a highly oscillatory system response. The criteria established requires that the phase angle of eq'n (3.7) be limited to a maximum value of approximately 30^o lagging over the frequency range of interest (0 - 3Hz).

Returning once again to eq'n (3.7) it can be seen, through calculation, that the roots of the denominator polynomial correspond to the high frequency complex conjugate poles of the system shown in Fig. 3.1. It is therefore apparent that the compensation to be performed involves the cancellation of the effect of these roots and replacing them with roots that meet the phase angle requirements stated earlier. If the previous root locus plots are examined in the light of this statement it can be observed that the best result obtained did in fact follow this line of reasoning.

The Bode plot for the machine function calculated for the indicated values are shown in Fig. 3.7 and 3.8.

Trial and error is again applied at this point so as to select the coefficients of $G_c(s)$ which produce a good overall phase angle

response for the whole system. In the selection of these coefficients for $G_c(s)$ it was attempted to synthesize a function which gave good results for a range of exciter gains. A design was selected for k_e = 75 after which k_e was changed to 140 and $G_c(s)$ was subsequently redesigned to suit this case. Finally, a compensator was selected which should be applicable for both cases.

The method of pole-zero selection for $G_c(s)$ was based on the following procedure. The zero of $G_c(s)$ was placed directly below the system pole to be compensated. The zero was placed beneath the pole so that the overall phase lag would not be excessive. The residue associated with this machine pole should now be quite small because of the compensator zero.

In the previous section the dominant root was selected so that the real part was greater than or equal to 2.7 to attain a short settling time. For the compensator poles to be nondominant their real part should be between 5 and 10 times further away from the $j\omega$ axis than the real part of the dominant pole. This now leaves one to select the imaginary part so as to satisfy the overall phase angle criteria.

Figures 3.9 and 3.10 show the Bode plots for the compensated system of eq'n (3.7). The compensator used was designed to be applicable for a k_e of 75 and 140.

A computer plot of the root locus is constructed for the above compensator and is shown in Fig. 3.11. The plot verifies that the system's high frequency pole is effectively cancelled from the system response and is replaced with the compensator pole which is sufficiently removed to have a negligible contribution. Referring to Fig. 3.4 indi-

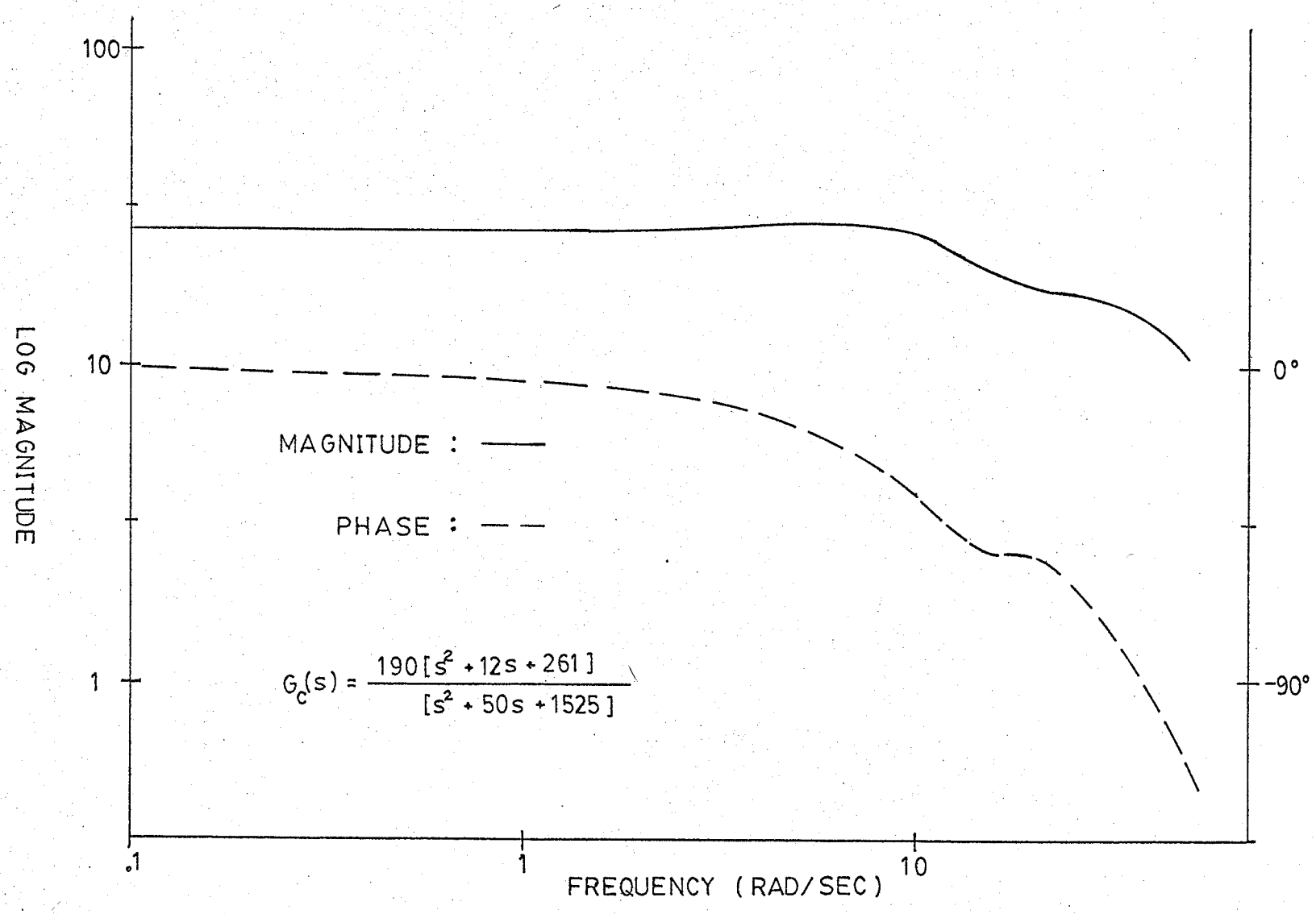

FIG. 3.9 Bode Plot of torque signal with compensation (k_e = 75)

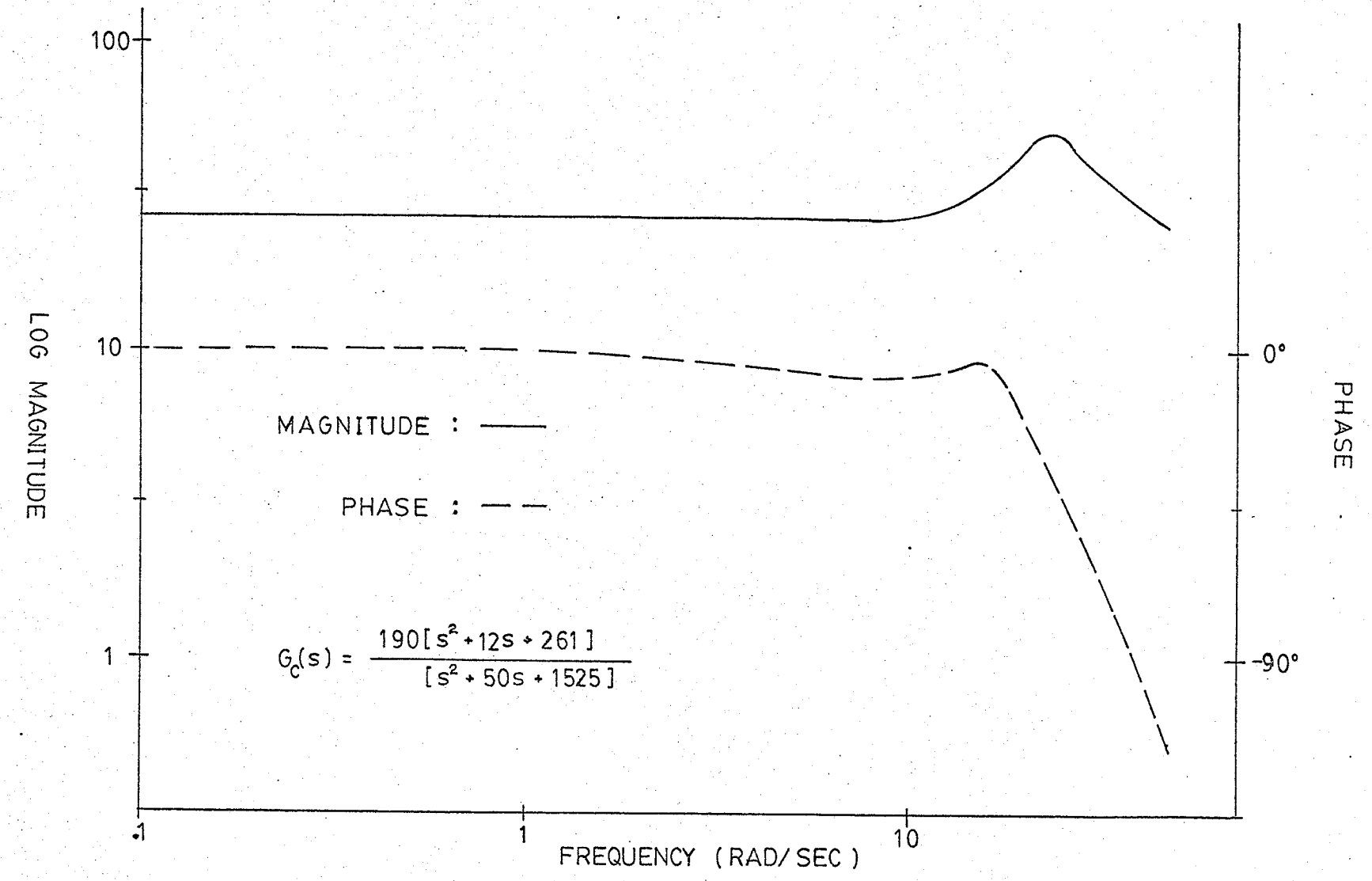

FIG. 3.10 Bode plot of torque signal with compensation (k_e = 140)

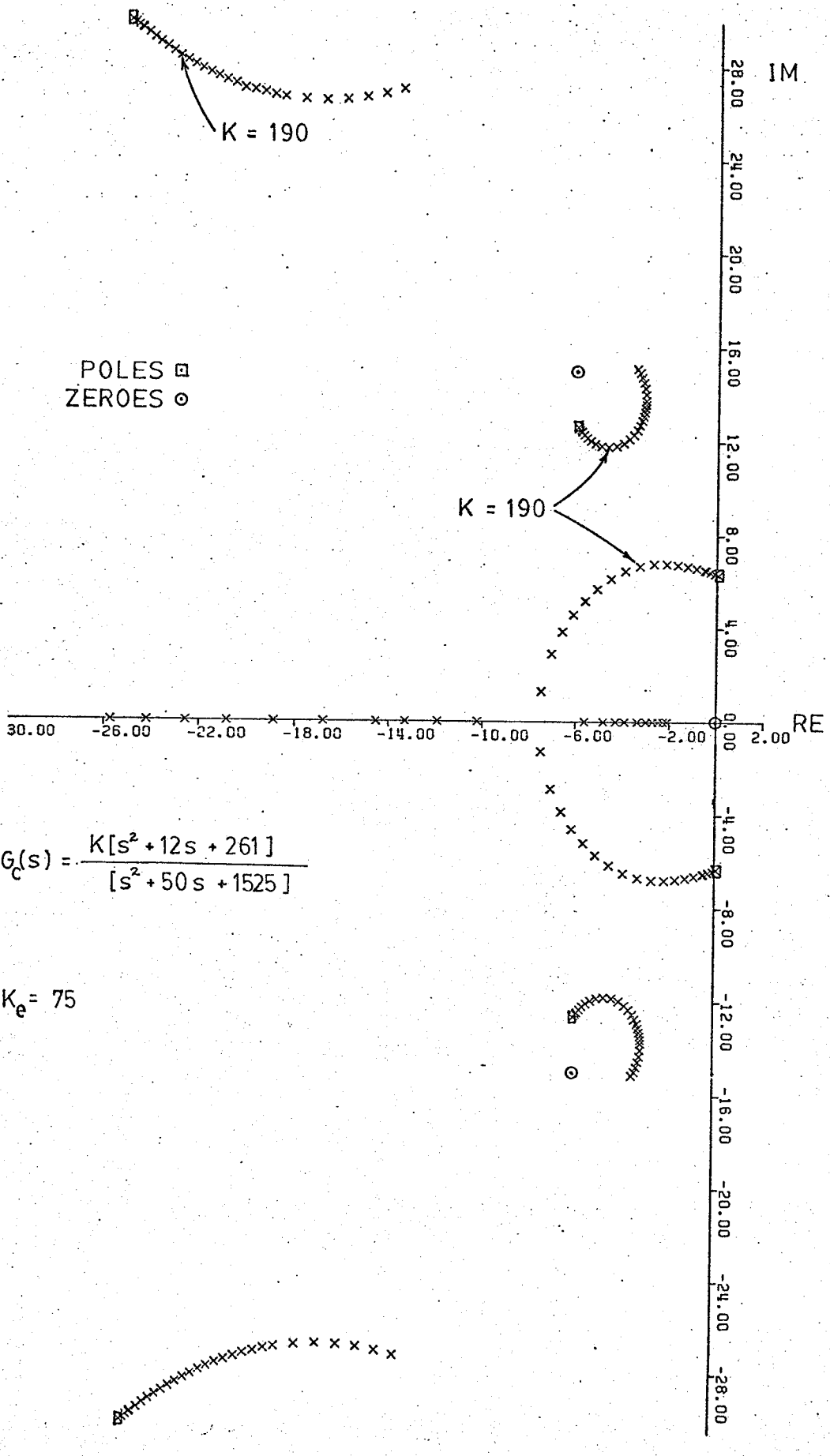

$$G_c(s) = \frac{K[s^2 + 12s + 261]}{[s^2 + 50s + 1525]}$$

$K_e = 75$

FIG. 3.11

cates that the major difference in the two design methods rests with the compensator pole locations. The final system root corresponding to this pole is further out into the left hand S-plane for the case illustrated in Fig. 3.11. The dominant root locations of Fig. 3.11 are satisfactory when the gain factor k is set to 190. The compensated characteristic root locations can be seen to be relatively insensitive to gain variations.

In summary it can be stated that the final design of a suitable form of compensator can best be accomplished with the use of S-plane techniques and frequency response methods. A design based solely on one method of analysis could produce good results provided enough trials were made. Using a second method however, allows a greater confidence in the solution obtained.

d) Analog Computer Results

To check the above analysis in the time domain the Heffron Phillips model was programmed onto an analog computer. The computer diagram for the model is shown in Fig. 3.12. All the computer variables have been scaled according to standard practice [12] and the procedure is shown in Appendix C.

In Fig. 3.13 the computer simulation of the system for the unstable operating condition using different values of T_e and T_{dz}' are shown for comparison.

In Fig. 3.14 the computer representation of the complex compensator is illustrated.

Fig. 3.15 shows the response of the uncompensated system to a disturbance using two values of exciter gain. The disturbance level for all the computer solutions which follow will be kept at this level so

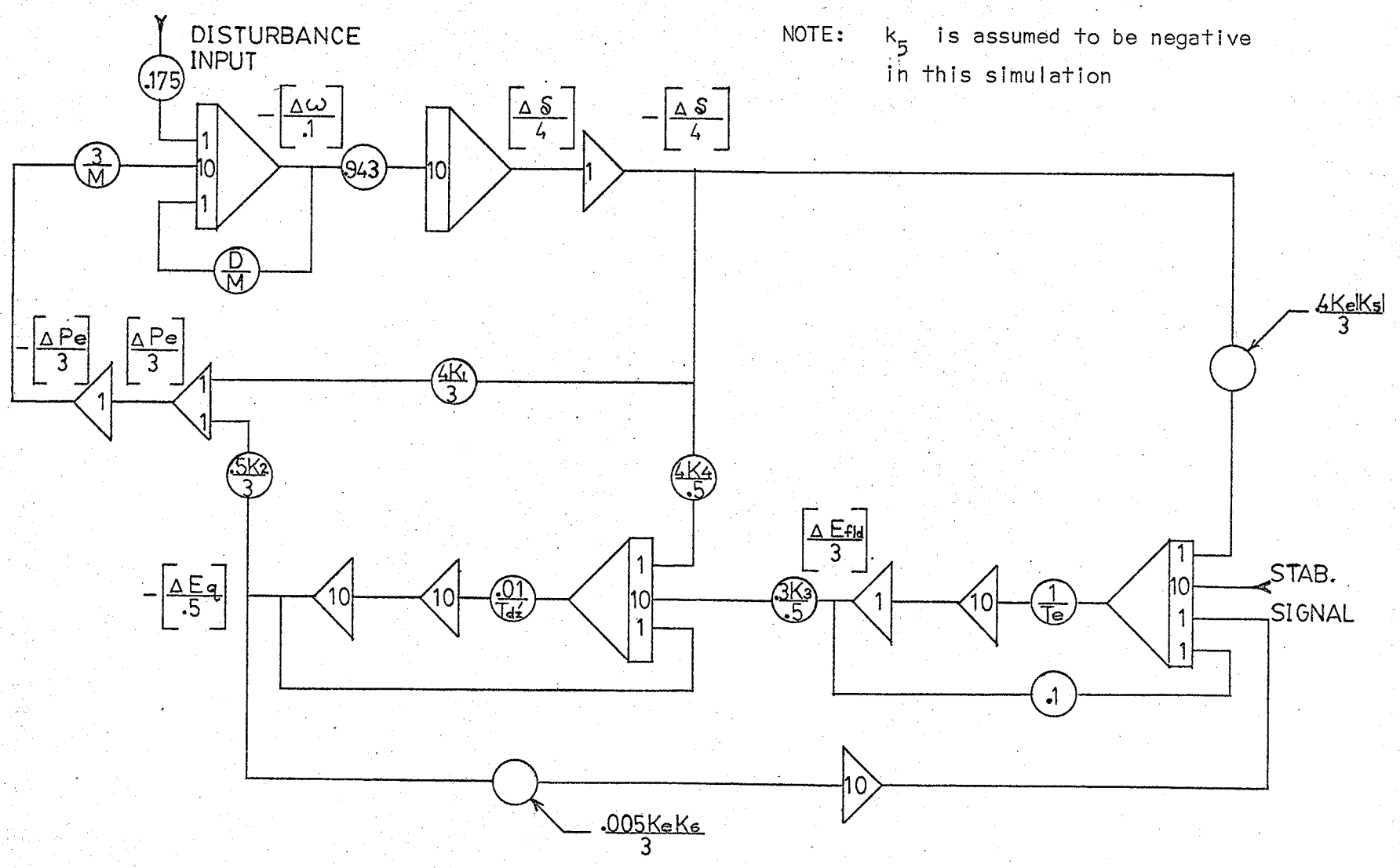

FIG. 3.12 Analog computer simulation of the Heffron Phillips model

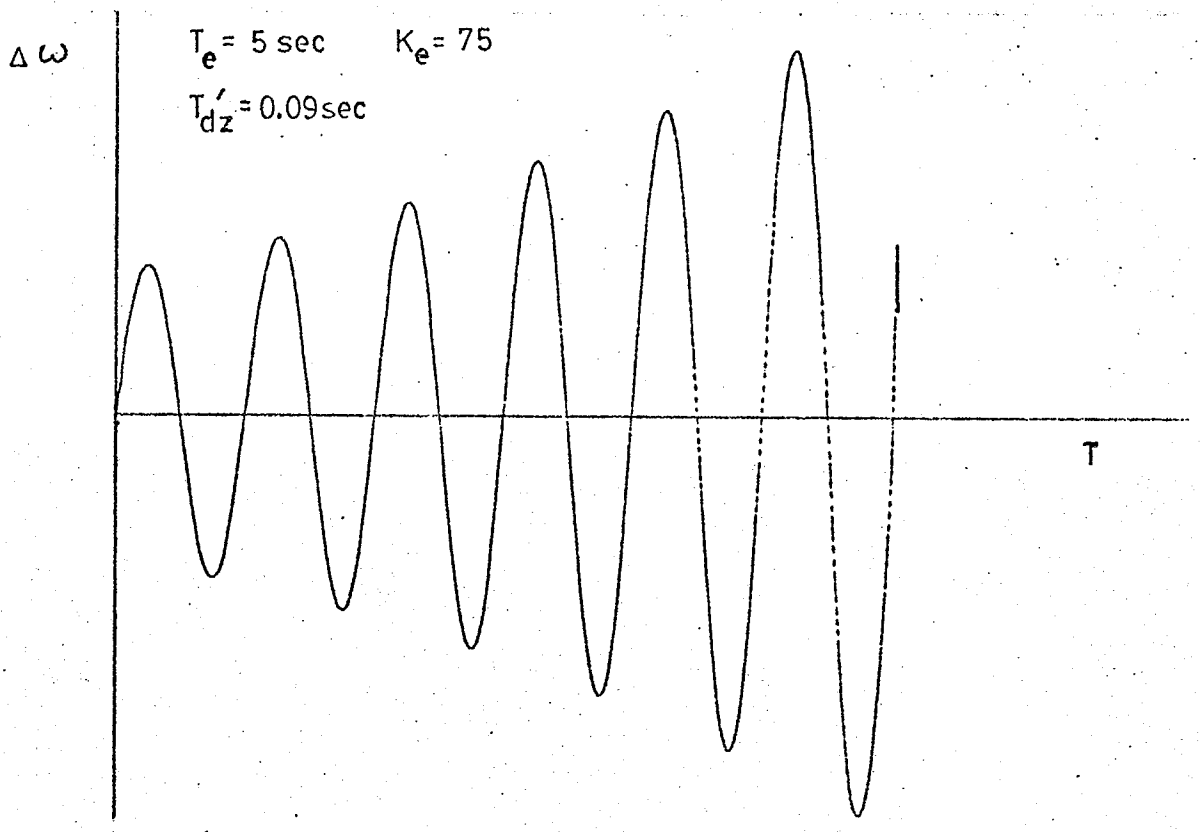

Fig 3.13(a)

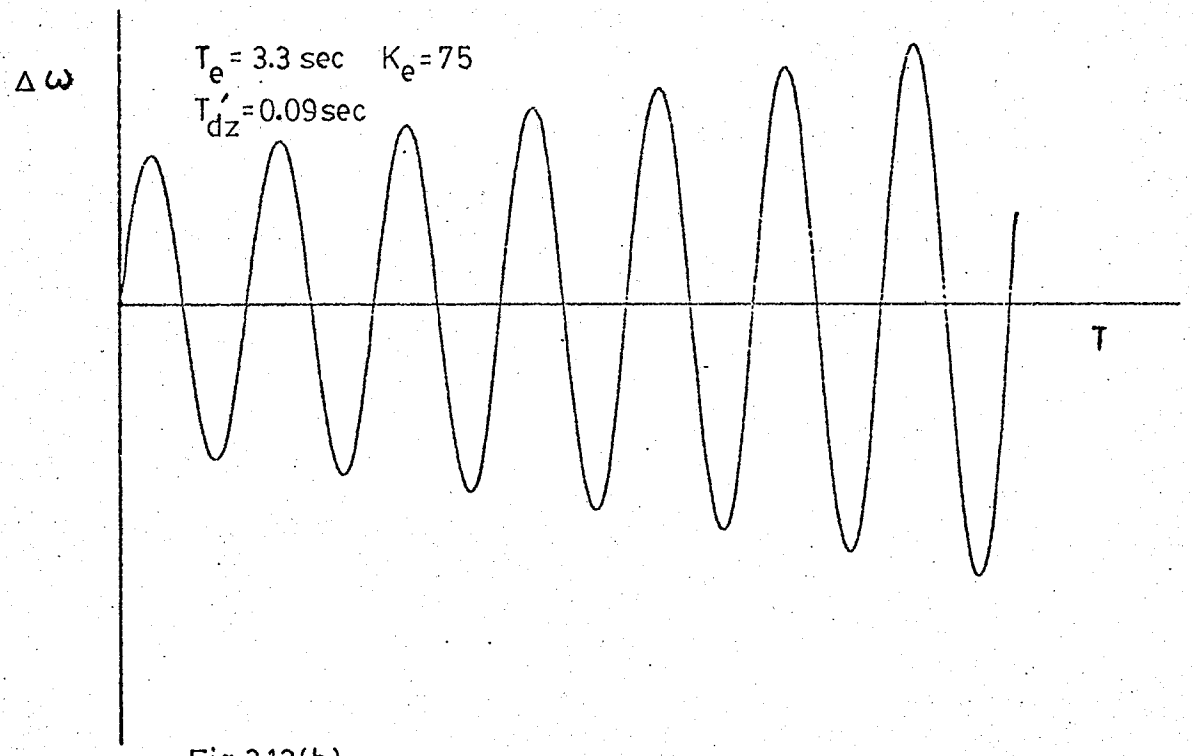

Fig 3.13(b)

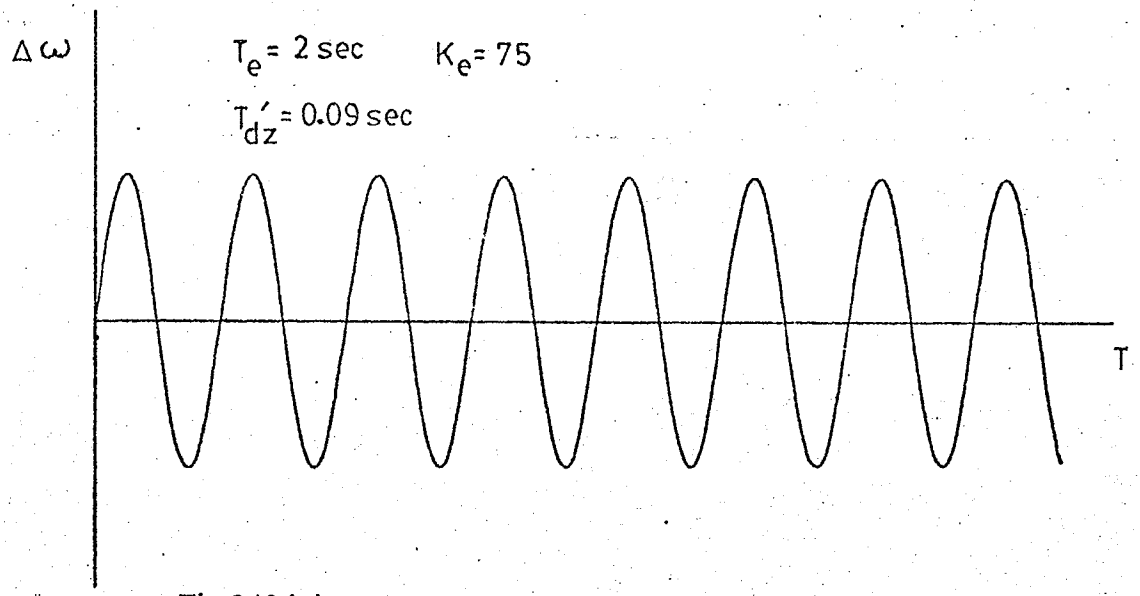

Fig 3.13 (c)

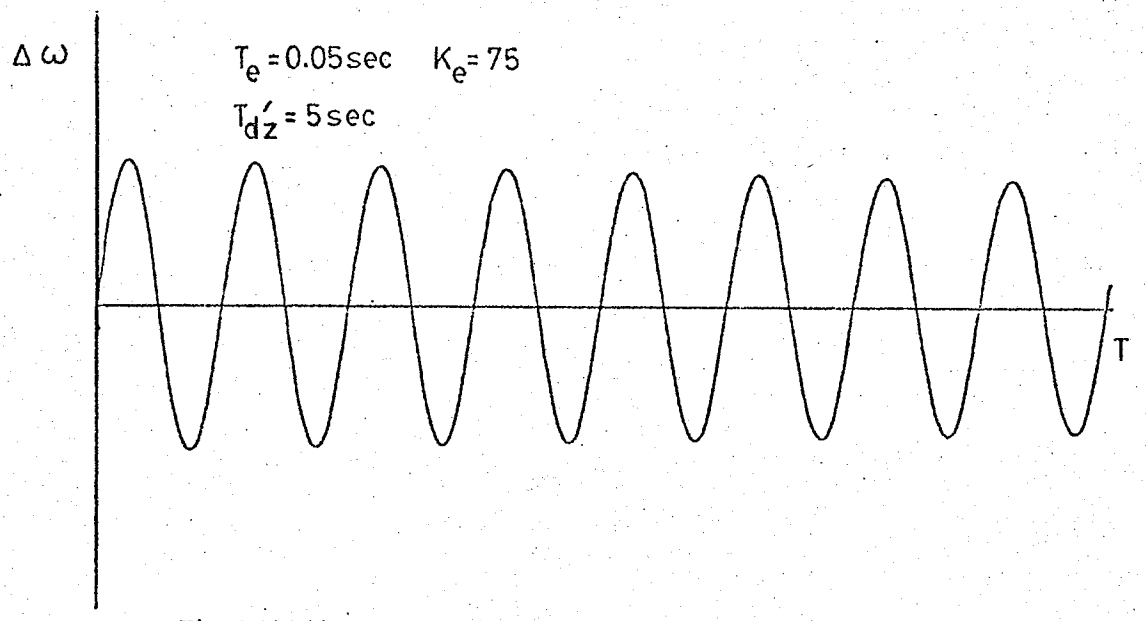

Fig 3.13(d)

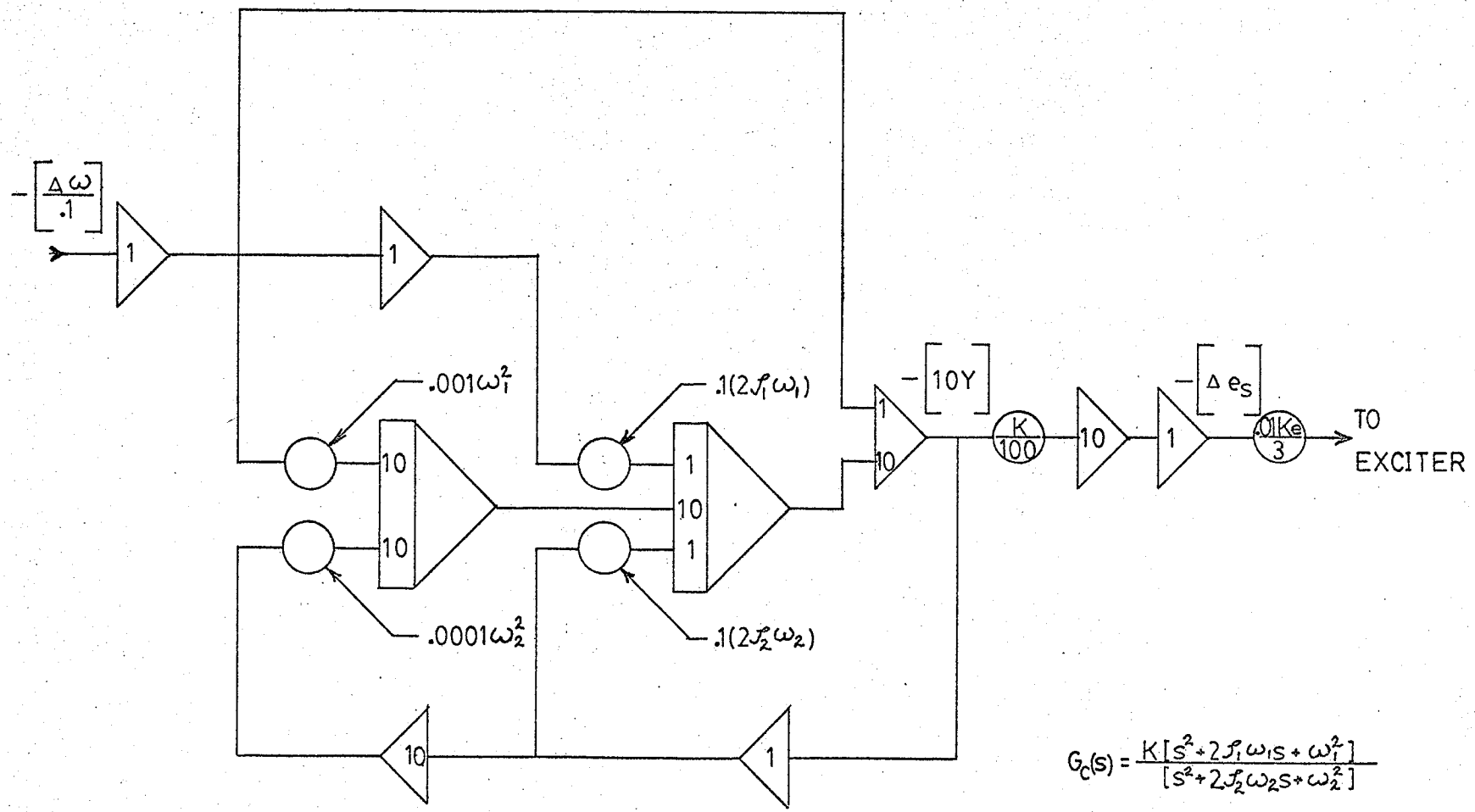

FIG. 3.14 Analog computer simulation of the complex compensator

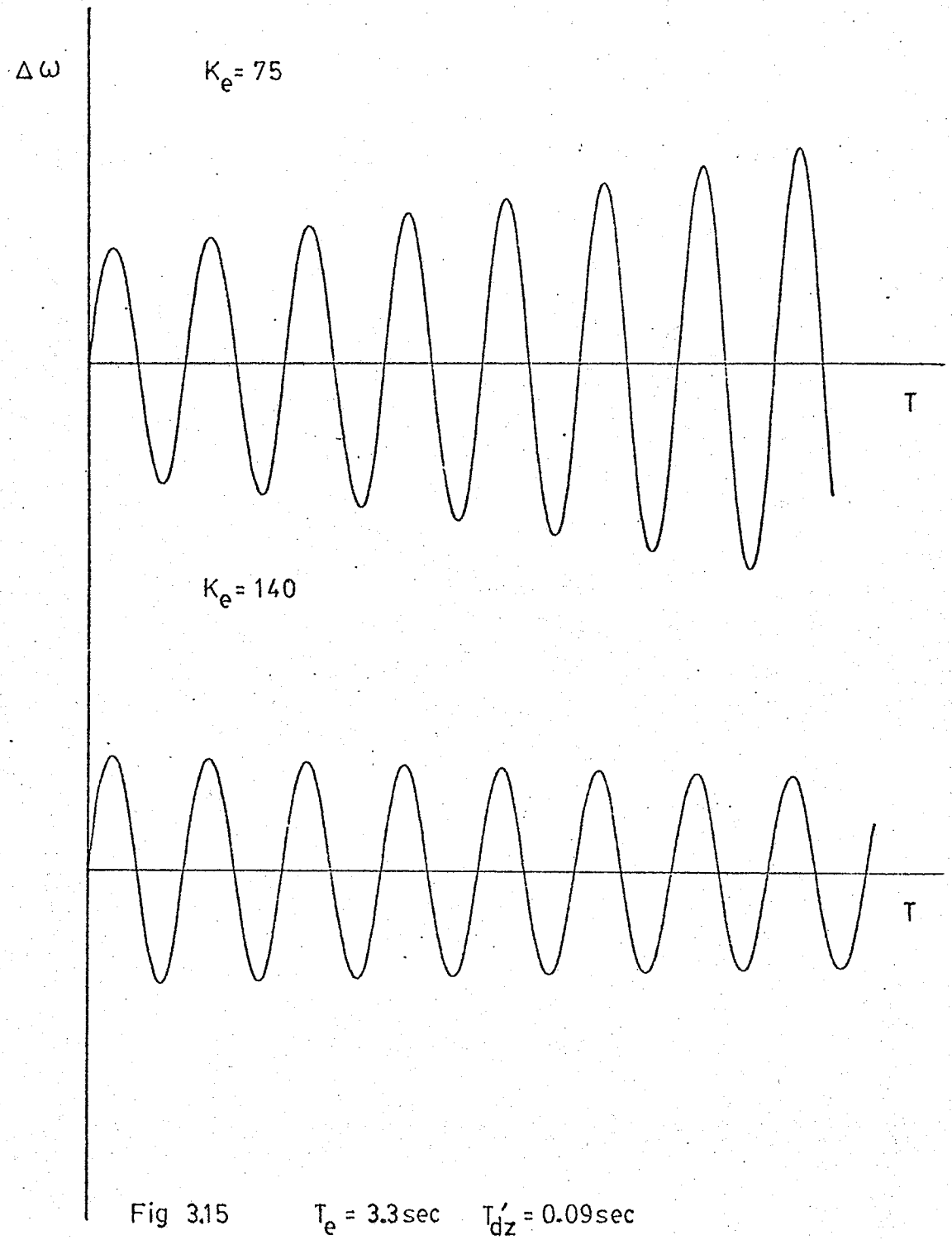

Fig 3.15 T_e = 3.3 sec T'_{dz} = 0.09 sec

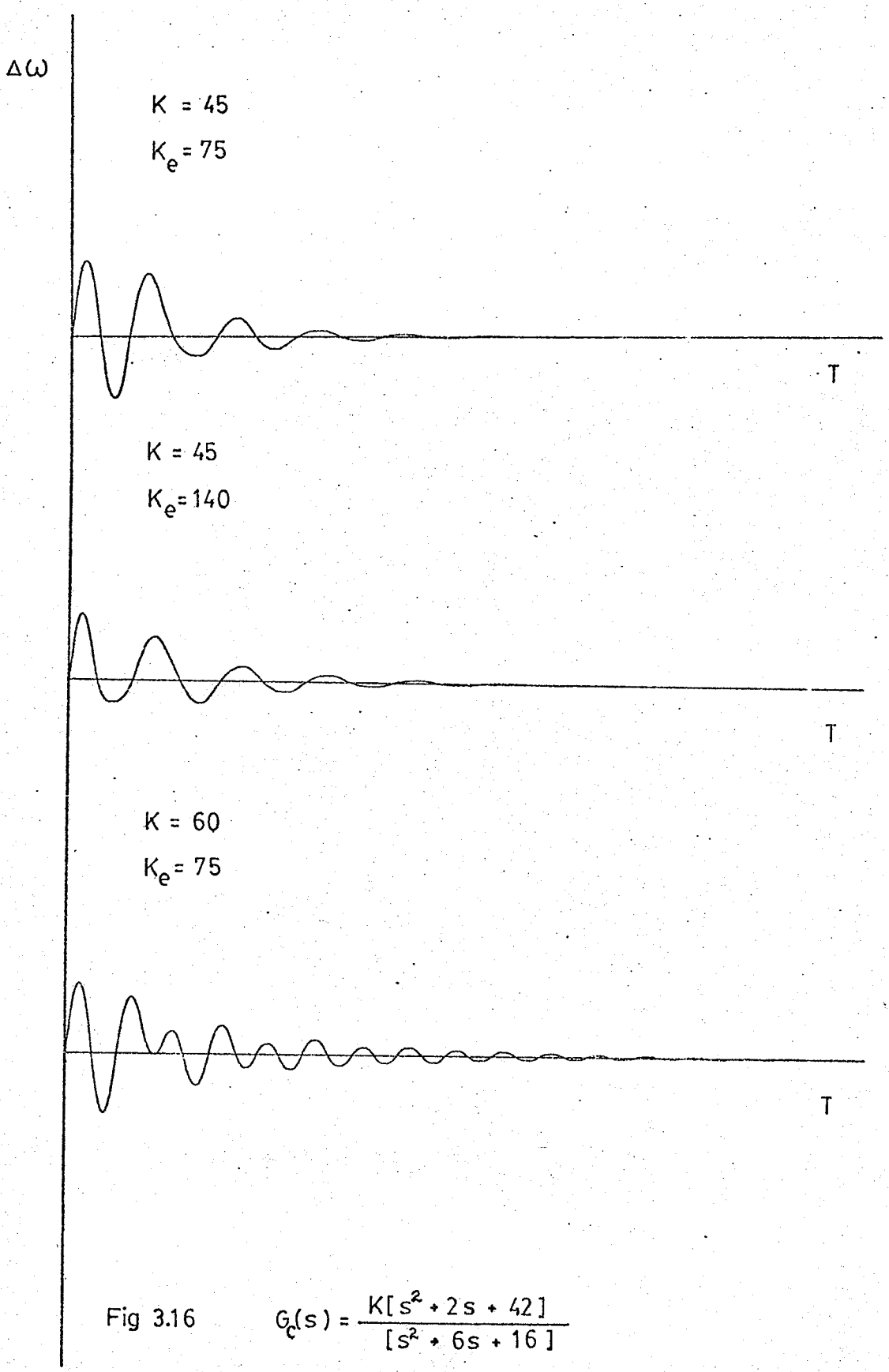

Fig 3.16 $G_c(s) = \frac{K[s^2 + 2s + 42]}{[s^2 + 6s + 16]}$

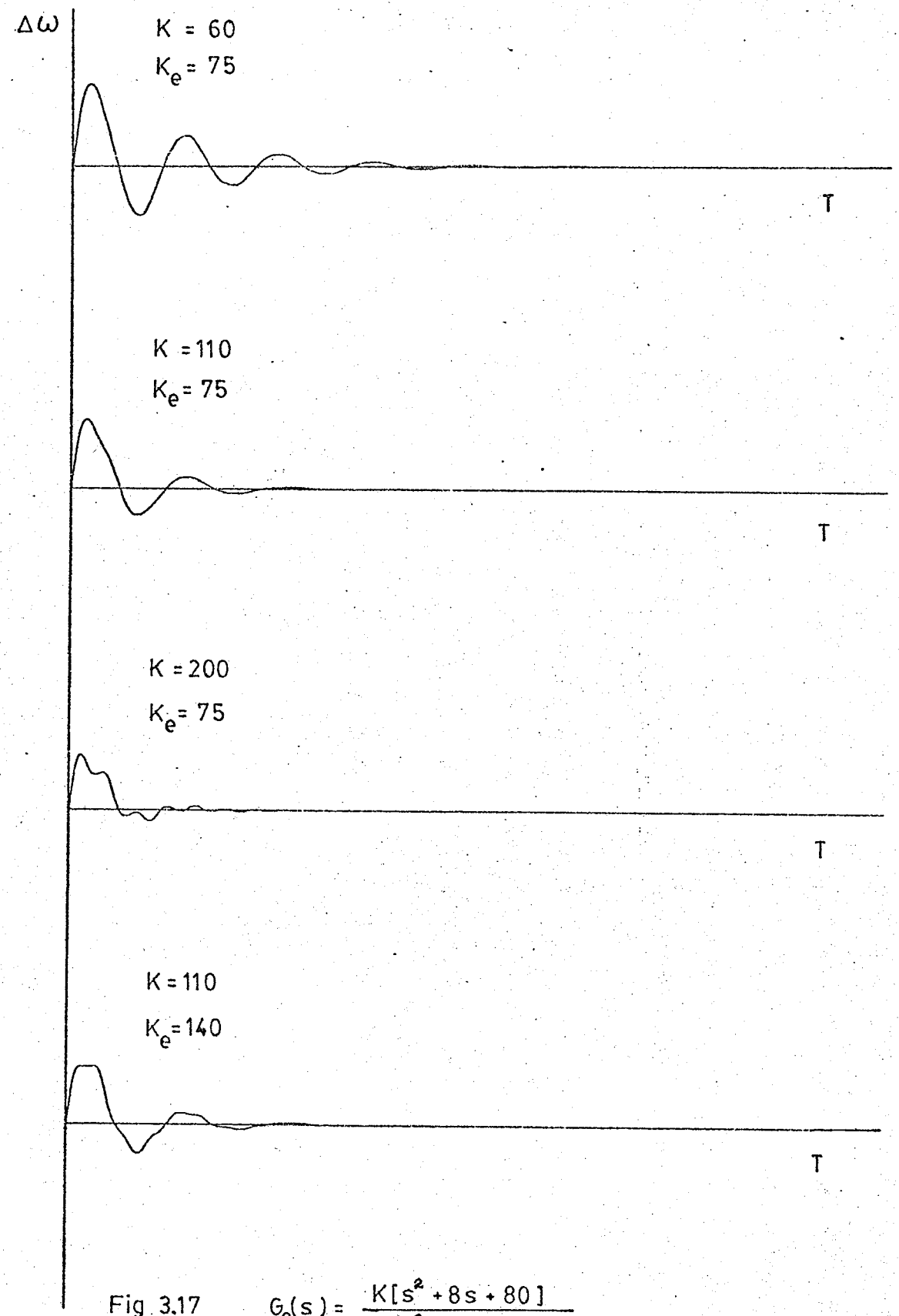

Fig 3.17 $G_c(s) = \dfrac{K[s^2 + 8s + 80]}{[s^2 + 20s + 296]}$

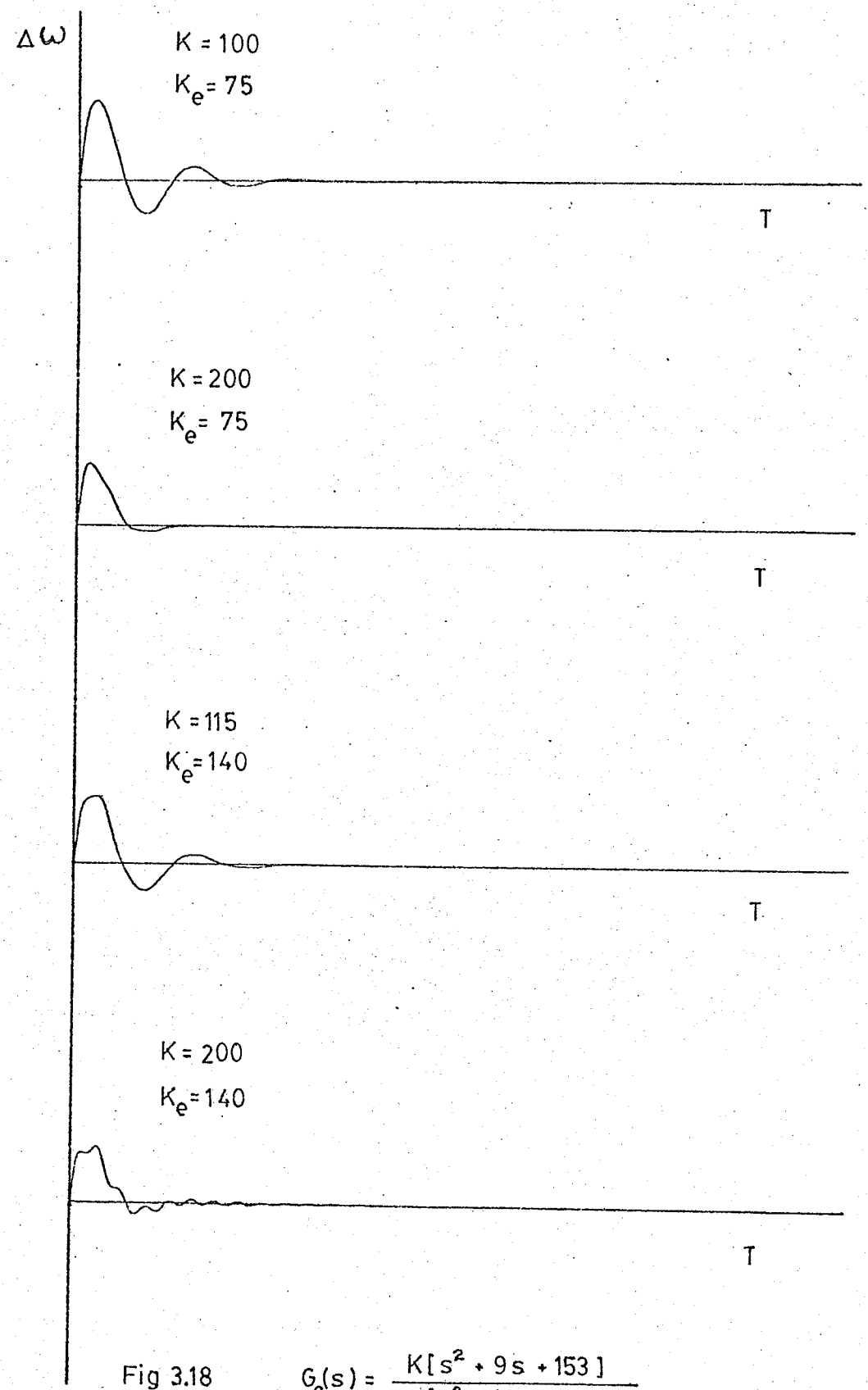

Fig 3.18 $G_c(s) = \dfrac{K[s^2 + 9s + 153]}{[s^2 + 21s + 594]}$

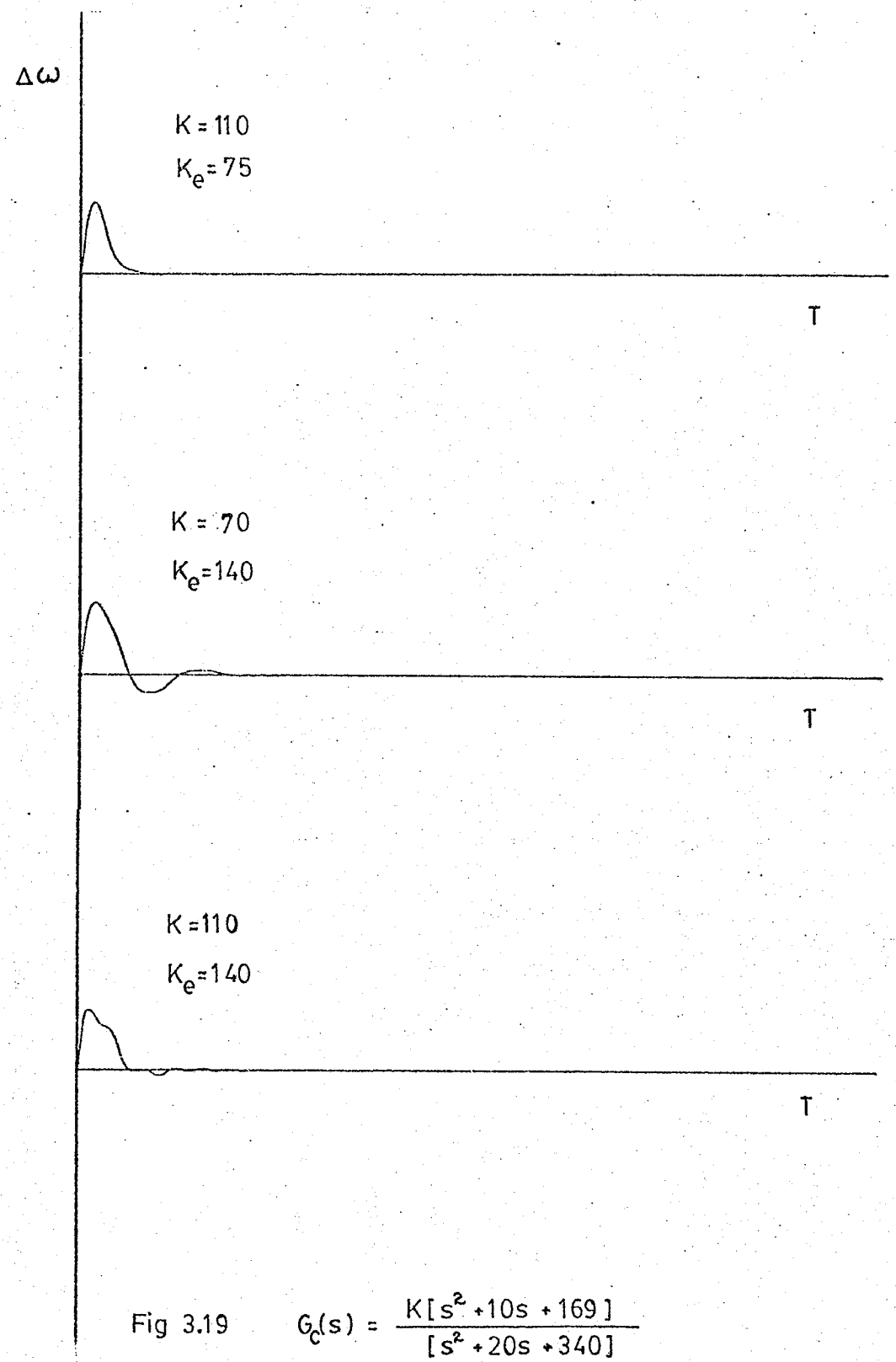

Fig 3.19 $G_c(s) = \frac{K[s^2 + 10s + 169]}{[s^2 + 20s + 340]}$

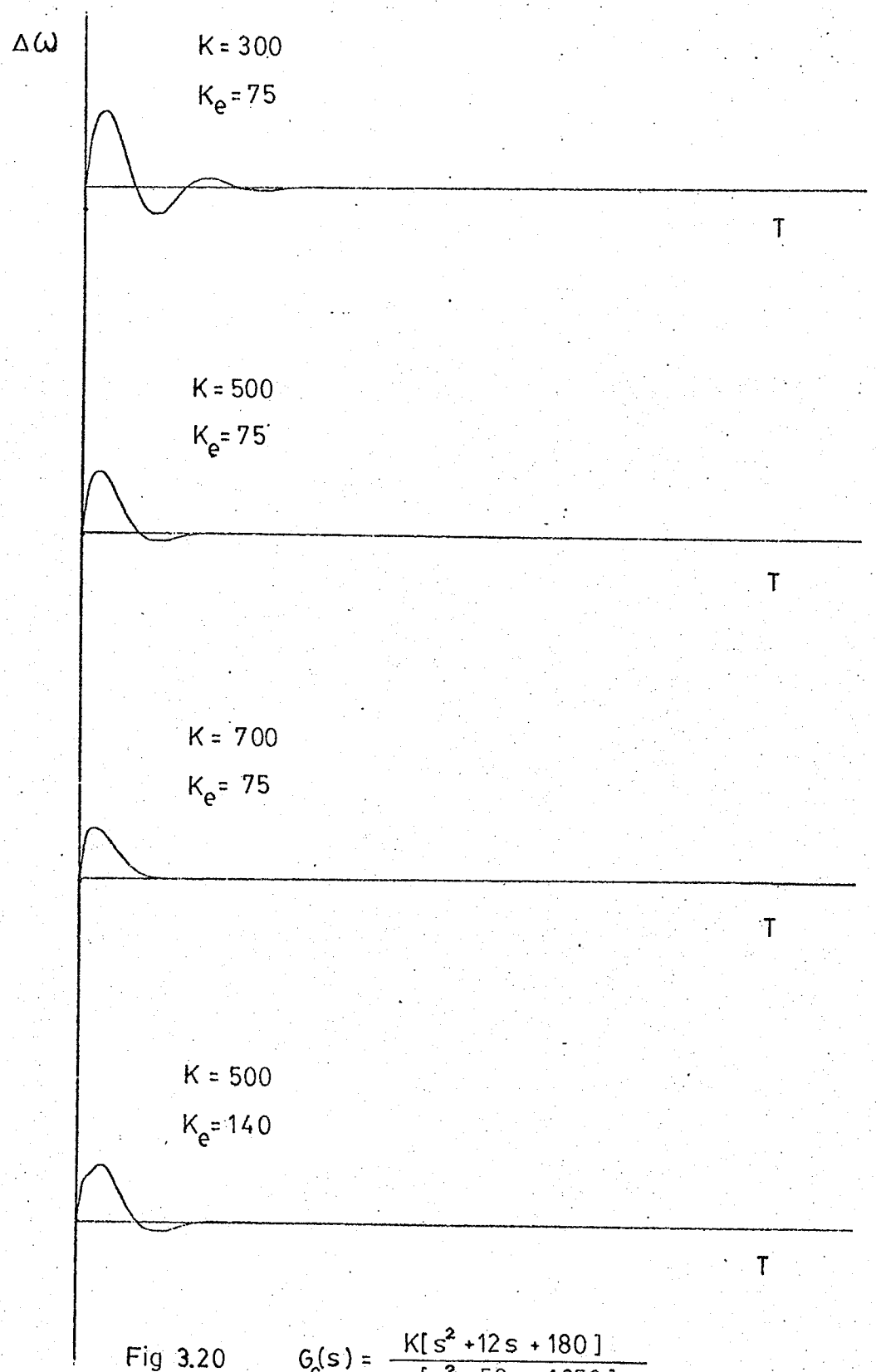

Fig 3.20 $G_c(s) = \dfrac{K[s^2 + 12s + 180]}{[s^2 + 50s + 1850]}$

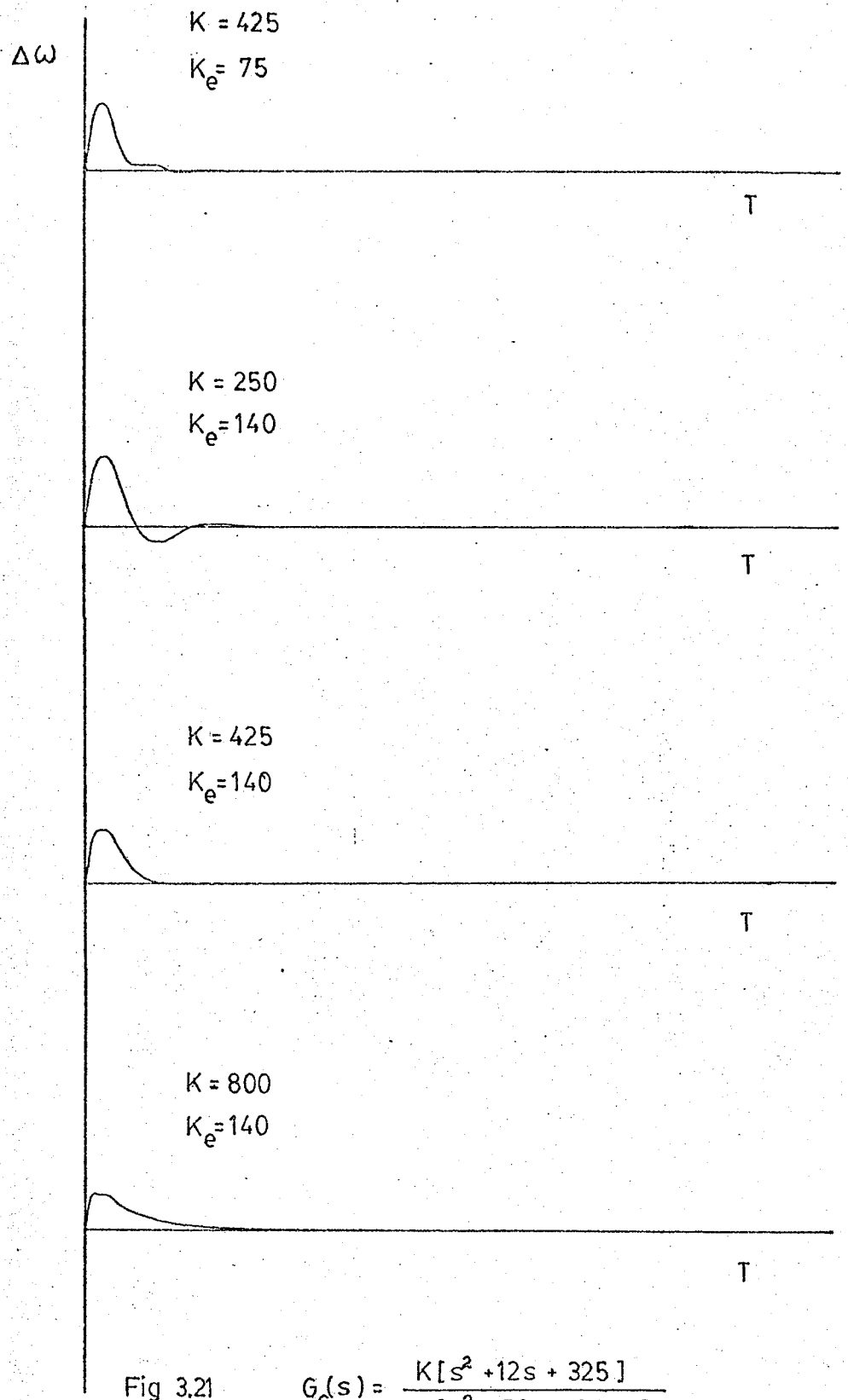

Fig 3.21 $G_c(s) = \dfrac{K[s^2 + 12s + 325]}{[s^2 + 50s + 2225]}$

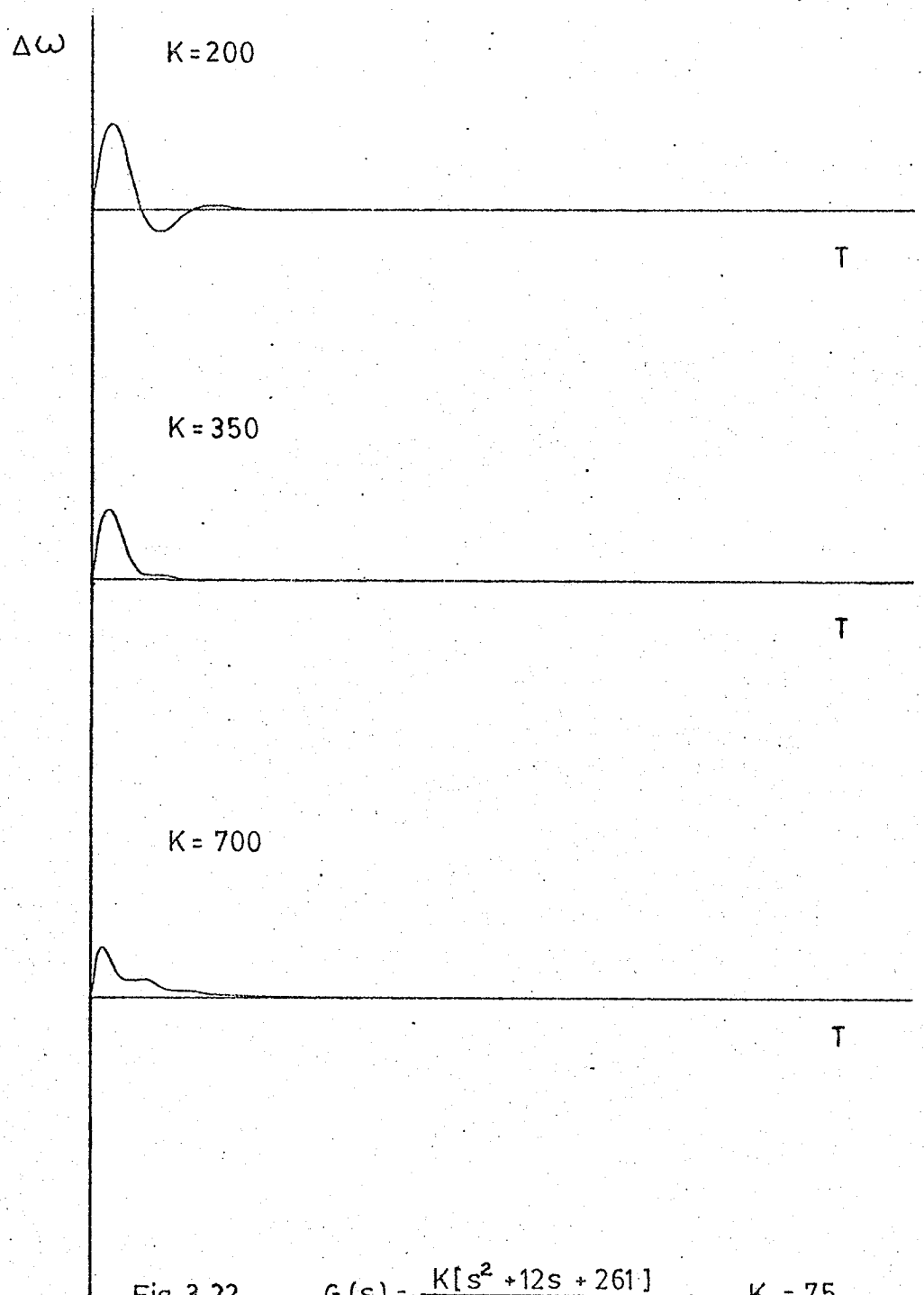

Fig 3.22 $G_c(s) = \frac{K[s^2 + 12s + 261]}{[s^2 + 50s + 1525]}$ $K_e = 75$

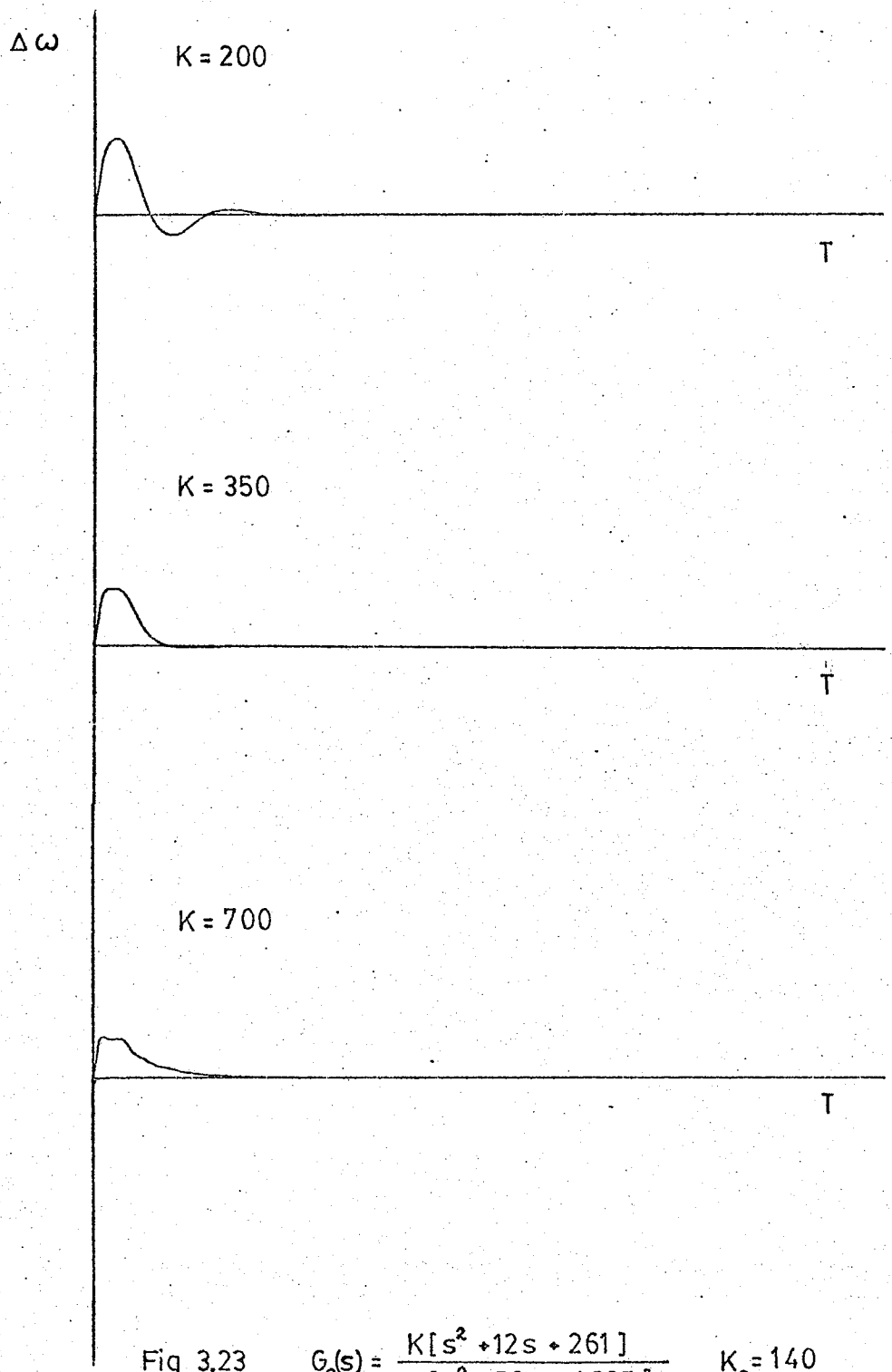

Fig 3.23 $G_c(s) = \frac{K[s^2 + 12s + 261]}{[s^2 + 50s + 1525]}$ $K_e = 140$

that an easy comparison of the results can be made.

Fig. 3.16 to 3.19 show the computer simulation for the different cases examined with the root locus technique. The simulations utilized the operating point determined in Chapter II with T_e set to 3.3 seconds. The results show each compensator's performance with high and low exciter gain and various values of compensator gain.

Fig. 3.20 and 3.21 indicate the performance of the compensators derived using frequency response techniques. Fig. 3.20 shows the results obtained for a compensator specifically designed for a k_e of 75 while Fig. 3.21 corresponds to the design for k_e = 140.

Finally, Fig. 3.22 and 3.23 shows the performance of the compensator which complies with the requirements imposed by the root locus approach and the frequency response method for a low and high exciter gain.

3. Comparison To A Real Root Compensator

a) Compensator Description

The compensation illustrated in Fig. 3.22 and 3.23 appears to be quite satisfactory. To be able to make a competent judgement on the usefulness of the above form of compensation, a comparison to an alternate form of compensation already used with success should be tried.

The compensator selected for comparison is a simple real root compensator presently being applied with success at Manitoba Hydro's Kettle Rapids Generating Station. The mathematical description of this compensator is

$$G_c(s) = \frac{ks}{1 + Ts} \qquad \text{- - - - - - - - - - - - - - - - - - - (3.8)}$$

This compensator has the obvious advantages of a simpler form which implies that it should be easier to analyze and implement. If its performance can be shown to be at least comparable to the complex root compensator then, the utility of the complex form would be doubtful.

b) Root Locus Approach

The root locus of the system described by eq'n (3.3) is plotted by computer for three values of T as shown. These plots are shown in Fig. 3.24, 3.25 and 3.26. In addition Fig. 3.27 shows a plot for k_e = 140 and T = 0.5 seconds. Examining the above results indicates that a T = 0.5 sec and k = 11 produces the best results. It should be noted that a much lower value of compensator gain is required and that the system roots are more sensitive to its variation.

c) Phase Angle Criteria

Analysis from a frequency response standpoint produces the Bode plot of Fig. 3.28, 3.29, 3.30 and 3.31 corresponding to T = 2 sec. and k_e = 75, T = 1 sec. and k_e = 75, T = 0.5 sec. and k_e = 75 and T = 0.5 sec and k_e = 140 respectively. Again the situation using a T of 0.5 sec. produces the best results.

d) Analog Computer Results

The real root compensator was programmed on the analog computer as per Fig. 3.32 and subsequently interconnected with the rest of the system representation to observe its performance in the time domain. The

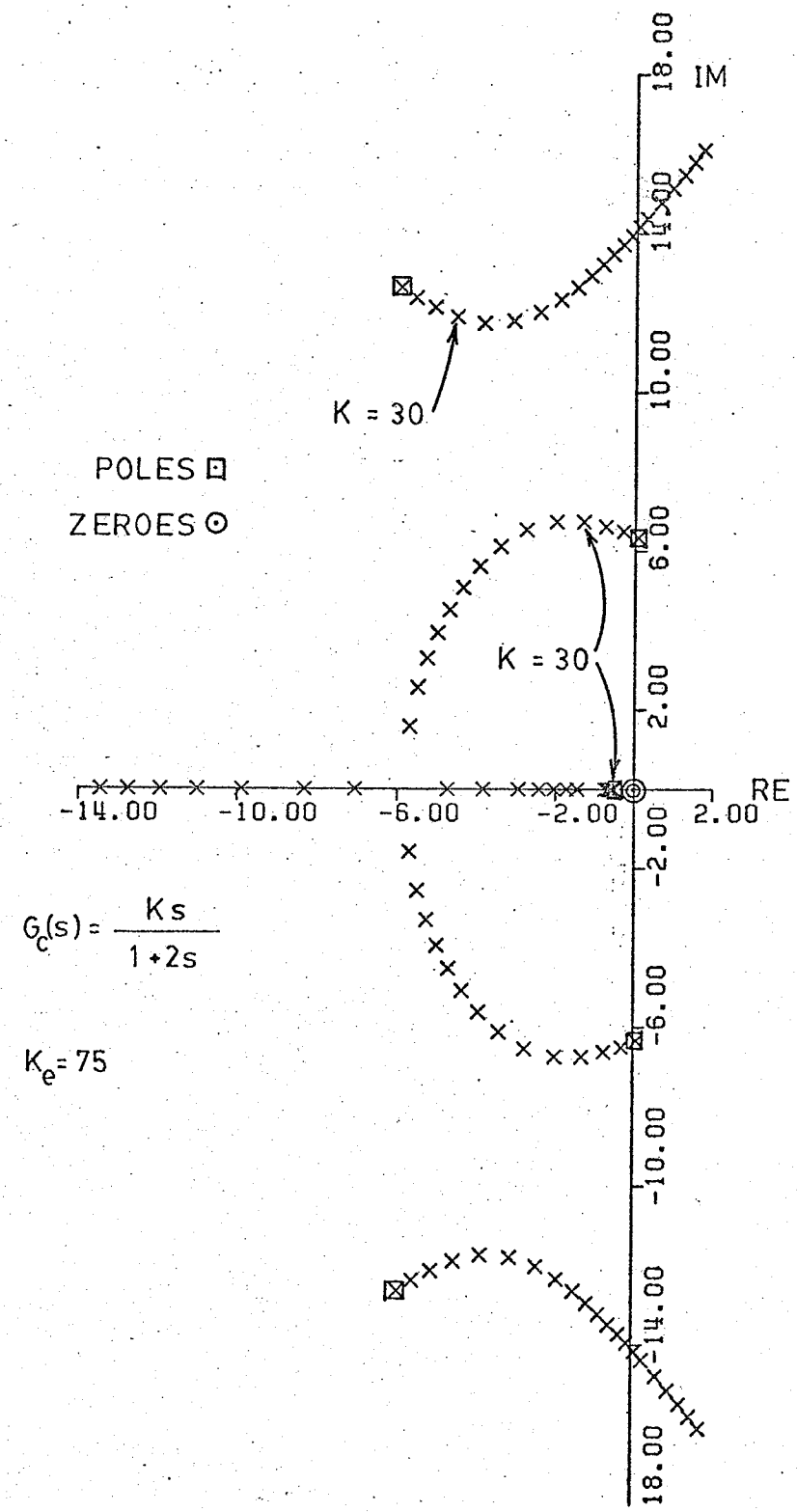
IM
RE
18.00
14.00
10.00
6.00
2.00
-2.00
-6.00
-10.00
-14.00
18.00
-14.00
-10.00
-6.00
-2.00
2.00
K = 30
K = 30
POLES ⊡
ZEROES ⊙
$G_c(s) = \frac{Ks}{1+2s}$
$K_e = 75$

FIG. 3.24

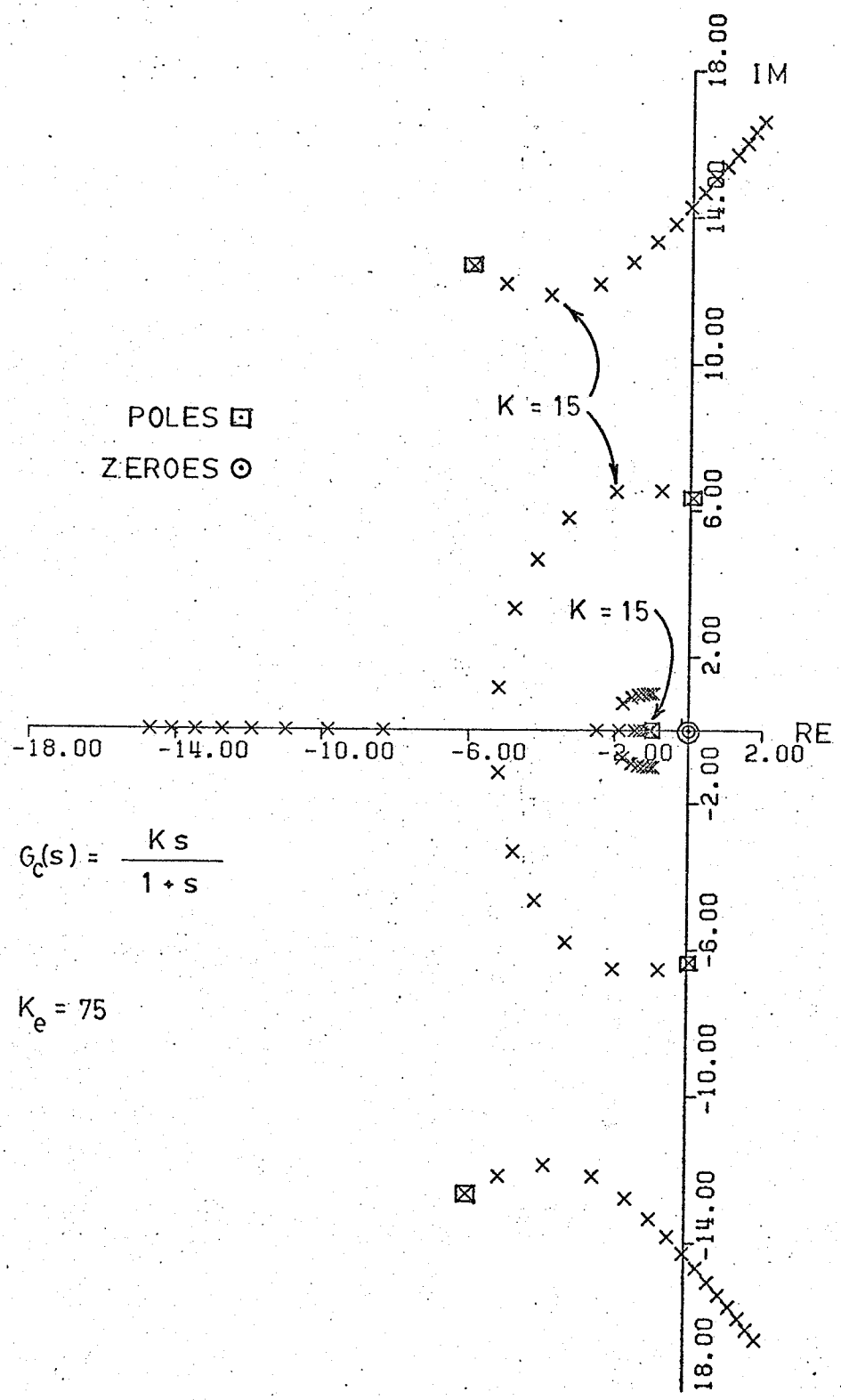
IM
RE
18.00
14.00
10.00
6.00
2.00
-2.00
-6.00
-10.00
-14.00
-18.00
-18.00
-14.00
-10.00
-6.00
-2.00
2.00
POLES ⊡
ZEROES ⊙
K = 15
K = 15
$G_c(s) = \frac{K s}{1 + s}$
$K_e = 75$

FIG. 3.25

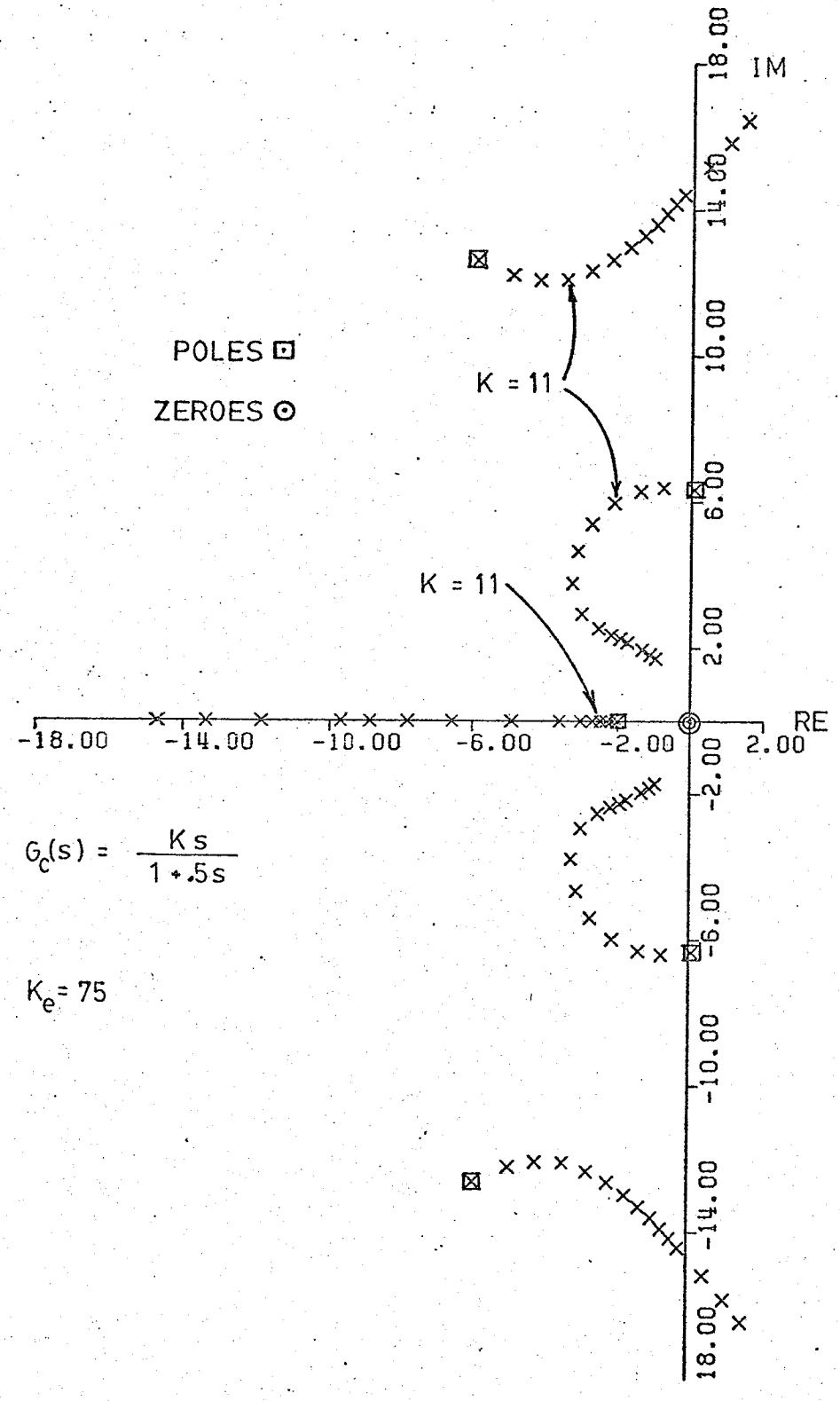
POLES ⊡
ZEROES ⊙
K = 11
K = 11
IM
RE
18.00
14.00
10.00
6.00
2.00
-2.00
-6.00
-10.00
-14.00
18.00
-18.00
-14.00
-10.00
-6.00
-2.00
2.00
$G_c(s) = \frac{Ks}{1+.5s}$
$K_e = 75$

FIG. 3.26

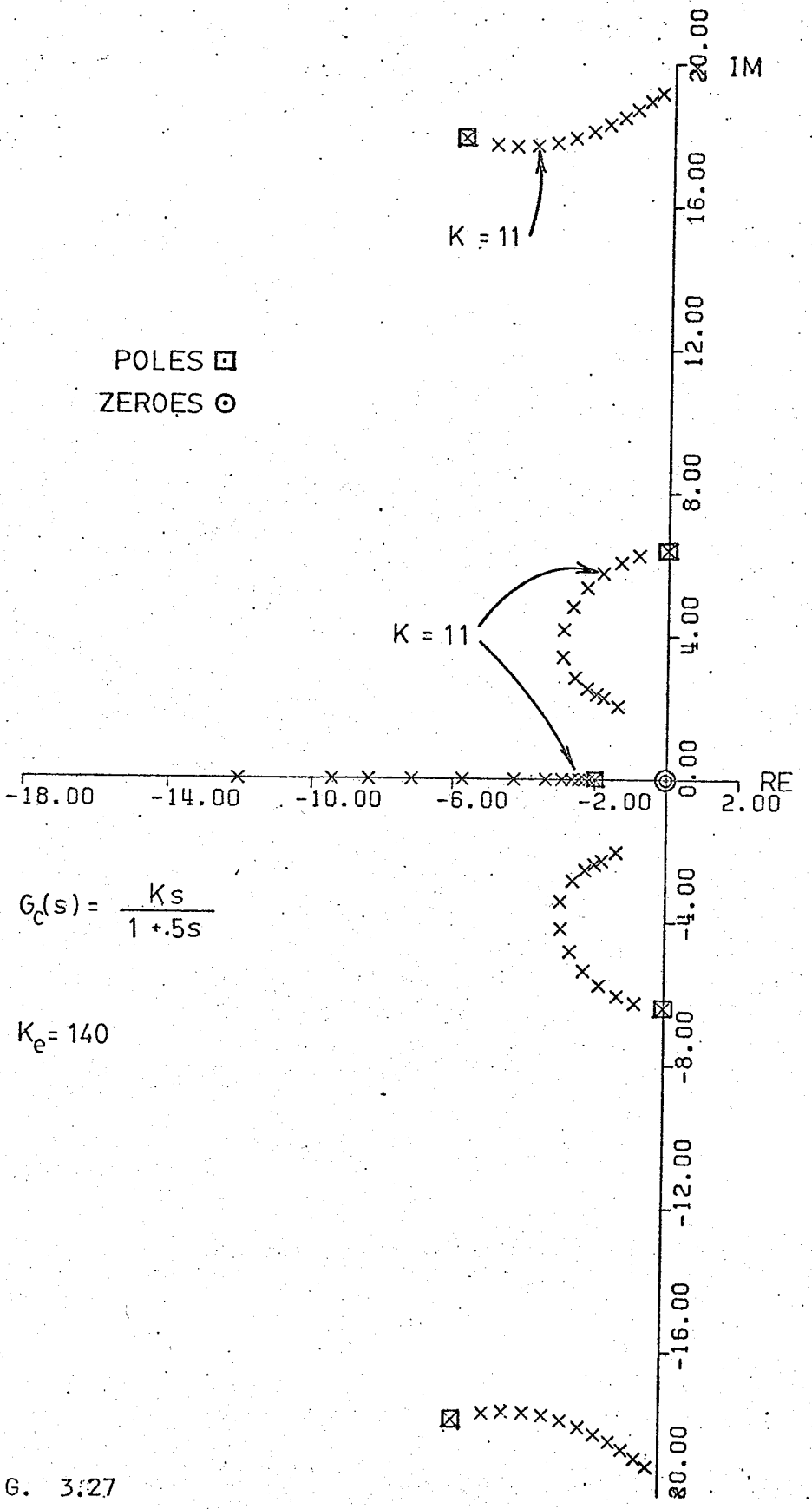
IM
RE
20.00
16.00
12.00
8.00
4.00
0.00
-4.00
-8.00
-12.00
-16.00
-20.00
-18.00
-14.00
-10.00
-6.00
-2.00
2.00
K = 11
K = 11
POLES ⊡
ZEROES ⊙
$G_c(s) = \frac{Ks}{1 + .5s}$
$K_e = 140$

FIG. 3.27

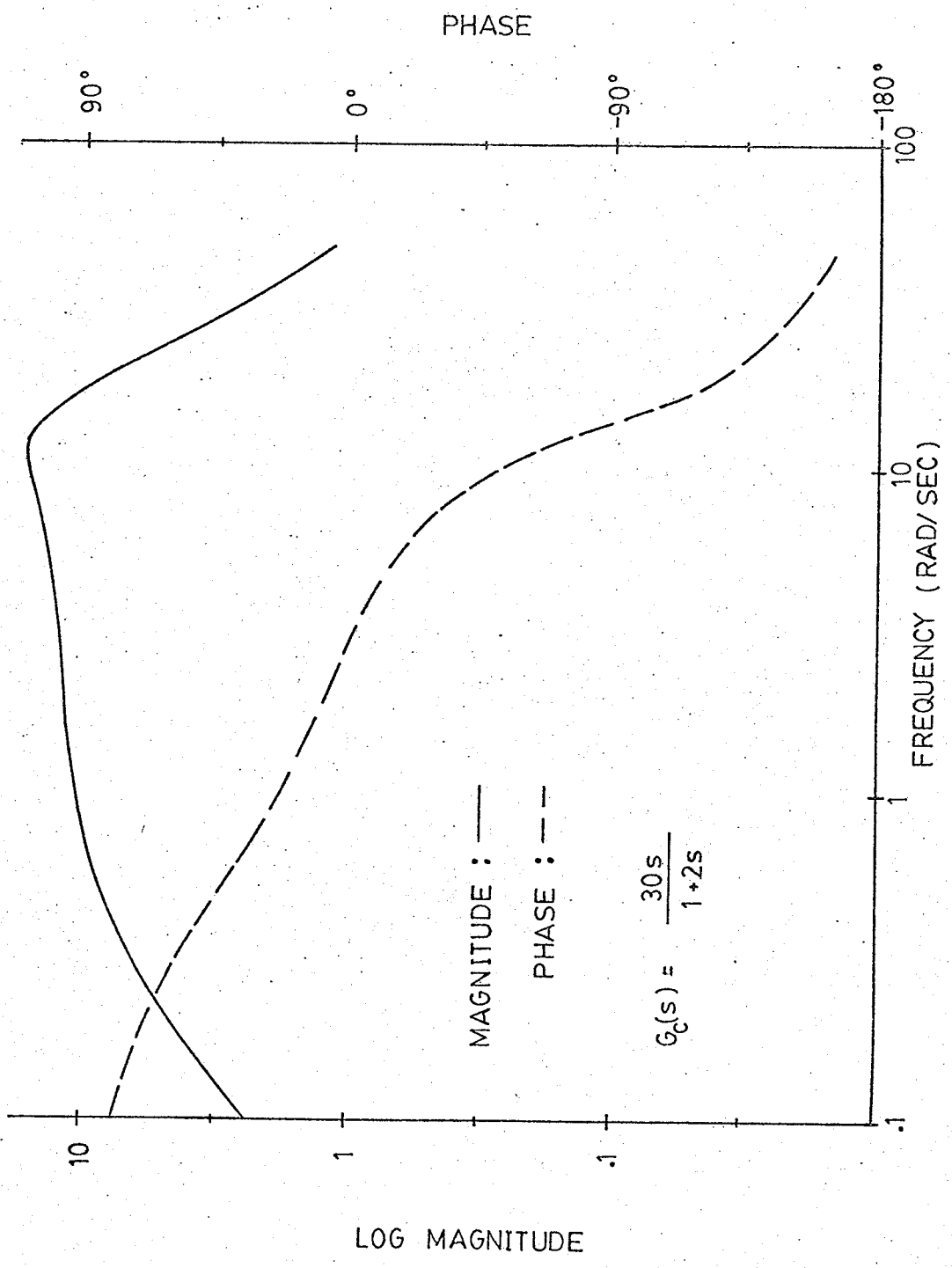

FIG. 3.28 Bode plot of torque signal with compensation (k_e = 75).

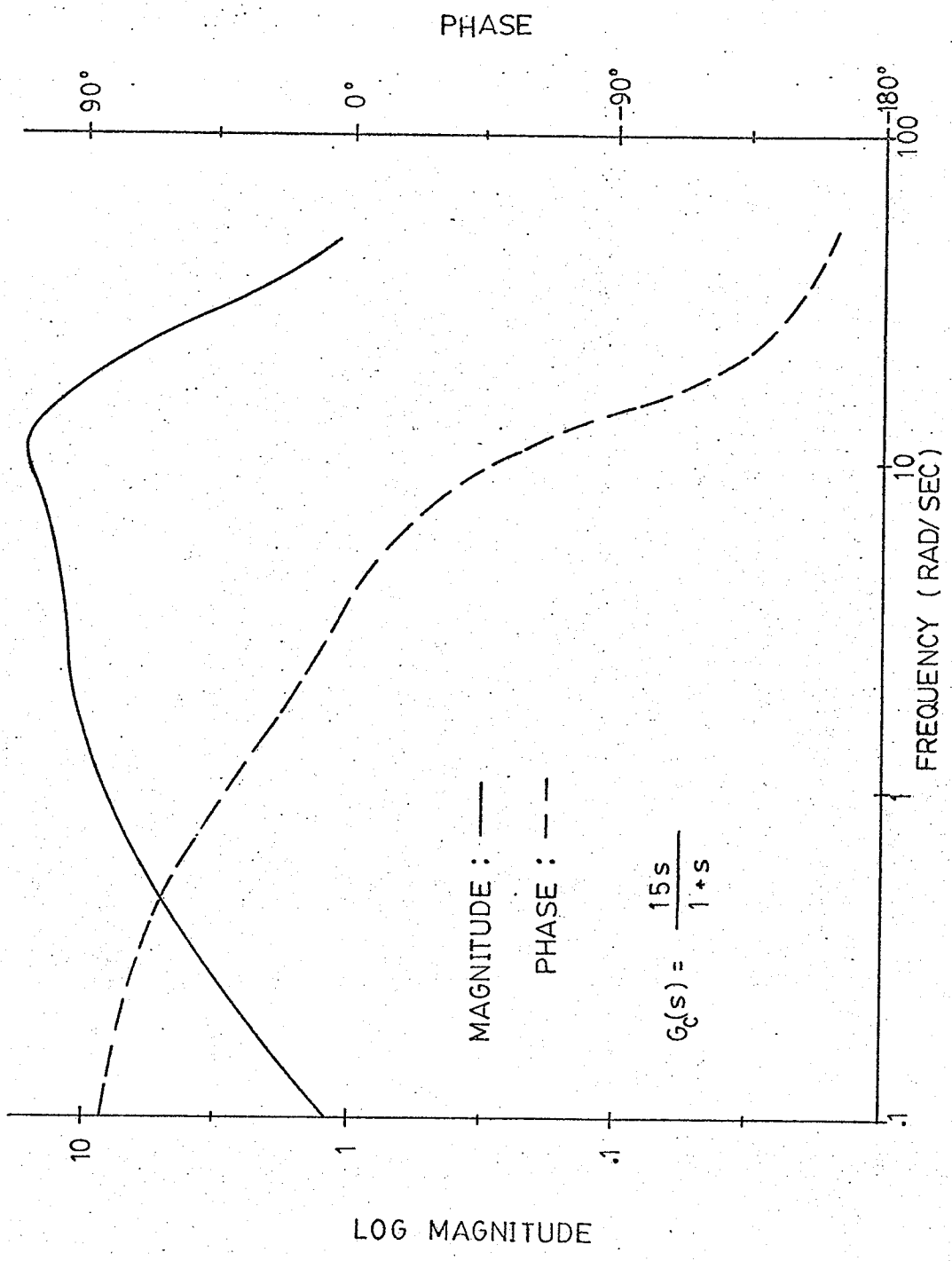

FIG. 3.29 Bode plot of torque signal with compensation (k_e = 75)

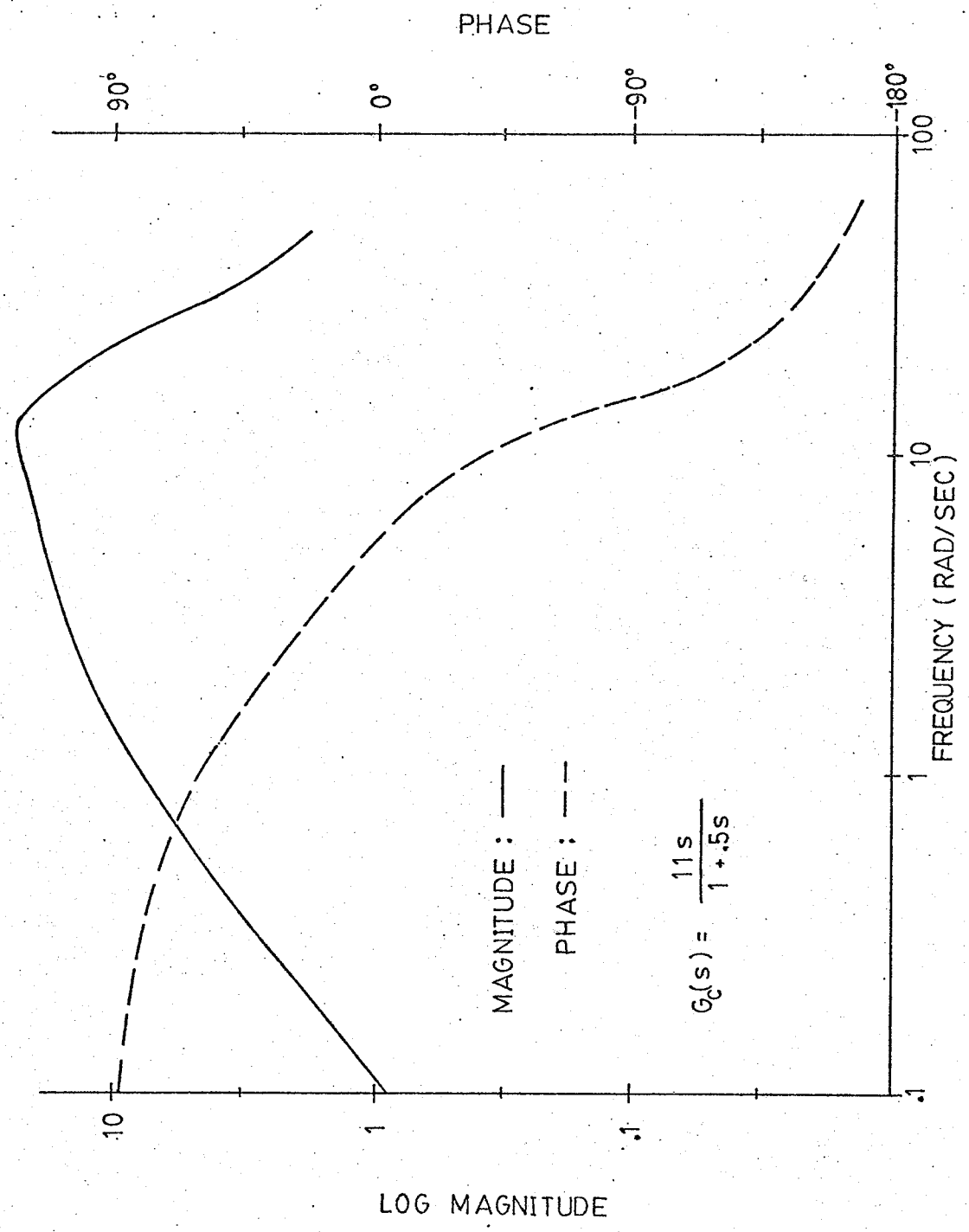

FIG. 3.30 Bode plot of torque signal with compensation (k_e = 75)

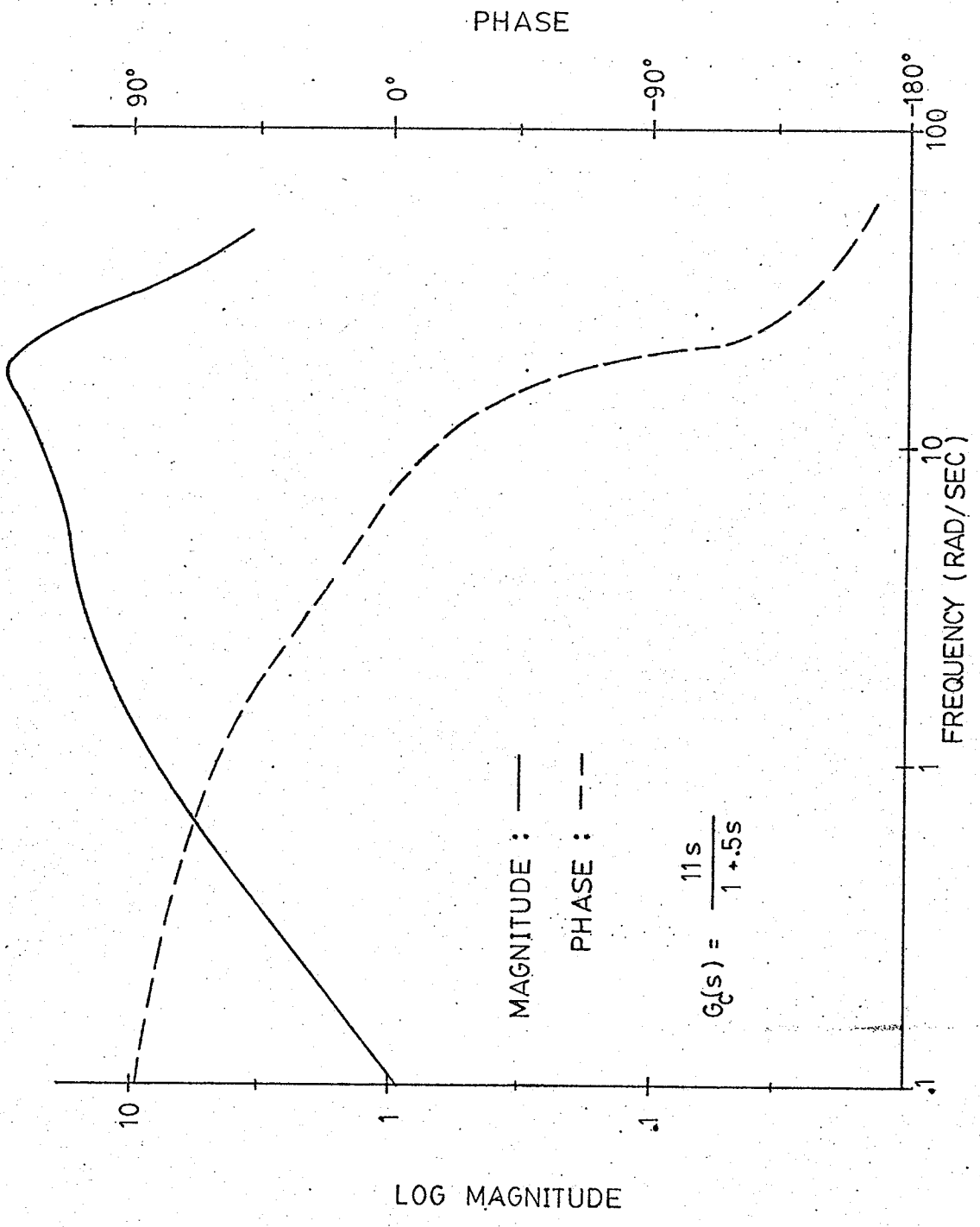

FIG. 3.31 Bode plot of torque signal with compensation (k_e = 140)

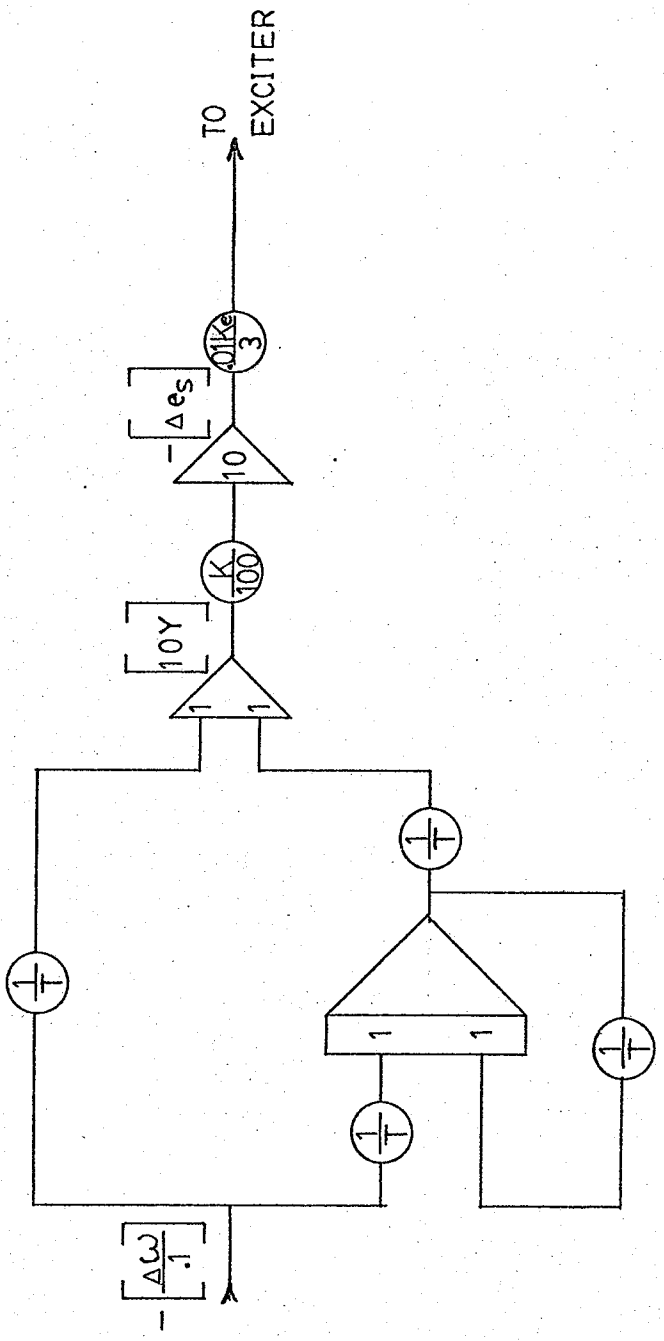

FIG. 3.32 Analog simulation of the real root compensator.

analog results for the three settings of T are shown in Fig. 3.33, 3.34 and 3.35. Comparing the best real root compensator to its complex root counterpart indicates that the real root compensator has approximately equal performance. The only notable exception occurs in the amount of overshoot observed. The complex compensator seems to have slightly better damping.

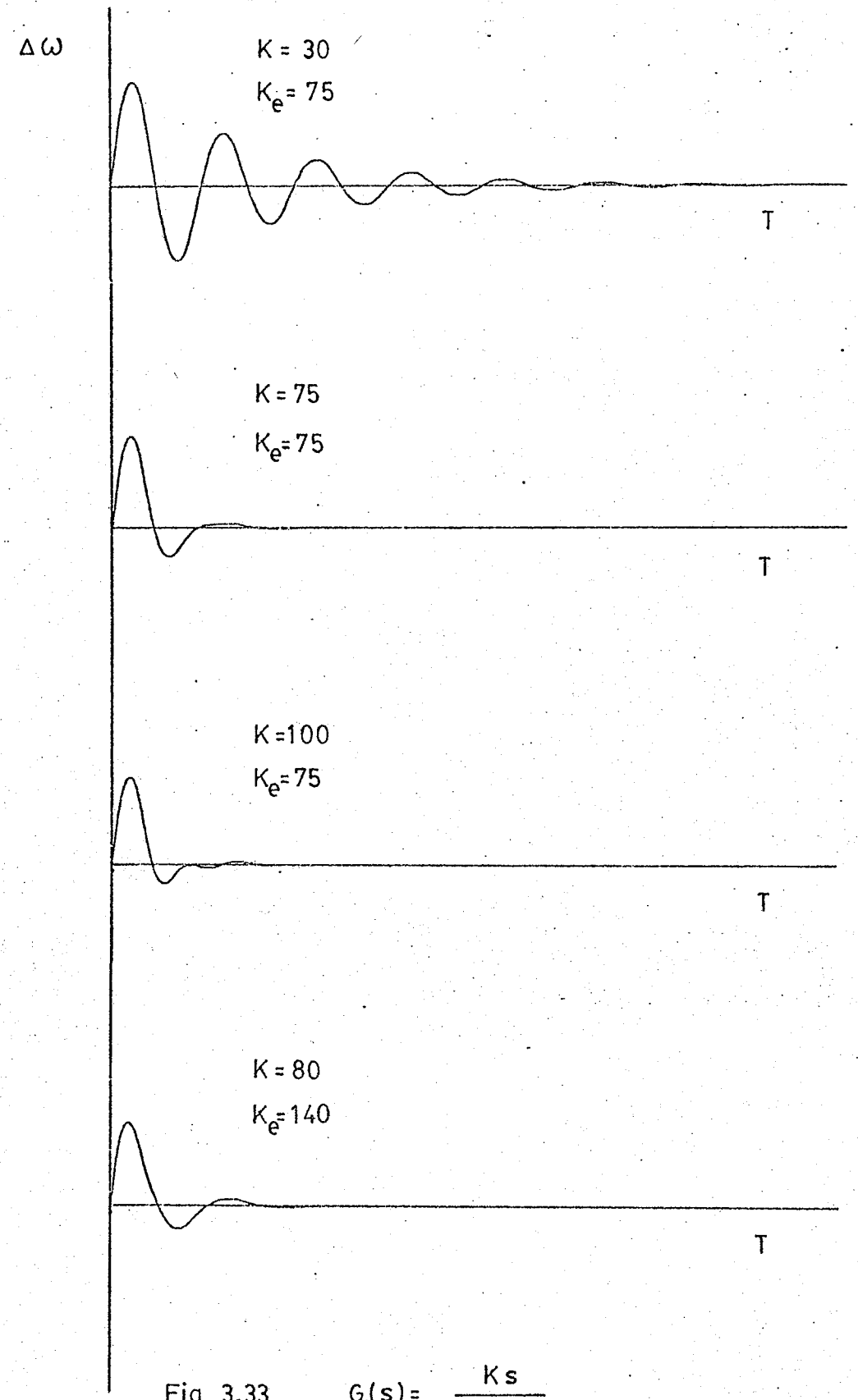

Fig 3.33 $G_c(s) = \frac{Ks}{1+2s}$

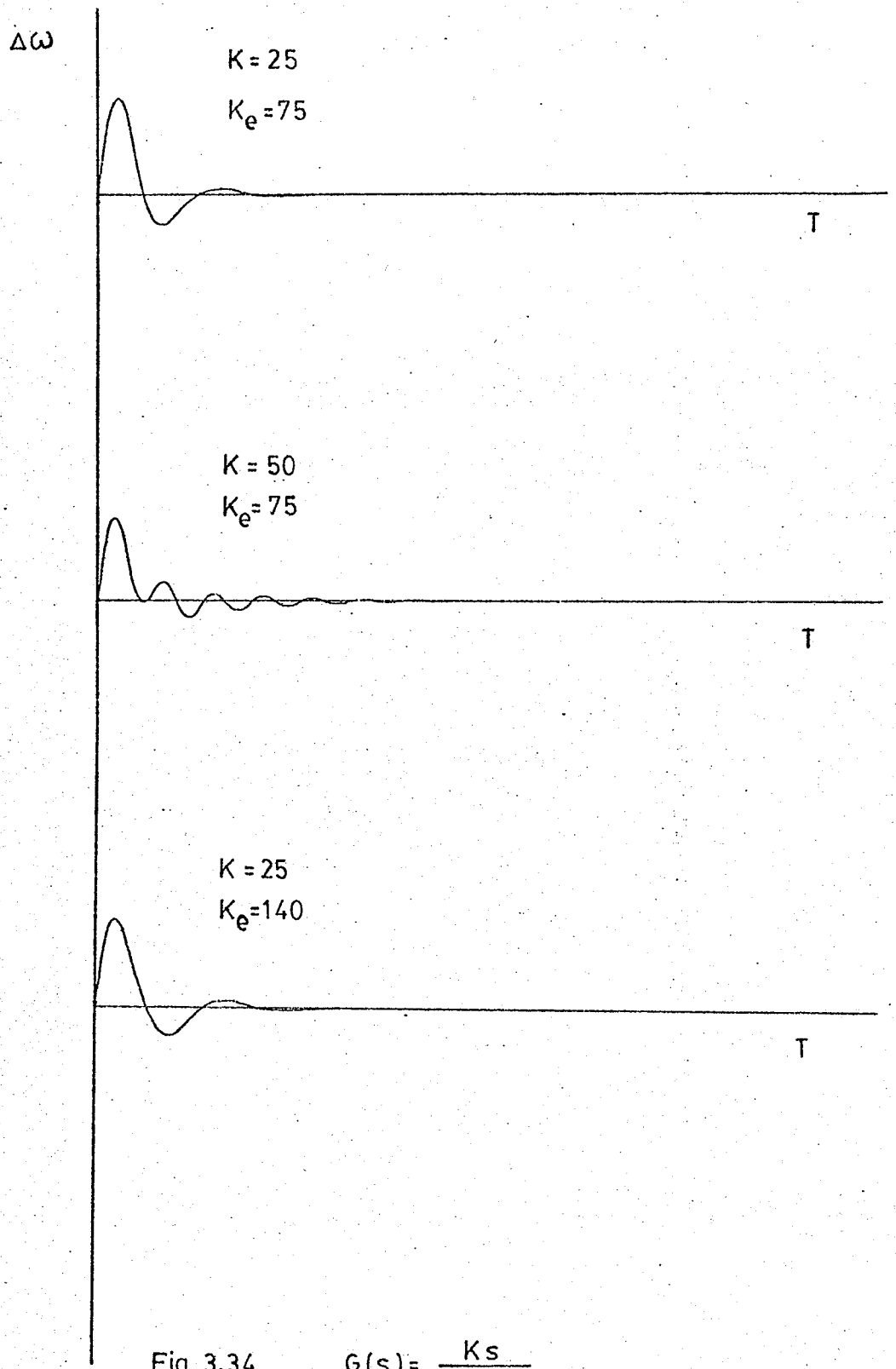

Fig 3.34 $G_c(s) = \frac{Ks}{1+s}$

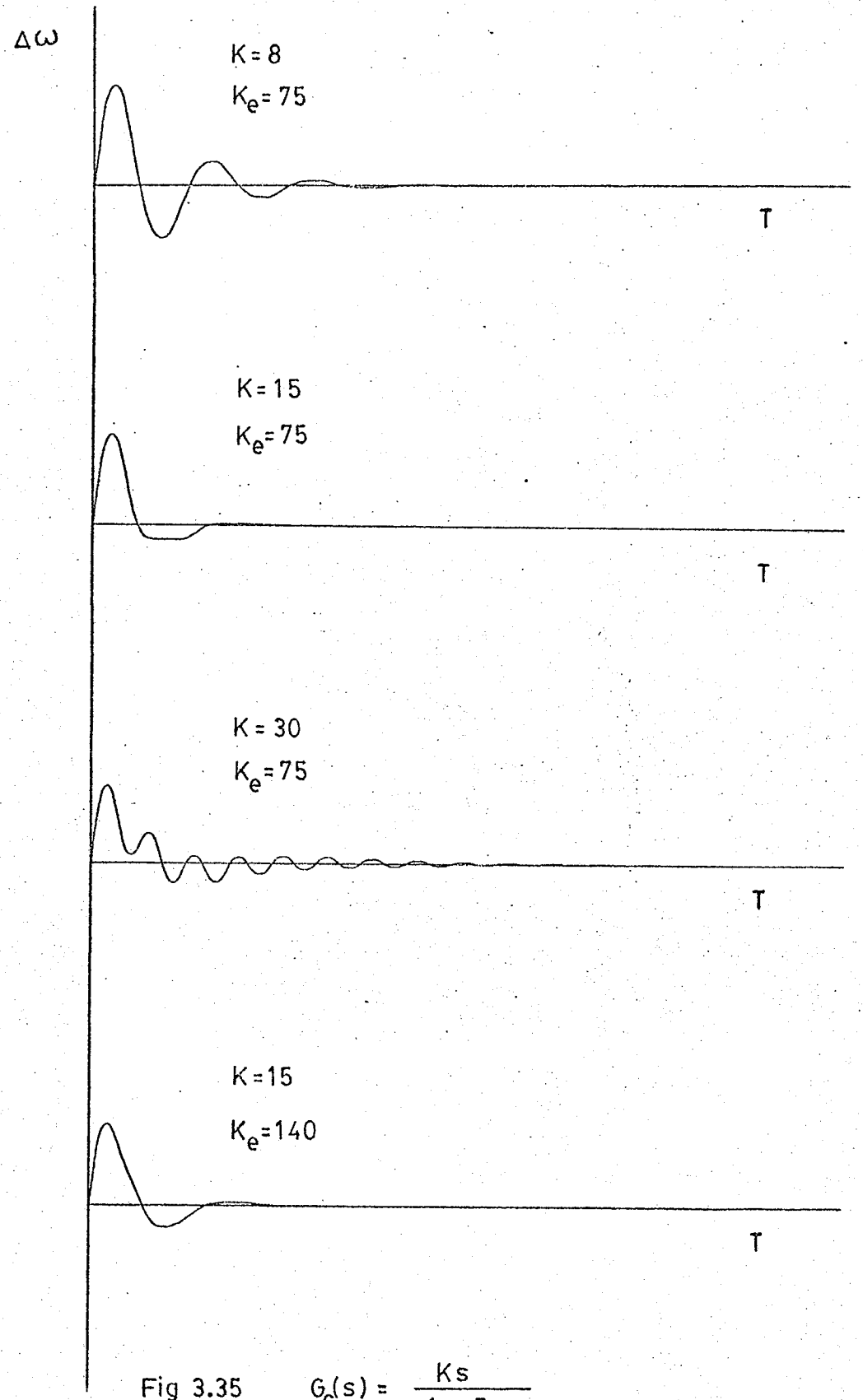

Fig 3.35 $G_c(s) = \frac{Ks}{1 + .5s}$

CHAPTER IV

IMPLEMENTATION ON A REAL SYNCHRONOUS MACHINE INFINITE BUS MODEL POWER SYSTEM

Although the computer testing of the two types of compensators indicates that their performance is approximatley equal these results can only be based on the assumption that the model used is correct. In order to confirm that this is in fact the case and at the same time observe the performance of the compensators on a real system, the two types of compensation are implemented on the model.

1. Complex Compensation

a) Circuit Description

As mentioned earlier the compensator will utilize terminal frequency as its input. The circuitry required to accomplish this will be dependent on the particular installation.

Fig. 4.1 shows the feedback circuit employed. The frequency transducer is connected in series with a meter circuit which provides continuous monitoring of terminal frequency. A 5000 ohm resistor is connected to ground at this point to develop a voltage signal for the stabilizer circuitry. The resistance value was selected to properly terminate the transducer as per manufacturers specifications. With the exception of the compensator itself the individual feedback circuit stages are realized using operational amplifers and the method of application can be found in any text on the subject [13].

The first stage of the circuit serves as a buffer and bandpass filter. A bandpass filter is required to remove any dc component in

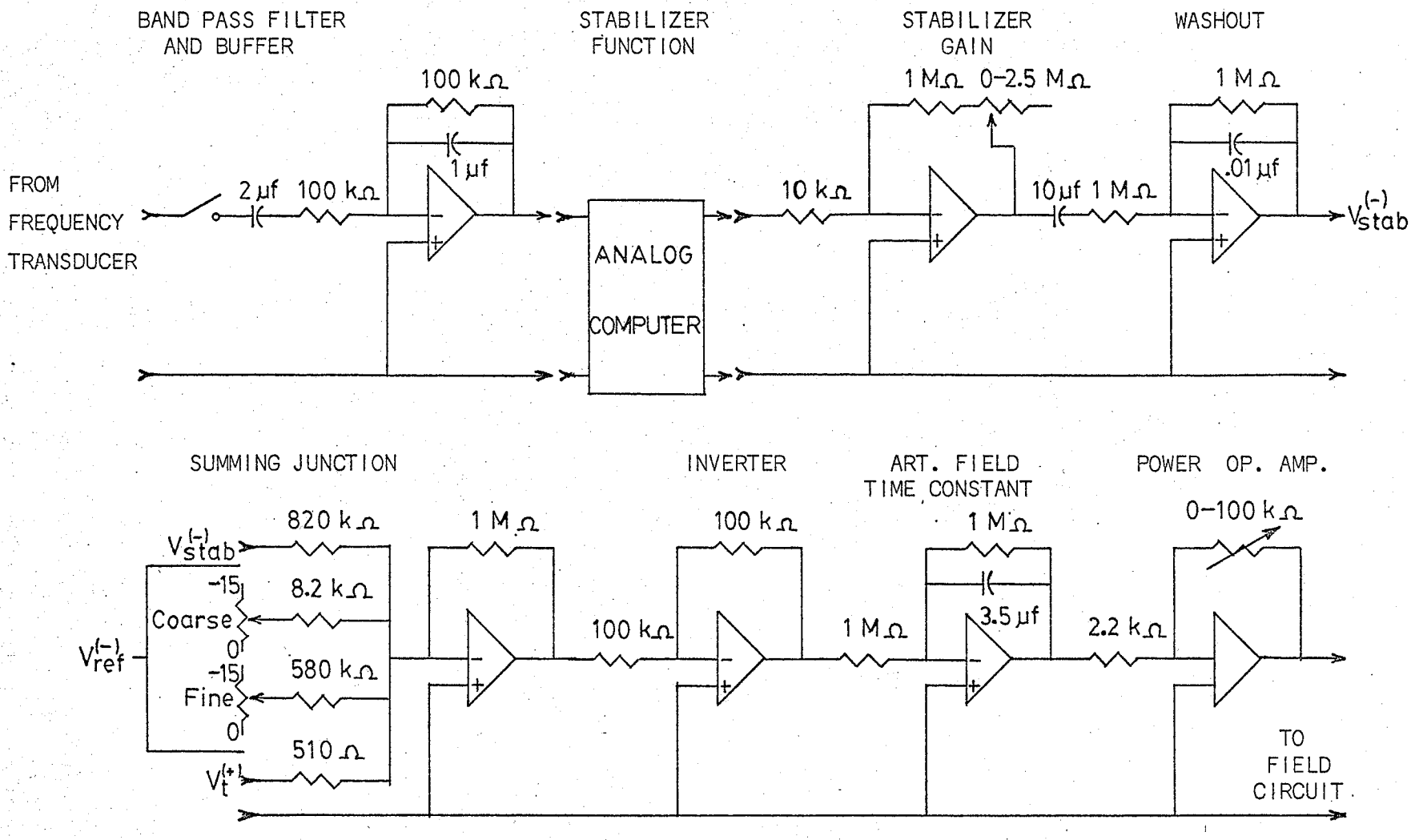

FIG. 4.1 Stabilizer feedback circuit - complex stabilizer

the transducer signal as well as a high frequency machine induced ripple component. A dc component cannot be tolerated since it could cause saturation problems in subsequent stages. The high frequency cut-off is set at 10 rad/sec. while the low frequency cut-off of the filter occurs at 5 rad/sec. The passband is between 0.8 Hz and 1.6 Hz which is sufficient for this system since the oscillation frequency of the system is around 1 Hz.

The following section of the feedback circuit is the stabilizer function itself. Although the complex stabilizer function can be realized using an active RC network the actual design would require the careful selection of network components as well as the use of a stabilized dc power supply. It was found that a complex form was not easily realized. In view of this and also conscious of the fact that the best stabilizing function may not correspond exactly to that predicted by analysis, it was decided to simulate the stabilizer on a TR - 20* analog computer. As long as the input and output voltages remained within $\pm$ 10 volts the computer would properly represent the function required. To ensure that this voltage level was not exceeded within the analog computer the stabilizer gain was implemented as a separate stage after the computer. As a consequence of using the analog computer, one could now set the coefficients of the compensator to those values which would best suit the system.

As indicated above, the compensator circuit is followed by a gain stage whose range of adjustment spans values from 100 to 350.

* Electronics Associates Incorporated.

The final stage prior to the summing junction of the voltage regulator serves as the "washout" or automatic zeroing function. It is added to the circuit, in accordance with standard practice, to eliminate the possibility of a steady state offset occurring in the terminal voltage as a result of the feedback signal and also to washout the effects of drift in the preceding circuitry. The washout function has the following form.

$$\text{WASHOUT} = \frac{Ts}{1 + Ts} \qquad \text{- - - - - - - - - - - - - - - - - - - (4.1)}$$

For practical operational amplifier circuits an infinite bandwidth is not possible and the amplifier circuit gain will thus drop off at high frequencies. It is therefore usual practice to include a high frequency cut-off in an operational amplifier circuit. As a result the actual washout transfer function implemented has the form:

$$\text{WASHOUT} = \frac{Ts}{(1+Ts)(1+T_1 s)} \qquad \text{- - - - - - - - - - - - - - - - (4.2)}$$

The high frequency cut-off has been set to 16 H_z while the value used for T is 10 seconds.

The output signal from the feedback circuit is now applied to the summing junction circuit. For a frequency derived signal positive feedback must be used. A terminal voltage feedback signal as well as a reference voltage are supplied at this point.

Each of the operational amplifier circuits are connected in the inverting mode and as a result the extra inverting circuit is required to impart the correct polarity to the signal.

The final stage before the exciter corresponds to the artifical time constant discussed earlier. The time constant actually implemented corresponds to 3.5 seconds. This is slightly different from the required value of 3.3 seconds due to limitations in component values. However, it is felt that the errors created would not be of major significance.

The exciter itself is modeled with a power operational amplifier as indicated earlier.

b) Parameter Determination and Oscillographic Results

In the actual performance testing of the complex stabilizer it is required to determine the values of exciter and stabilizer gains which will be used.

The testing is carried out for two values of exciter gain corresponding to $k_e = 75$ and $k_e = 140$. The feedback resistor settings are identical to those determined in Chapter II.

The value of stabilizer gain was determined by evaluating the transient gain of the circuit shown in Fig. 4.1. The routine followed is shown below.

Frequency Transducer

$$\text{Gain} = \frac{10^{-3}}{5} \qquad \frac{\text{AMPS}}{\text{Hz}}$$

Voltage Divider:

$$\text{Gain} = \frac{100000}{105000} \times 1 \text{ AMP} \times 5000\ \Omega$$

$$= 4761.9 \quad \frac{\text{VOLTS}}{\text{AMP}}$$

Bandpass Filter and Buffer Circuit:

$$\text{Transfer function} = \frac{-.2S}{(1+.1S)(1+.2S)}$$

Examination of the Bode plot over the frequency range of interest indicates that

$$\text{Gain} = 1$$

Stabilizer Circuit:

$$\text{Gain} \simeq 1 \frac{\text{VOLTS}}{\text{VOLTS}} \qquad \text{(By experimental measurement)}$$

Stabilizer Gain Stage.

$$\text{Gain} = \frac{1.0\text{x}.0^6 \text{ to } 3.5\text{x}10^6}{10^4} \qquad \frac{\text{VOLTS}}{\text{VOLT}}$$

Washout Stage:

$$\text{Gain} = \frac{1\text{x}10^6}{1\text{x}10^6} = 1 \frac{\text{VOLTS}}{\text{VOLT}}$$

Summing Junction:

$$\text{Gain} = \frac{1\text{x}10^6}{820\text{x}10^3} = \frac{1}{0.82} \qquad \frac{\text{VOLTS}}{\text{VOLT}}$$

Taking the product of the above values sets the stabilizer loop gain to the following range of values:

$$\text{Overall Gain} = 116 \text{ to } 407 \frac{\text{VOLTS}}{\text{Hz}}$$

Although the stabilizer function was determined by analysis it must be appreciated that the function actually implemented would quite probably require some minor adjustments to yield good results. This contention can be justified from the standpoint that there are inadequacies in the measurements and approximations which were used to analyze the system.

Adjustment and trial resulted in the selection of the following

stabilizer function.

$$G_c(s) = \frac{175\,[s^2 + 12s + 280]}{[s^2 + 50s + 1530]} \qquad \text{- - - - - - - - - - - - (4.3)}$$

It should be noted that the stabilizer gain actually used turned out to be less than that predicted by analysis. It was observed that too large a value of gain would result in the amplification of the ripple frequency component contained in the frequency transducer signal (the low pass filters could not remove this component completely). If a prominent ripple frequency component was fed back to the exciter loop it was found that a corresponding dither signal was superimposed on the system operating variables. As a result, the stabilizer gain has to be reduced to avoid this effect but yet kept high enough to maintain adequate damping.

In the oscillograms that follow power and frequency are recorded for the two values of exciter gain under different operating conditions. Fig. 4.2 (a) demonstrates the improvement in dynamic stability. It was observed that the stabilizer extended the dynamic stability limit of the generator beyond its own ratings. The value of terminal voltage used is quite low so as to accentuate the stability problem. Fig. 4.2(b) show the stabilizer's transient stability performance. The system is run at the operating point shown and a single phase switching operation (approximately 10 cycle duration) is performed. Stability is maintained. Fig. 4.2(c) gives an indication of the stabilizer's range of application. With the system running at the operating point shown, a transmission line switching operation is simulated. The transmission line equivalent reactance is switched from 0.94 pu to 0.50 pu and then back to 0.94 pu.

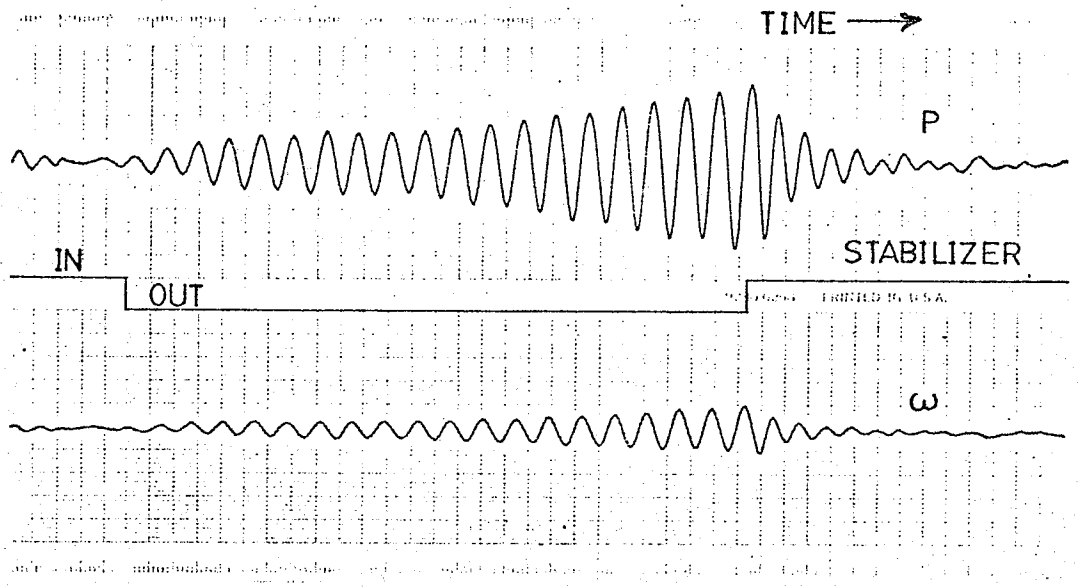

Fig 4.2(a)

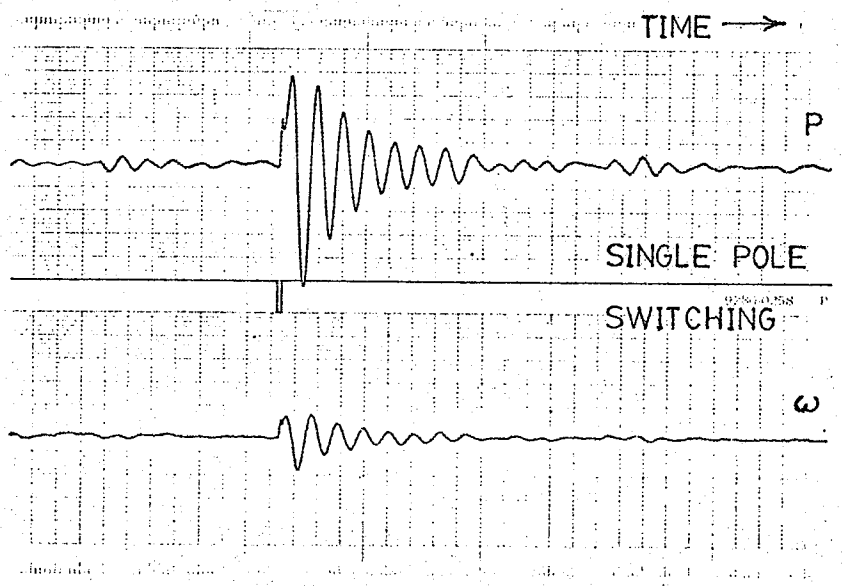

Fig 4.2(b)

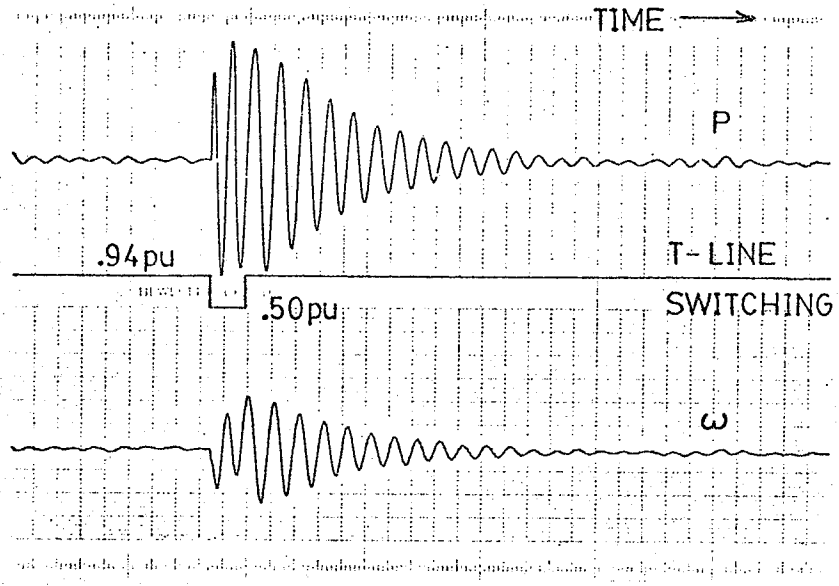

Fig 4.2(c)

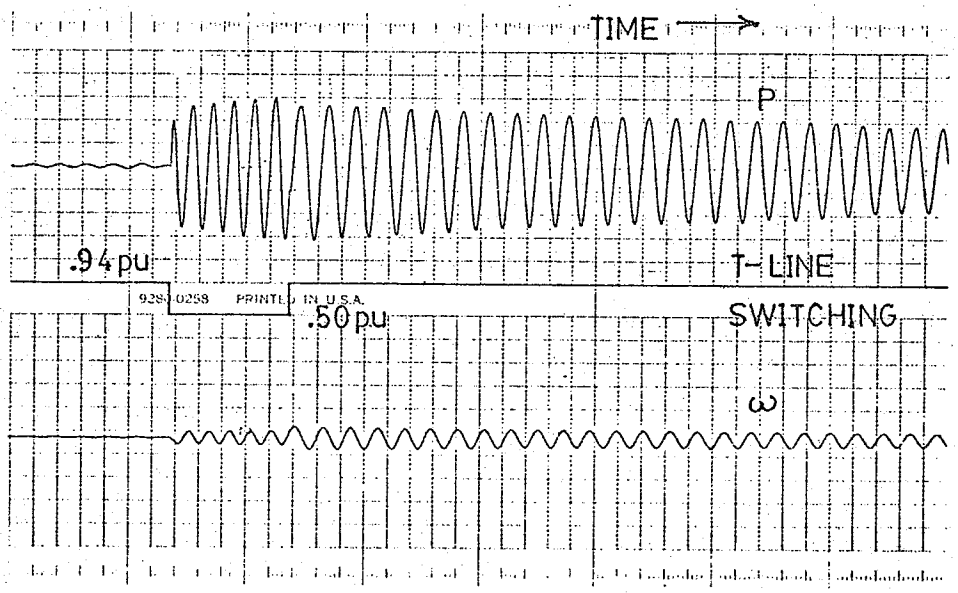

Fig 4.2(d)

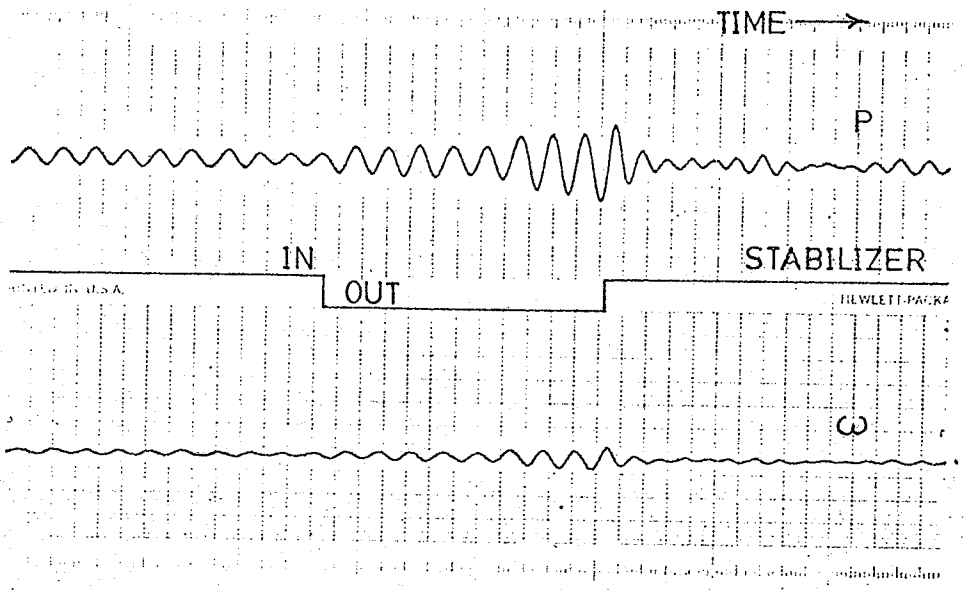

Fig 4.3(a)

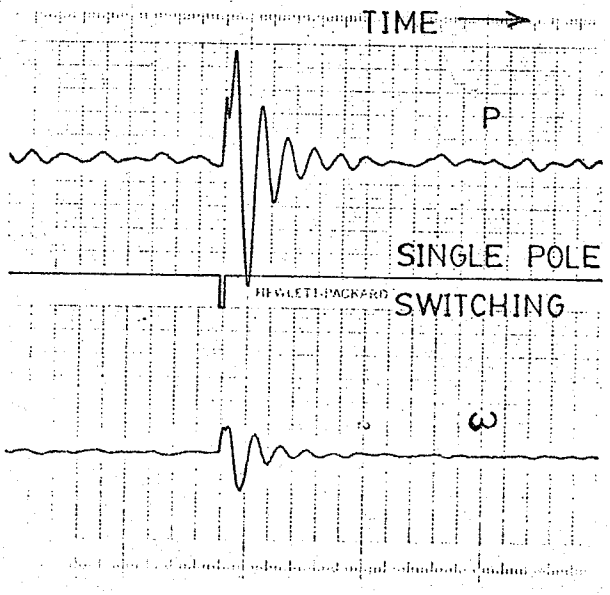

Fig 4.3(b)

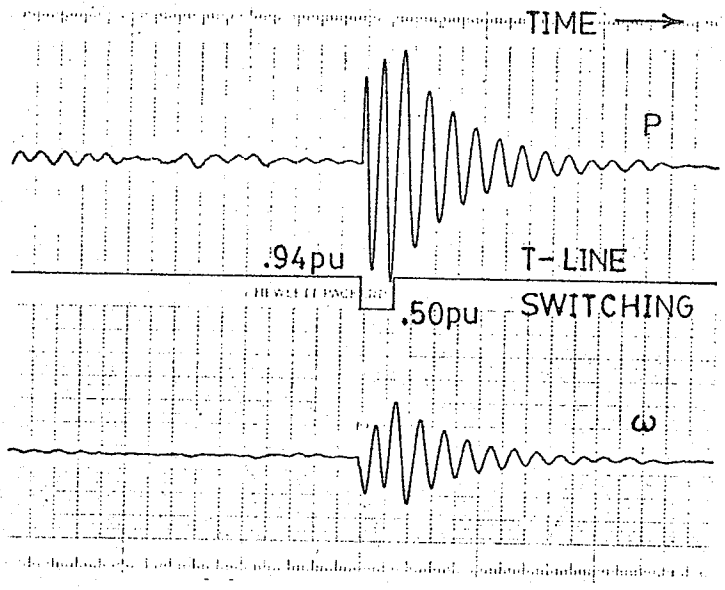

Fig 4.3(c)

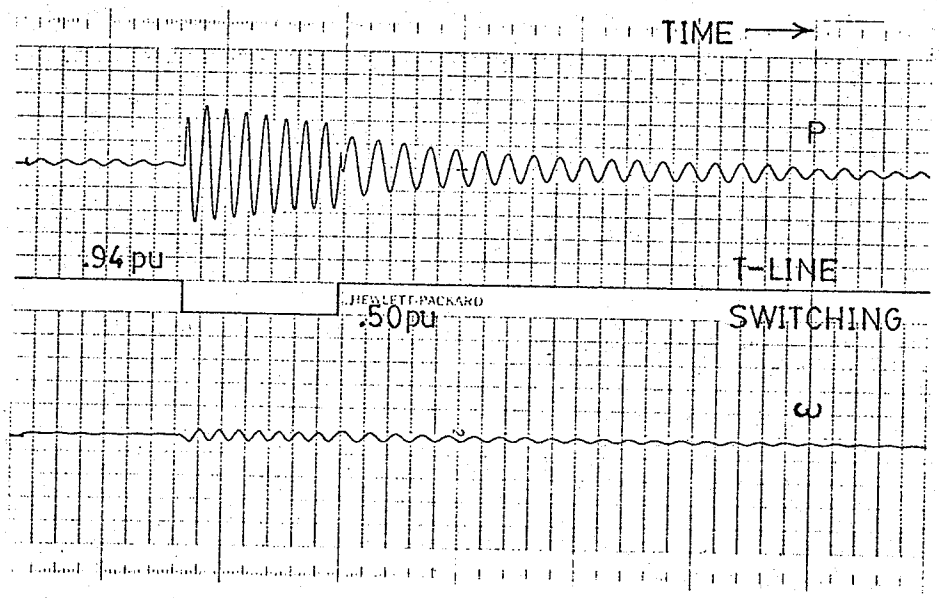

Fig 4.3(d)

This would be analogous to either reducing the length of the line or placing another line in parallel with an existing line. The impedance value was returned to its original value since the system response at the lower value turned out to be very oscillatory and would tend to instability if left alone. The same situation is repeated with the stabilizer removed and the result can be observed in Fig. 4.2 (d). The oscillograms show that the stabilizer performance is adequate for the particular situation it was designed for but, that it cannot be applied at all times. It would then seem apparent that a stabilizer is only applicable to a specific situation and that it cannot be applied for a general range of cases since it will either affect no improvement in the system stability or possibly even contribute to instability. A possible solution to the above dilemma could involve the design of several compensators to suit several operating configurations and the appropriate logic to bring the correct stabilizer into operation at the right time.

The above range of conditions are reexamined with the exciter gain increased to 140 in the oscillograms of Fig. 4.3. It should be noted that the higher exciter gain causes the system, by itself, to exhibit greater stability but that the observations made above can still be applied to these results.

2. Real Root Compensator

a) Circuit Description

The circuitry required to realize the real root compensation is shown in Fig. 4.4. Since the function considered has a much simpler form it was decided to implement it using operational amplifiers.

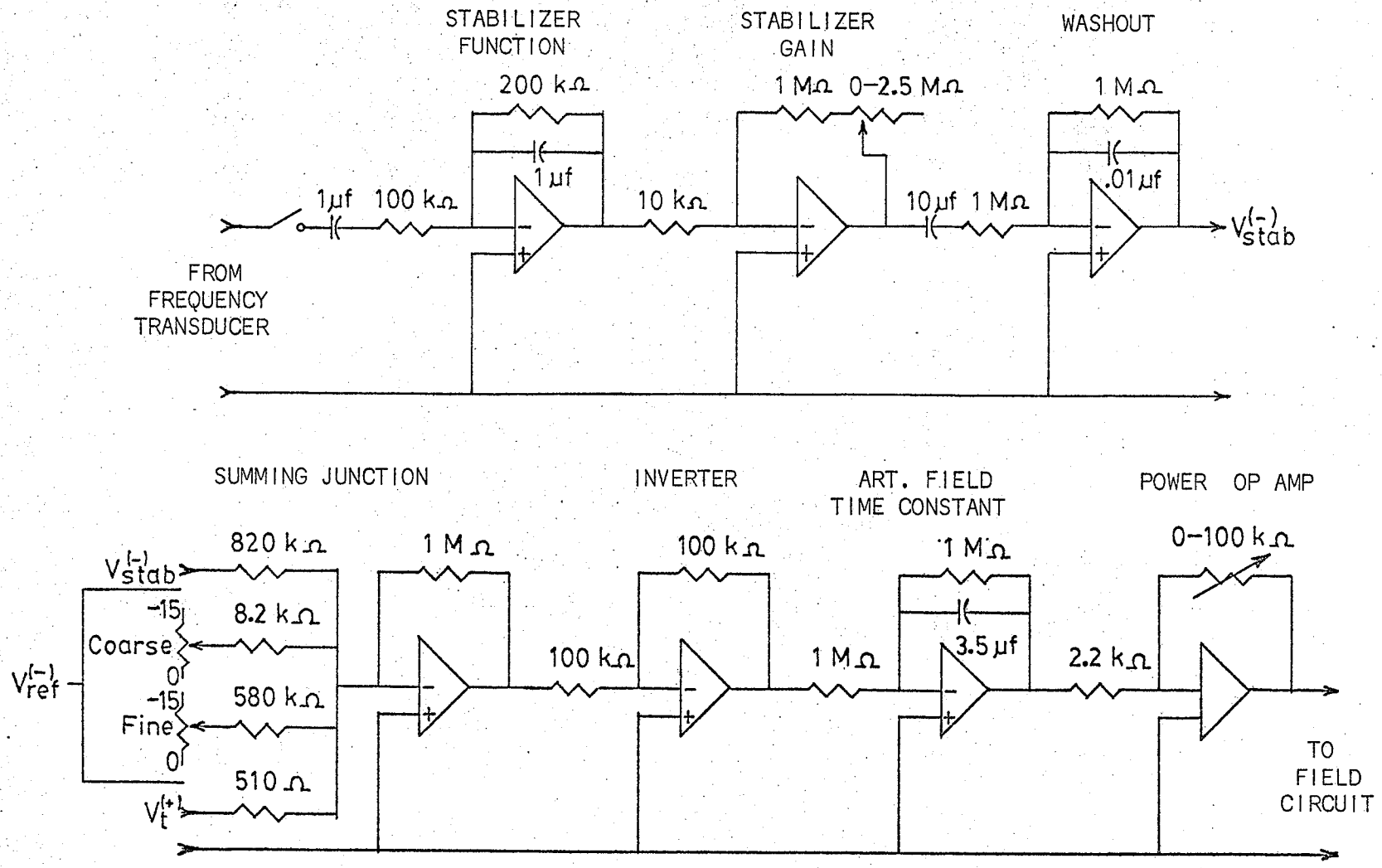

FIG. 4.4 Stabilizer feedback circuit - real root stabilizer

The first stage is the frequency transducer itself. There is also a high pass filter incorporated into the circuit to remove the ripple component from the transducer signal. This circuit is then followed by the gain stage and the washout stage as used previously. Although the stabilizer function itself has the form of a washout function, the additional stage was employed to obtain the correct signal polarity and also to eliminate any dc offset which may occur.

b) Parameter Determination and Oscillographic Results

The tests performed in the previous section are repeated for the real root stabilizer. As before, the range available in the stabilizer gain was determined prior to actual testing and the actual coefficients used were adjusted before the results were recorded.

The calculation of the feedback circuit gain is identical to the calculation of the preceding section except for the changes mentioned above. The gain of the stabilizer feedback circuit becomes:

$$\text{Overall gain} = \frac{100}{105} \times \frac{1}{0.82} \times (100 \rightarrow 350) \times (0.2)$$

$$= 23 \text{ to } 81$$

After adjustment the following real root stabilizer was used.

$$G_c(s) = \frac{60S}{1+(0.2)S} \qquad \text{- - - - - - - - - - - - - - - - - - (4.4)}$$

Fig. 4.5 and 4.6 show the performance of the stabilizer for k_e = 75 and 140 respectively. The situations examined are identical to those run previously for the complex stabilizer so as to facilitate comparison.

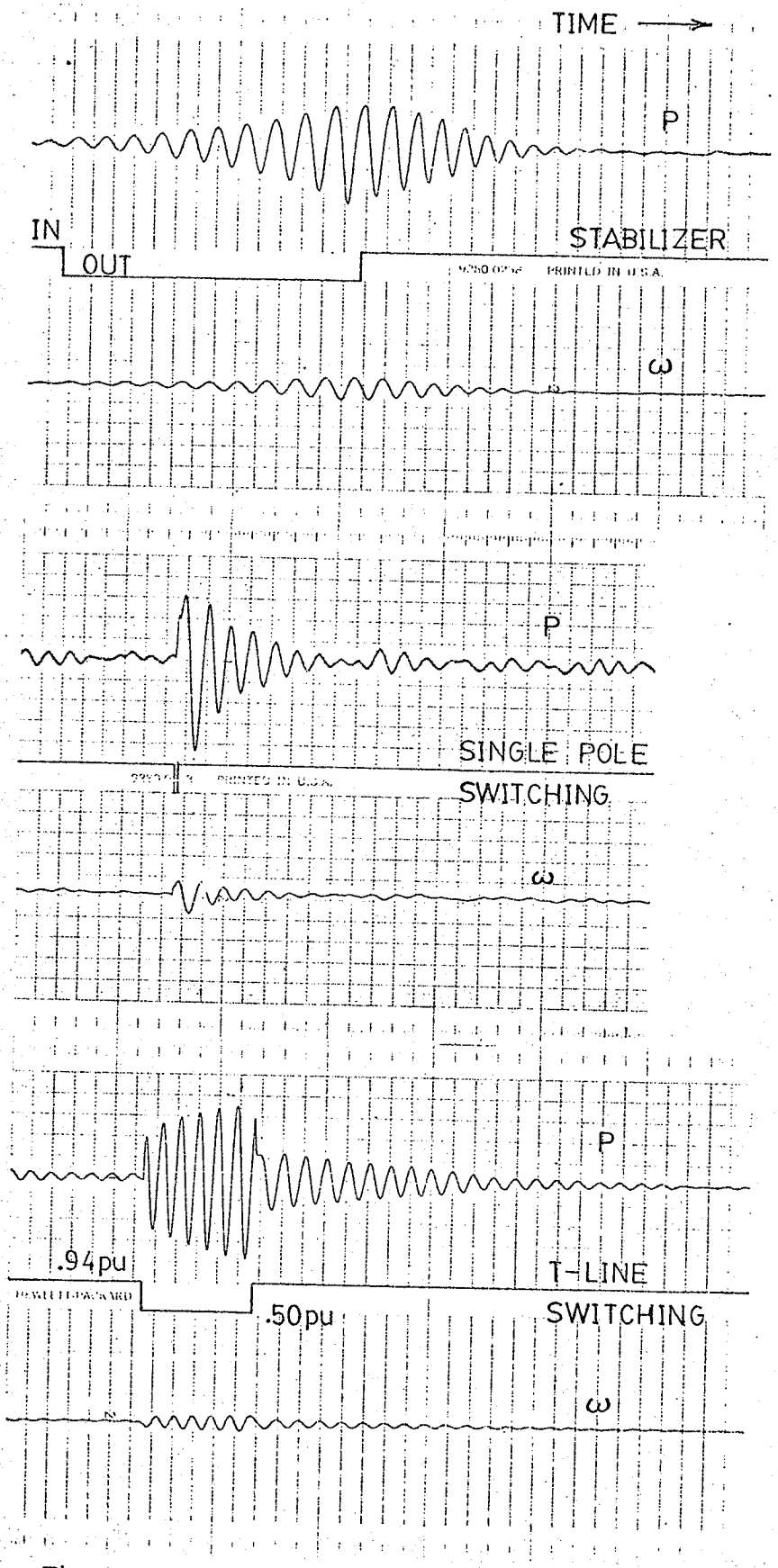
TIME
P
IN
OUT
STABILIZER
PRINTED IN U.S.A.
ω
P
SINGLE POLE
SWITCHING
ω
P
.94pu
T-LINE
.50pu
SWITCHING
ω

Fig 4.5

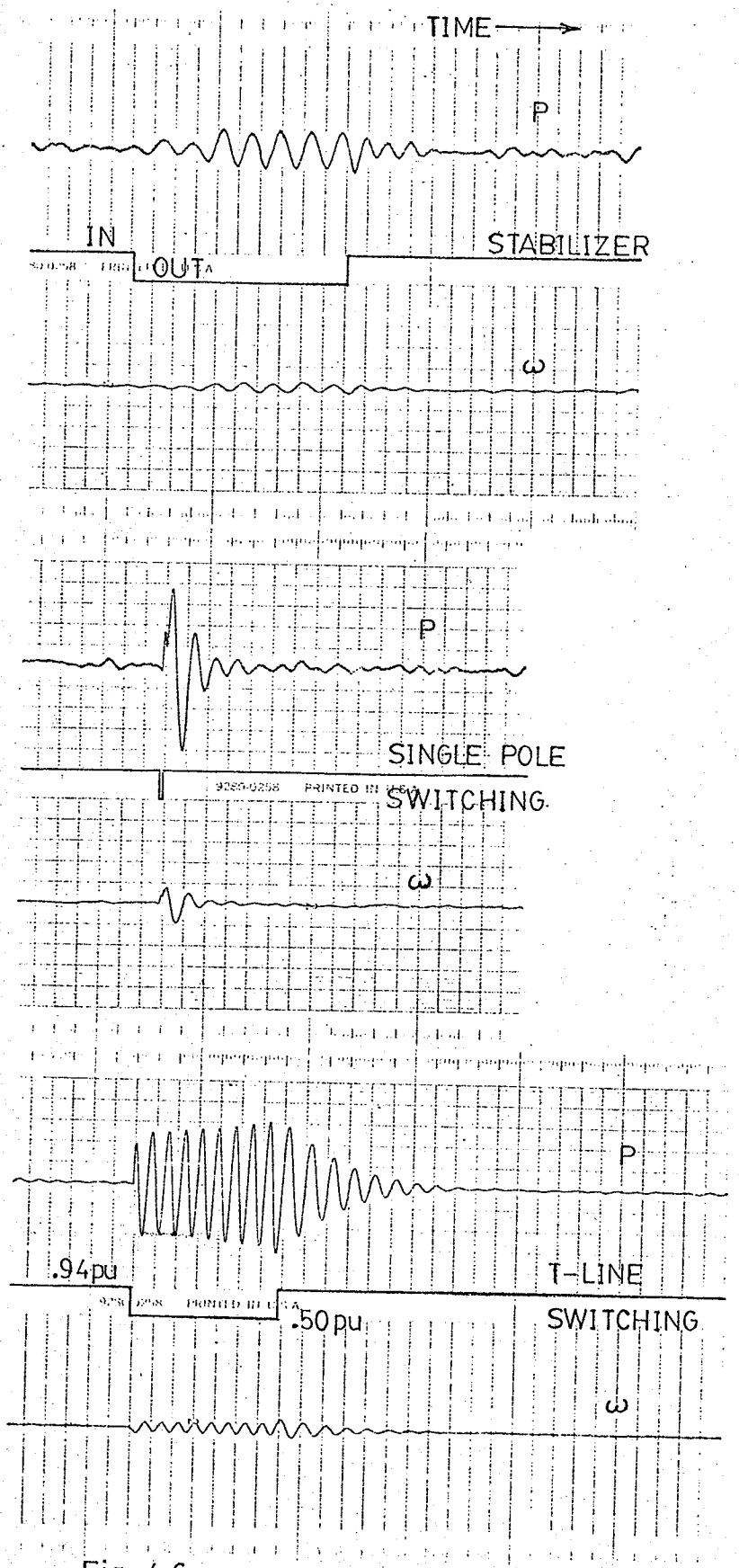
TIME
P
IN
OUT
STABILIZER
ω
P
SINGLE POLE
SWITCHING
ω
P
.94pu
.50pu
T-LINE
SWITCHING
ω

Fig 4.6

In comparing the results, one can conclude that the real root compensator's performance is comparable to that of the complex compensator. Implementation of a real root compensator would therefore seem to be the most practical course of action. However, the real root compensator suffers from the same pitfall associated with the complex root compensators in that it cannot be generally applied to all operating conditions.

CHAPTER V

CONCLUSIONS

The purpose of this work was to examine the effect that complex compensation could have on the improvement of stability for a power system. In this respect, a specific situation was selected which is usually characterized by instability. The situation studied is described by a block of generation connected to a large system through a long transmission line. The compensator design was based on parameters obtained from measurements taken on a real model power system. To test the compensator obtained through analysis, analog computer simulations were performed and the compensation was implemented on the real model power system. The same system was reexamined using real root compensation.

The following conclusion became evident as a consequence of this study.

- A properly designed real root compensator can perform just as well as a complex compensator selected for the same situation.
- Although complex compensation can enhance system stability its mathematical form is involved resulting in a more difficult problem of analysis. In addition, the realization of such a compensator can prove to be very difficult. Usually this would mean the use of more components than a comparable real root stabilizer. More components would tend to raise the possibility of circuit malfunctions. All of these factors taken together would seem to indicate that a complex compen-

sator would be more expensive to produce.

- A real root compensator of the form $\frac{ks}{1+Ts}$ was considered in this study. Implementation of a real root compensator possessing two poles and two zeros could possibly yield better results but this would require analysis of the specific situation being considered. At any rate, the study would seem to indicate that real root compensation is the best form to use.
- Whether the compensation is real or complex, the fact remains that a single compensator cannot provide proper stabilization for all the operating cases encountered on a system. As a solution, one can design several compensators and employ the proper logic to select the compensation required. An alternate approach, which seems to be the present trend, would involve the use of minicomputers to monitor the status of all operating variables continuously and, as the situation arose, apply the appropriate remedial action.
- The value of stabilizer gain used must not be excessive since the amplification of unwanted signals could result. This must be considered as a factor in the synthesis of any stabilizer function.
- In the identification of the machine parameters of the real power system model a technique employing frequency response methods was employed. This method allows the determination of all the required machine parameters. However, the analysis of the data is rather complex. This disadvantage can be

tolerated when the standard tests fail to yield the desired information as was the case in this investigation.

BIBLIOGRAPHY

1. Heffron, W.G., Phillips, R.H. "Effect of modern amplidyne voltage regulators on underexcited operation of large turbine generators," AIEE Trans. (Power Apparatus and Systems), Vol. 71, pp 692 - 697, August 1952.

2. Transmission and Distribution Reference Book. Westinghouse.

3. Byerly, R.T., Kimbark, E.W. Stability of Large Electric Power Systems. IEEE Press. 1974.

4. Fleming, R.J. Automatic Control in Electric Power Systems. University of Saskatchewan - Power systems control course notes.

5. DeMello, F.P., Concordia, C. "Concepts of synchronous machine stability as effected by excitation control", IEEE Trans. PAS, Vol. 88, No. 4, pp. 316 - 329, April 1969.

6. Slemon, G.R. Magnetoelectric Devices - Transducers, Transformers and Machines. Wiley, 1966.

7. Dorf, R.C. Modern Control Systems. 2nd Edition, Addison - Wesley, 1974.

8. Jones, C.V. The Unified Theory of Electrical Machines. Butterworths, 1967.

9. Lawrence, R.R. Principles of Alternating Current Machinery. McGraw-Hill, 1940.

10. Watson, W., Manchur, G. "Synchronous machine operational impedances from low voltage measurements at the stator terminals, "IEEE Trans. PAS, Vol. 93, No. 3, pp. 777 - 784, May/June 1974.

11. Ogata, K. Modern Control Engineering. Prentice-Hall, 1970.

12. Electronic Associates Inc. Handbook of Analog Computation, 2nd Edition, 1965.

13. Wait, J.V., Huelsman, L.P., Korn, G.A. Introduction to Operational Amplifier Theory and Applications. McGraw-Hill, 1975.

14. Dandeno, P.L.,Kundur, P. "Stability performance of 555 MVA turbo alternators - digital comparisons with system operating tests" IEEE Trans. PAS, Vol. 93, No. 3, pp. 767 - 776, May/June 1974.

APPENDIX A

Heffron-Phillips Constants Equations

The Heffron Phillips constants used in the analysis of a synchronous machine infinite bus system are obtained through the use of the following equations.

$$k_1 = \frac{E_{q_0} E_0}{A} [r_e \sin \delta_0 + (X_e + X_d') \cos \delta_0]$$

$$+ \frac{i_{q_0} E_0}{A} [(X_q - X_d')(X_e + X_q) \sin \delta_0 - r_e (X_q - X_d') \cos \delta_0]$$

$$k_2 = [\frac{r_e E_{q_0}}{A} + i_{q_0} (1 + \frac{(X_e + X_q)(X_q - X_d')}{A})]$$

$$k_3 = [1 + \frac{(X_e + X_q)(X_d - X_d')}{A}]^{-1}$$

$$k_4 = \frac{E_0 (X_d - X_d')}{A + (X_e + X_q)(X_d - X_d')} [(X_e + X_q) \sin \delta_0 - r_e \cos \delta_0]$$

$$k_5 = \frac{e_{d_0}}{e_{t_0}} X_q [\frac{r_e E_0 \sin \delta_0 + (X_e + X_d') E_0 \cos \delta_0}{A}]$$

$$+ \frac{e_{q_0}}{e_{t_0}} X_d' [\frac{r_e E_0 \cos \delta_0 - (X_e + X_q) E_0 \sin \delta_0}{A}]$$

$$k_6 = \frac{e_{q_0}}{e_{t_0}} [1 - \frac{X_d' (X_e + X_q)}{A}] + \frac{e_{d_0}}{e_{t_0}} X_q \frac{r_e}{A}$$

where

$$A = [r_e^2 + (X_e + X_d')(X_q + X_e)]$$

The steady state operating values of δ_0, E_{q_0}, E_0, e_{d_0} and e_{q_0} are obtained with the following eq'ns.

$$E_{q_0} = \sqrt{(e_{t_0} + I_{q_0} X_q)^2 + (I_{p_0} X_q)^2}$$

$$E_0 = \sqrt{(e_{t_0} - I_{p_0} r_e - I_{q_0} X_e)^2 + (I_{p_0} X_e - I_{q_0} r_e)^2}$$

$$\sin \delta_0 = \frac{e_{t_0} I_{p_0} (X_q + X_e) - r_e X_q (I_{p_0}^2 + I_{q_0}^2)}{E_{q_0} E_0}$$

$$\cos \delta_0 = \frac{e_{t_0} (e_{t_0} - I_{q_0} (X_q - X_e) - I_{p_0} r_e}{E_{q_0} E_0}$$

$$- \frac{X_e X_q (I_{p_0}^2 + I_{q_0}^2)}{E_{q_0} E_0}$$

$$i_{q_0} = [I_{p_0} (e_{t_0} + I_{q_0} X_q) - I_{p_0} I_{q_0} X_q] / E_{q_0}$$

$$i_{d_0} = [I_{p_0}^2 X_q + I_{q_0} (e_{t_0} + I_{q_0} X_q)] / E_{q_0}$$

$$e_{q_0} = [(e_{t_0} + I_{q_0} X_q) / E_{q_0}] \, e_{t_0}$$

$$e_{d_o} = i_{q_0} X_q$$

If it is assumed that the external resistance is zero the expressions for the six constants becomes:

$$k_1 = \frac{X_q - X_d'}{X_e + X_d'} \; i_{q_0} \; E_0 \sin \delta_0 + \frac{E_{q_0} \; E_0 \cos \delta_0}{X_e + X_q}$$

$$k_2 = \frac{E_0 \sin \delta_0}{X_e + X_d'}$$

$$k_3 = \frac{X_d' + X_e}{X_d + X_e}$$

$$k_4 = \frac{X_d - X_d'}{X_e + X_d} \; E_0 \sin \delta_0$$

$$k_5 = \frac{X_q}{X_e + X_q} \; \frac{e_{d_0}}{e_{t_0}} \; E_0 \cos \delta_0 - \frac{X_d'}{X_e + X_d'} \; \frac{e_{q_0}}{e_{t_0}} \; E_0 \sin \delta_0$$

$$k_6 = \frac{X_e}{X_e + X_d'} \; \frac{e_{q_0}}{e_{t_0}}$$

It should be noted that all quantites are in per unit on the machine base.

The nomenclature used is as follows:

e_q = quadrature - axis voltage

e_d = direct - axis voltage

i_q = quadrature - axis current

i_d = direct - axis current

e_t = terminal voltage

X_d = direct - axis synchronous reactance

X_q = quadrature - axis synchronous reactance

X_d' = direct - axis transient reactance

X_e = equivalent system reactance (external to machine)

r_e = equivalent system resistance (external to machine)

δ = angle between the quadrature axis and the infinite bus voltage.

I_p = real component of load current

Iq = reactive component of load current

Subscript 0 denotes steady state value.

Upon examination of the paper presented by deMello and Concordia [5], one will observe that the expression for k_4 does not correspond to that given above. The expressions for k_1 - k_6 enumerated previously correspond to those originally proposed by Heffron and Phillips [1]. In the development by deMello and Concordia the location of the constant k_3 has been altered so as to appear in t he field expression. In order that the diagrams remain equivalent the original expression for k_4 (shown above) must be divided by k_3 to obtain the expression given by deMello and Concordia.

APPENDIX B

Synchronous Machine Operational Impedances From Low Voltage Measurements at the Stator Terminals - A Sample Calculation

The procedure employed to obtain the machine parameters is presented using the test data corresponding to the d-axis with open circuit field. The synchronous machine is analyzed through the use of an electrical equivalent network consisting of parallel branches of RL elements as shown in Fig. 1. The model is an exact equivalent to the transfer function determined for voltage changes applied to the stator terminals. The development to be followed is identical to that given in reference [10].

On a per phase basis the ratio of stator voltage to stator current results in

$$\frac{V_s}{kI_s} = R_s + s\, L_d(s)$$

where R_s is the dc stator resistance measured at operating temperature and $L_d(s)$ is the operational inductance associated with the direct - axis. The factor k is a constant to account for the measurement arrangement ($k = 2$ for the d - axis). Manipulation yields:

$$\frac{V_s}{kR_sI_s} = 1 + \frac{sLd(s)}{R_s}$$

The quantity on the left hand side of the equality sign correponds to the measured transfer function whose data is analyzed to fit the following general form.

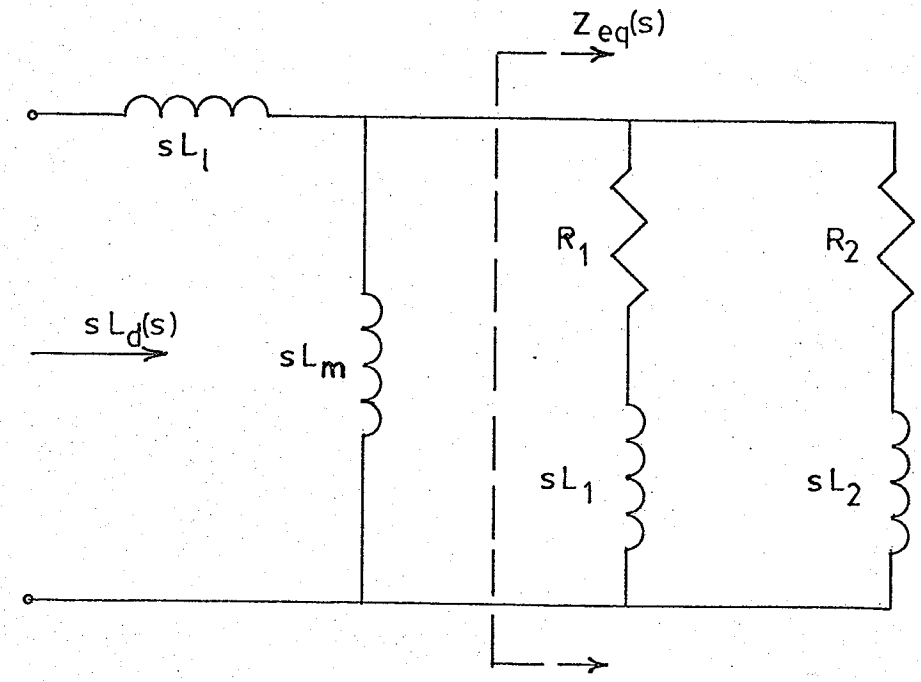

FIG. 1 D - axis equivalent circuit referred to the stator terminals.

$$\frac{V_s}{kR_s I_s} = \frac{(1+sT_1)(1+sT_2)(1+sT_3)}{(1+sT_4)(1+sT_5)}$$

Using a least squares optimization routine the curve obtained through experiment is fitted to the analytic form and the resulting break frequencies are derived. Fig. 2 shows the Fortran listing of the main program for this case. The numerical result is:

$$\frac{V_s}{kR_s I_s} = \frac{[1+(0.115)s][1+(0.0318)s][1+(0.0029)s]}{[1+(0.102)s][1+(0.0230)s]}$$

The above expression has the form:

$$\frac{V_s}{kR_s I_s} = \frac{Y_{(s)}}{Z_{(s)}}$$

and

$$1 + \frac{sL_{d(s)}}{R_s} = \frac{Y_{(s)}}{Z_{(s)}}$$

Therefore

$$L_{d(s)} = \frac{R_s}{s}\left(\frac{Y_{(s)} - Z_{(s)}}{Z_{(s)}}\right)$$

From above

$$Y_{(s)} = 1 + (0.15)s + (4.096\times10^{-3})s^2 + (1.093\times10^{-5})s^3$$

and

$$Z_{(s)} = 1 + (0.125)s + (2.346\times10^{-3})s^2$$

```
      $JOB  WATFIV   CURVE FIT D AXIS C C FIELD
.1          REAL*8 F(20),X(7),E(20),W(251),ESCALE
 2          COMMON /TRANS/ XX(20),Y(20),C(20)
 3          DIMENSION A(20)
 4          DOUBLE PRECISION XX,Y,A,C,DATAN,DSQRT,B(20),H(20)
 5          M=20
 6          READ,(A(I),Y(I),C(I),I=1,M)
 7          DO 2 I=1,M
 8          C(I)=C(I)/.57295779D2
 9        2 XX(I)=2.D0*3.1416D0/A(I)
10          N=7
11          X(1)=.119130D0
12          X(2)=.33423D-1
13          X(3)=.3018D-2
14          X(4)=.58743D-3
15          X(5)=.10636D0
16          X(6)=.2395D-1
17          X(7)=.53970D-3
18          DO 10 I=1,M
19       10 E(I)=1.D-4
20          ESCALE=1.D1
21          IPRINT=2
22          MAXFUN=350
23          LW=251
24          CALL LEAST(M,N,F,X,E,ESCALE,IPRINT,MAXFUN,W,LW)
25          PRINT25
26       25 FORMAT('0','FREQ RAD/SEC',19X,'MAGNITUDE',20X,'PHASE',20X,
          *       'MEAS MAGN',15X,'MEAS PHASE')
27          DO 4 I=1,20
28          H(I)=DSQRT((1.+(X(1)*XX(I))**2.)=(1.+(X(2)*XX(I))**2.)*
          *       (1.+(X(3)*XX(I))**2.)*(1.+(X(4)*XX(I))**2.)/((1.+(X(5)*
          *       XX(I))**2.)*(1.+(X(6)*XX(I))**2.)*(1.+(X(7)*XX(I))**2.)))
29          B(I)=DATAN(X(1)*XX(I))+DATAN(X(2)*XX(I))+DATAN(X(3)*
          *       XX(I))+DATAN(X(4)*XX(I))-DATAN(X(5)*XX(I))-DATAN(X(6)*
          *       XX(I))-DATAN(X(7)*XX(I))
30          B(I)=.57295779D2*B(I)
31          C(I)=.57295779D2*C(I)
32          PRINT35,XX(I),H(I),B(I),Y(I),C(I)
33       35 FORMAT(' ',D14.6,15X,D14.6,14X,D14.6,11X,D14.6,10X,D14.6)
34        4 CONTINUE
35          STOP
36          END

37          SUBROUTINE CALFUN(M,N,F,X)
38          REAL*8 F(M),X(N)
39          DOUBLE PRECISION DSQRT,XX,Y,C,B(20),DATAN,DABS
40          COMMON /TRANS/ XX(20),Y(20),C(20)
41          DO 6 K=1,7
42          IF(X(K))3,6,6
43        3 X(K)=-X(K)
44        6 CONTINUE
45          DO 12 I=1,M
46          B(I)=DATAN(X(1)*XX(I))+DATAN(X(2)*XX(I))+DATAN(X(3)*
          *       XX(I))+DATAN(X(4)*XX(I))-DATAN(X(5)*XX(I))-DATAN(X(6)*
          *       XX(I))-DATAN(X(7)*XX(I))
47       12 F(I)=DABS(Y(I)-DSQRT((1.+(X(1)*XX(I))**2.)*(1.+(X(2)*XX(I))**2.)*
          *       (1.+(X(3)*XX(I))**2.)*(1.+(X(4)*XX(I))**2.)/((1.+(X(5)*
          *       XX(I))**2.)*(1.+(X(6)*XX(I))**2.)*(1.+(X(7)*XX(I))**2.))))
          *       +10.*DABS(C(I)-B(I))
48          RETURN
49          END
```

FIG. 2 Fortran listing of the main program for the least squares optimizing routine "LEAST".

Now R_s = 11.9 ohms.

After calculation

$$Ld_{(s)} \doteq \frac{(0.30)[1+(0.064)s][1+(0.0070)s]}{[1+(0.10)s][1+(0.023)s]}$$

From reference [14] the equivalent expression for the above is

$$Ld_{(s)} = \frac{[1+(\frac{Ld'}{Ld''} T_{do}')s][1+(\frac{Ld''}{Ld'} T_{do}'')s]}{[1+(T_{do}')s][1+(T_{do}'')s]}$$

Examination of the two previous expressions allows one to immediately say:

$$T_{do}' \simeq 0.10 \text{ sec.} \qquad T_{do}'' \simeq 0.02 \text{ sec.}$$

T_{do}' is the open circuit transient field time constant while T_{do}'' is the subtransient value. For the stability studies undertaken only the value for T_{do}' was used.

Returning again to Fig. 1, it can easily be deduced that

$$sLd_{(s)} = sL\ell + \frac{(sLm)(Zeq(s))}{sLm + Zeq(s)}$$

Solving for Z eq (s):

$$Z \text{ eq } (s) = \frac{(sLm)(Ld(s) - L\ell)}{(Lm + L\ell) - Ld(s)}$$

If we let $Ld(s) = Ldu\ (\frac{N(s)}{D(s)})$

where Ldu is the per unit d axis inductance on the machine base (Ldu = $L\ell$ + Lm where $L\ell$ and Lm are respectively the leakage induct-

ance and the mutual inductance), the expression for Z eq (s) now becomes:

$$Z\ eq\ (s) = \frac{sLm(N_{(s)} - \frac{L\ell}{Ldu} D_{(s)})}{D_{(s)} - N_{(s)}}$$

The values for $L\ell$ and Lm were determined through previous tests and are as shown.

$$L\ell \simeq 0.05\ pu \qquad Lm \simeq 0.25\ pu$$

From the above

$$N_{(s)} = 1 + (0.0706)s + (4.407 \times 10^{-4})s^2$$

$$D_{(s)} = 1 + (0.125)s + (2.346 \times 10^{-3})s^2$$

After calculation we arrive at the following form:

$$Z\ eq\ (s) = \frac{Req\ (1+sTx)(1+sTy)}{(1+sTm)}$$

From analysis of Fig. 1 Z eq (s) can also be expressed as:

$$Z\ eq\ (s) = \frac{\frac{R_1R_2}{R_1+R_2}\left[1 + s\left(\frac{L_1}{R_1} + \frac{L_2}{R_2}\right) + s^2\frac{L_1L_2}{R_1R_2}\right]}{\left[1 + s\left(\frac{L_1L_2}{R_1+R_2}\right)\right]}$$

If we let

$$R_p = \frac{R_1R_2}{R_1+R_2}, \quad T_1 = \frac{L_1}{R_1} \quad \text{and} \quad T_2 = \frac{L_2}{R_2}$$

then, by substitution and factoring

$$Z \text{ eq } (s) = \frac{R_p[1+sT_1][1+sT_2]}{[1+R_p(\frac{T_1}{R_2}+\frac{T_2}{R_1})s]}$$

Equating like terms of this final expression and the earlier version produces:

$$R_p = Req$$

$$T_1 = Tx$$

$$T_2 = T_y$$

$$R_p(\frac{T_1}{R_2} + \frac{T_2}{R_1}) = T_m$$

Using the first and last equations of the above set allows the establishment of the following matrix equation.

$$\begin{bmatrix} 1 & 1 \\ T_2 & T_1 \end{bmatrix} \begin{bmatrix} 1/R_1 \\ 1/R_2 \end{bmatrix} = 1/R_p \begin{bmatrix} 1 \\ T_m \end{bmatrix}$$

Deriving Z eq (s) numerically gives:

$$Z \text{ eq } (s) = \frac{(3.69)[1+(0.059)s][1+(0.0010)s]}{[1+(0.035)s]}$$

Using this equation the following values become evident.

$T_1 = 0.059$ sec. $\qquad T_2 = 0.001$ sec.

$T_m = 0.035$ sec. $\qquad R_p = 3.7$ ohms

Upon solution we have:

$R_1 = 8.9$ ohms $\qquad R_2 = 6.3$ ohms

and subsequently

$L_1 = .53$ H $\qquad L_2 = .01$ H.

To determine the value of X_d'' the equivalent reactance of the whole network is determined (resistance values are neglected). The value obtained is:

$$X_d'' = 0.06 \text{ pu.}$$

To determine the value of X_d' the equivalent reactance of the network with the last shunt branch removed is determined. The value is:

$$X_d' = 0.22 \text{ pu.}$$

Finally the value for X_d is obtained by removing both shunt branches from the networks and determining the equivalent reactance. This corresponds to L_{du} (in per unit) obtained earlier and thus

$$X_d = 0.30 \text{ pu}$$

In an analogous manner the values of the other machine parameters are calculated using the data from the rest of the tests performed. The pertenant results are shown in the table of Chapter II.

APPENDIX C

Analog Computer Simulation

Scaling

In order that the signal levels present at any location in the model should not exceed $\pm$ 10 volts, thereby avoiding saturation which could create errors in the results, the simulation must be properly scaled. In addition, the signals should not be too small so that they are not of the same order as noise signals. The process of scaling involves writing the appropriate equations for each part of the model and estimating the maximum expected value for each variable. The equations are then rewritten to obtain reasonable pot settings and amplifier gains throughout the simulation.

The scaled analog computer simulation diagram is shown in Fig. 3.12. If we first examine the power - frequency section of the model the following equation becomes evident.

$$\Delta\omega = \frac{-\Delta P_e + \Delta P_m}{Ms+D}$$

$$\Delta\omega = -\frac{\Delta P_e}{M} - \frac{D\Delta\omega}{M} + \frac{\Delta P_m}{M}$$

The estimated maximum values for each variable are:

$\Delta\omega$ - .10 pu

ΔP_e - 3 pu

ΔP_m - 1 pu

Therefore

$$.1\left[\frac{\Delta\dot{\omega}}{.1}\right] = -\left(\frac{3}{M}\right)\left[\frac{\Delta P_e}{3}\right] - \left(\frac{.1D}{M}\right)\left[\frac{\Delta\omega}{.1}\right] + \left(\frac{1}{M}\right)\left[\frac{\Delta P_m}{1}\right]$$

and thus:

$$\left[\frac{\Delta\dot{\omega}}{.1}\right] = -10\left(\frac{3}{M}\right)\left[\frac{\Delta P_e}{3}\right] - \left(\frac{D}{M}\right)\left[\frac{\Delta\omega}{.1}\right] + 10\left(\frac{1}{M}\right)\left[\frac{\Delta P_m}{1}\right]$$

From measurements

$$D = 1.8 \text{ pu} \qquad M = 5.7 \text{ sec.}$$

The required pot settings become:

$$3/M = 0.526 \qquad \frac{D}{M} = 0.316$$

and

$$\frac{1}{M} = 0.175$$

The pot settings turn out to be satisfactory.

For the frequency - angle section of the model:

$$\Delta\delta = \frac{377}{S}\,\Delta\omega$$

or

$$\Delta\dot{\delta} = 377\,\Delta\omega$$

The estimated maximum value for $\Delta\delta$ is 4 radians resulting in the following:

$$\left[\frac{\Delta\dot{\delta}}{4}\right] = 10(.943)\left[\frac{\Delta\omega}{.1}\right]$$

Examining the area of the model associated with electrical power gives:

$$\Delta P_e = k_2 \Delta Eq + k_1 \Delta\delta$$

The estimated maximum value for ΔEq is 0.5 pu.

Therefore:

$$\left[\frac{\Delta P_e}{3}\right] = \left(\frac{.5k_2}{3}\right)\left[\frac{\Delta Eq}{.5}\right] + \left(\frac{4k_1}{3}\right)\left[\frac{\Delta\delta}{4}\right]$$

For the signals contributing to field voltage the appropriate equation is:

$$\Delta E_{fld} = \frac{k_e}{1+sT_e}\ (-k_5\Delta\delta - k_6\Delta Eq)$$

or

$$\Delta \dot{E}_{fld} = \frac{-k_e k_5}{T_e}\ \Delta\delta - \frac{k_e k_6}{T_e}\ \Delta Eq - \frac{1}{T_e}\ \Delta E_{fld}$$

The estimated maximum value for ΔE_{fld} is 3 pu.

Therefore:

$$\left[\frac{\Delta \dot{E}_{fld}}{3}\right] = \left(\frac{4k_e k_5}{3T_e}\right)\left[\frac{\Delta\delta}{4}\right] - \left(\frac{0.5\ k_e k_6}{3\ T_e}\right)\left[\frac{\Delta Eq}{0.5}\right]$$

$$- \left(\frac{1}{T_e}\right)\left[\frac{\Delta E_{fld}}{3}\right]$$

Since k_e is large it can be seen that the pot settings will not be reasonable. To alleviate the problem divide numerator and denominator by 10.

$$\left[\frac{\Delta \dot{E}_{fld}}{3}\right] = -\left(\frac{0.4\ k_e k_5}{3\ T_e/10}\right)\left[\frac{\Delta\delta}{4}\right] - 10\left(\frac{0.005\ k_e k_6}{3\ T_e/10}\right)\left[\frac{\Delta Eq}{0.5}\right]$$

$$- \left(\frac{0.1}{T_e/10}\right)\left[\frac{\Delta E_{fld}}{3}\right]$$

Using values obtained earlier for each of the constants shows that the pot settings are now reasonable.

Finally, if we consider the equation relating q - axis voltage, we obtain:

$$\dot{\Delta Eq} = \frac{-k_4 \Delta\delta}{T'_{dz}} + \frac{k_3}{T'_{dz}} \Delta E_{fld} - \frac{1}{T'_{dz}} \Delta Eq$$

The resulting scaled equation is:

$$\left[\frac{\dot{\Delta Eq}}{0.5}\right] = - \left(\frac{4k_4}{0.5T'_{dz}}\right)\left[\frac{\Delta\delta}{4}\right] + 10\left(\frac{0.3k_3}{0.5T'_{dz}}\right)\left[\frac{\Delta E_{fld}}{3}\right] - \left(\frac{1}{T'_{dz}}\right)\left[\frac{\Delta Eq}{0.5}\right]$$